Meteorological, Sea Ice, and Oceanographic Conditions in the Labrador Sea during 2020

Igor Yashayaev, Ingrid Peterson, and Zeliang Wang

Fisheries and Oceans Canada
Ocean and Ecosystem Sciences Division
Bedford Institute of Oceanography
P.O. Box 1006, 1 Challenger Drive
Dartmouth, Nova Scotia B2Y 4A2

Canada

Foreword

This document has been peer-reviewed and will be published by Fisheries and Ocean Canada as Canadian Science Advisory Secretariat Research Document, possibly with minor modifications. The series documents the scientific basis for the evaluation of aquatic resources and ecosystems in Canada. As such, it addresses the issues of the day in the time frames required and the documents it contains are not intended as definitive statements on the subjects addressed but rather as progress reports on ongoing investigations.

ABSTRACT

In the Labrador Sea, the coldest and freshest North Atlantic basin south of the Greenland-Iceland-Scotland Ridge, wintertime surface heat losses result in the formation of dense waters that play an important role in ventilating the deep ocean and driving the global ocean overturning circulation. In the winter of 2020, the central Labrador Sea lost more heat through surface cooling than in the previous winter. However, the surface heat loss remained near-normal for a third straight year, contrasting a 27-year record high in 2015 and above-normal losses in 2016 and 2017. The 2020 winter (Dec-Mar) NAO index was above-normal and the highest after reaching its record high in 2015. However, the sea level pressure pattern was not associated with strong westerly winds along the Labrador coast. This led to, respectively, near-normal and above-normal winter and spring air temperatures in the Labrador Basin domain. Both winter and spring sea surface temperatures in the Labrador Basin were above-normal. Winter sea ice extent was below-normal in the Davis Strait, Northern Labrador Shelf and Labrador Shelf regions. Spring sea ice extent was also below-normal in all three regions. With respect to temperature anomalies averaged annually over the central Labrador Sea, the upper 100 m layer was the coldest in the 2002-2020 period in 2015 and 2018. After 2018, this layer attained above-normal annual temperatures in 2019-2020, reaching a 2011-2020 temperature high in 2019, then slightly cooling yet remaining above-normally warm through 2020. The intermediate, 200-2000 m, layer of the Labrador Sea started to cool immediately after hitting a record warm point of the 1972-2020 period in 2011. This cooling trend was mainly driven by strengthening and progressively deepening winter convection in 2012 and during 2014-2018. The key factor that has contributed to the recurrent deepening of convective mixing in the three straight winters following the winter of 2015 was not as much air-sea heat exchange as the water column preconditioning set by convective mixing in the previous years. Such multiyear persistence of deepening winter convection, continuing through the winter of 2018, when it exceeded 2000 m in depth, has resulted in the most voluminous, densest and deepest formation of Labrador Sea Water since 1994. In the winter of 2019 the situation has however changed with winter convection not generally exceeding 1400 m and the intermediate layer starting to warm to the point of fully reversing the seawater density trend to negative. Even though, wintertime mixing reached marginally deeper in 2020 (by 100 m or so), and the intermediate layer slightly cooled, the negative density trend prevailed. Between 2018 and 2020, the annual mean intermediate layer density reduced by about 0.01 kg/m^3. Overall, the changes in the depth of winter convection and intermediate layer properties between these years imply that the effect of the water column preconditioning on winter convection has weakened since 2018. Vertical distributions of dissolved oxygen and CFC (chlorofluorocarbons or CFCs, industrially Freons, are the anthropogenic gases that are commonly used as tracers of convectively-formed water masses spreading in the ocean) concentrations in the central Labrador Sea based on quality controlled drift-corrected measurements assembled since 1990 follow very closely multiyear events of recurrently persistent renewal of dense deep Labrador Sea water in the Atlantic Ocean. Bedford Institute of Oceanography North Atlantic model simulations suggest that the transport of the Labrador Current generally decreased between 1995 and 2014, increased between 2014 and 2019, and slightly decreased in 2020. The Atlantic meridional overturning circulation index based on this model demonstrates a general weakening trend since mid-1990s until 2004, then slight strengthening lasting until 2011, then weakening again until the overturning weakest point was reached in 2019. The overturning circulation started to strengthen in 2020, but it is too early to associate this short-term increase with a reversal of the current negative trend in the Atlantic meridional overturning circulation.

INTRODUCTION

The Labrador Sea is located between Greenland and the Labrador coast of eastern Canada, with its deep semi-enclosed basin bounded by the West Greenland and the Newfoundland-Labrador shelves. Cold, low-salinity waters of polar origin circle the Labrador Sea in a counterclockwise current system that includes both the northward flowing West Greenland Current (WGC) on the eastern side and the southward flowing Labrador Current (LC) on the western side (Figure 1). Distinctively warmer and saltier patches of water can be found underneath the offshore extensions of the WGC and LC. These are variations of the Atlantic Water originating in the low latitudes of the Atlantic Ocean, and following first the North Atlantic Current and then the Gulf Stream. As the Atlantic Water flows into and around the Labrador Sea, following its eastern, northern and eventually western boundaries, it mixes with other masses, progressively cooling and freshening.

Spatial distribution and temporal changes in temperature, salinity, density, dissolved oxygen and other environmental variables in the upper and deep layers of the Labrador Sea respond to a wide range of external and internal oceanic factors. The external factors include exchanges with land, e.g., continental runoff, and atmosphere, e.g., radiation, latent and sensible heat, and momentum fluxes, precipitation, evaporation and exchanges with other substances (such as anthropogenic gases). The internal factors include inflows of warmer and saltier, and colder and fresher waters from the adjacent North Atlantic and Arctic, respectively, and local oceanic processes such as lateral mixing and winter convection. Naturally, the physical, chemical and biological processes and seawater properties are subjected, both vertically and horizontally, to seasonal, interannual and decadal variations across the region. In addition, instantaneous conditions and process development depend on the cumulative effect of past heat, salt and freshwater gains and respective temperature, salinity and density changes termed as ocean preconditioning (Yashayaev and Loder, 2017).

Since 1990 except for 2017, the Bedford Institute of Oceanography (BIO) of Fisheries and Oceans Canada (DFO) has been conducting annual occupations of the oceanographic section Atlantic Repeat 7-West (AR7W). This section spanning the Labrador Sea, (Figure 1) was first included as both one-time (A1E) and repeat (AR7W) hydrographic lines in the World Ocean Circulation Experiment (WOCE) array (Lazier et al., 2002; Kieke and Yashayaev, 2015; Yashayaev et al., 2015a).

During more than three decades of its existence, the annual survey of the AR7W line provided the most critical high-quality observations used to quantify and understand both physical processes and full-depth ocean variability in the subpolar North Atlantic. The observations collected on the AR7W line became an important contribution of Canada to the international Global Climate Observing System (GCOS), the Climate Variability (CLIVAR) component of the World Climate Research Programme (WCRP) and the Global Ocean Ship-based Hydrographic Investigations Program (GO-SHIP). These observations were repeatedly used and accentuated in numerous high-impact publications (e.g., Dickson et al., 2002; Curry et al., 2003; Thornalley et al., 2018; Lozier et al., 2019; Fröb et al., 2017; Holliday et al., 2020), special journal issues (e.g., Yashayaev, 2007b; Yashayaev et al. 2015b; also Yashayaev et al. 2015a; Kieke and Yashayaev, 2015), books (e.g., Dickson et al., 2008), the Fourth and Fifth Assessment Reports (AR) of the Intergovernmental Panel on Climate Change (IPCC; e.g. Bindoff et al., 2007; Rhein et al., 2013), the International Council for the Exploration of the Sea's (ICES) Reports on Ocean Climate (IROC, e.g., González-Pola et al., 2020) and Northwest Atlantic Fisheries Organization (NAFO) reports (e.g., Yashayaev et al., 2020).

The annually visited Labrador Sea oceanographic section AR7W spans approximately 900 km from Misery Point, Labrador, to Cape Desolation, Greenland. With more than three decades of coast-to-coast surface-to-bottom observations systematically collected on AR7W between June of 1990 and August of 2020 (meeting WOCE quality requirements for temperature, salinity and dissolved oxygen until June of 2019) presently available, we are able to construct and analyze interannual and decadal variations, and long-term trends in all key ecosystem variables at any point below 200 m, i.e., where the contribution of the seasonal cycle to their total variance is relatively small.

Additionally, the scope of the DFO-led Deep-Ocean Observation and Research activities includes occupations of the Extended Halifax line, maintaining deep-water oceanographic moorings in the Labrador Sea, such as the Hamilton Bank mooring (Figures 1 and *15*), and on the Scotian Slope and deployments of profiling Argo floats in both regions.

The following four sections, **Meteorological Observations**, **Remotely-Sensed Sea Surface Temperature**, **Sea Ice Observations** and **In-Situ Oceanographic Observations**, introduce the data sources used to produce this report, each starting with brief descriptions of respective data and methods, and present general climatological and environmental metrics obtained with these data. The seasonality in the seawater properties and its impacts on the reported ocean state variables and other general issues concerning shipboard survey data synthesis limitations are discussed in **Adequacies and Limitations of In-Situ Observations for Monitoring Interannual Changes in the Labrador Sea**. The next section, **Winter Convection and Hydrographic Conditions in the Central Labrador Sea**; provides a detailed view and discusses the mechanisms of both long and short term variability in the Labrador Sea. In the **Numerical Model Results** section, the past BIO North Atlantic Model results are updated to include the year of reporting and to connect the changes in water mass characteristics and boundary current systems. The key results and Labrador Sea condition parameters are summarized in the **Summary** section.

This document is also in support of the Atlantic Zone Monitoring Program (AZMP) Science Advisory Report (DFO, 2021).

METEOROLOGICAL OBSERVATIONS

NORTH ATLANTIC OSCILLATION (NAO) INDEX

The NAO is an important teleconnection pattern influencing atmospheric processes in the Labrador Sea (Barnston and Livezey, 1987; Hauser et al., 2015). When the North Atlantic Oscillation (NAO) is in its positive phase, low-pressure anomalies over the Icelandic region and throughout the Arctic combined with high-pressure anomalies over the Azores and across the subtropical Atlantic produce stronger-than-average westerlies across the mid-latitudes. Conditions over the northwestern Atlantic including the Labrador Sea region are colder and drier than average. A negative NAO indicates a relative weakening of either the Icelandic low or the Azores high or both, which decreases the pressure gradient across the North Atlantic resulting in weakening of the westerlies and brings warmer conditions than usual. Both NAO phases are associated with basin-wide changes in the intensity and location of the North Atlantic atmospheric jet stream and storm track, and in large-scale modulations of the zonal and meridional heat and moisture transport (Hurrell, 1995), resulting in the modification of the temperature and precipitation patterns. Even though the focus of this report is on the past three decades, we present and analyze 73-year long NAO, winter surface heat loss and oceanographic records to relate the recent conditions to the major shifts in the atmospheric situations over the North Atlantic.

NAO indices computed using two versions of the NAO index are shown in Figure 2 (upper panel). The station-based NAO index (green) is the difference in winter (December, January, February, March) sea level atmospheric pressure between the Azores and Iceland (Hurrell et al., 2018). The PC-based NAO index (blue) is associated with the first empirical orthogonal function (EOF) of standardized monthly 500-mb height anomaly fields for the Northern Hemisphere. The spatial pattern of this EOF shows a high over southern Greenland, and a low near the latitude of the Azores.

The wintertime NAO exhibits significant multi-decadal variability (Hurrell, 1995). An upward trend of the NAO index from the 1960s to the 1990s was noted by Visbeck et al. (2001), although since the peak in the 1990s there has been a slight downward trend. Recent studies reveal an atmospheric circulation pattern, complementary to NAO, which becomes more prominent in years of low NAO (Hauser et al., 2015). Further study of this phenomenon will help to improve understanding and forecasting capabilities of atmospheric and oceanic conditions.

In 2010, the NAO index reached a record low (Figure 2, upper panel). In 2011, the NAO index rebounded from the record low but still remained well below the 30-year average (1981-2010). In 2012, however, the NAO index was strongly positive, up to a level comparable to those in early 1990s showing the highest winter index over the last twenty years. There was a significant change in the winter NAO index in 2013, when it became moderately negative. In 2014, the NAO index returned to its high positive phase, slightly lower than the 2012 value, making it the second highest in the last twenty years. In 2015 there was another high NAO event, the largest positive NAO magnitude in the 123-year long instrumental record.

In 2020, while both station-based (green) and PC-based (blue) winter (Dec–Mar) NAO indices were strongly positive, continuing the positive anomalies observed since 2014, and, actually, the highest since 2015 (Figure 2, upper panel), the sea level pressure pattern was not associated with strong westerly winds along the Labrador coast (Figure 2, lower right). The reason of this dissociation becomes evident when comparing the maps of the mean sea level pressure (SLP) in winter (December, January, February, March) for the 1981-2010 mean and for 2020 over the North Atlantic (Figure 2, middle row). In 2020, a strengthening of both the Icelandic Low and the Azores High can be seen, so that a low pressure anomaly is present east of Greenland and extending westward into the northeastern Labrador Sea region (bottom left panel). This pattern is associated with positive southeastward to eastward vector wind anomalies in the central Labrador Sea region (bottom right panel) rather than with anomalous winds along the Labrador coast that winter, such that the coastal conditions are similar to those with the winter NAO index is near-normal.

AIR TEMPERATURE

The air temperature data used are from the NCEP Reanalysis dataset, provided by the NOAA/OAR/ESRL PSD, Boulder, Colorado, USA, from their Web site at https://www.esrl.noaa.gov/psd/. The NCEP Reanalysis is a joint project between the National Centers for Environmental Prediction (NCEP) and the National Center for Atmospheric Research (NCAR). The goal of this joint effort is to produce a new Surface Air Temperature and Sea Surface analysis using historical data (1948 onwards) and to produce analyses of the current atmospheric state (Kalnay et al., 1996).

Time series plots of winter and spring air temperature anomalies in the Labrador Basin are shown in Figure 3, for the box 55-60°N, 50.0-52.5°W (Figure 4, left panel). In 2020, winter and spring air temperatures were near-normal and 0.5-1.0 SD above-normal respectively. The maps of surface air temperature anomalies based on the NCEP Reanalysis and averaged over the winter and spring seasons of 2020 are shown in Figure 4. In winter (left panel), air temperature

anomalies are near-normal in the central Labrador Sea, with a positive anomaly in the northern Labrador Sea. Typically, a positive winter temperature anomaly is associated with a negative-to-normal NAO index, while a positive mode of NAO often brings strong westerlies along the Labrador coast resulting in negative air temperature anomalies in the Labrador Sea. However, although the Icelandic Low was strengthened in the winter of 2020, the SLP anomaly pattern was not associated with strong westerlies along the Labrador coast, and therefore negative air temperature anomalies in the Labrador Sea region.

AIR-SEA HEAT FLUX

The cumulative air-sea heat flux integrated over individual-year cooling seasons (cumulative winter surface heat flux/loss in Figures 3 and 13) was computed using 6-hourly heat flux and daily-mean radiation data obtained from the U.S. National Centers for Environmental Prediction (NCEP) Reanalysis (Kalnay et al., 1996). The two available versions of NCEP Reanalysis products, R1 and R2, are jointly used to provide the most extensive up-to-date data coverage.

The total or cumulative surface heat loss incurred in a cooling season was estimated by integrating the net surface heat flux over the Labrador Basin from start to end of a time period showing continuous cooling. Each fall-to-spring cooling period (also cooling cycle) was defined individually from the first date when the net surface heat flux became consistently positive (sea-to-air) to the moment since when its negative values (air-to-sea) prevailed.

Specifically, the net heat flux values used in this integration were computed as a sum of incoming and outgoing shortwave and longwave radiative, and latent and sensible turbulent heat flux components extracted for the region of interest from the NCEP/NCAR Reanalysis fields. As already noted, the start and end points of each cooling cycle were associated with the net flux reversals in fall and spring (Yashayaev and Loder, 2009).

The highest annual heat losses during 1974-2020 were achieved in 1993 and 2015 (e.g. negative anomaly to the negative heat flux). Since 1998, the top six cumulative surface heat losses have occurred in 2008, 2012, 2014, 2015, 2016 and 2017. The heat loss in 2019 was the lowest in six consecutive years, while in 2020 it increased again (consistent with the winter NAO index at a 5-year high in 2020). However, as in the two preceding years, in 2020, the cumulative winter surface heat flux was within the multiyear half standard deviation bounds (Figure 3, third panel from top).

REMOTELY-SENSED SEA SURFACE TEMPERATURE

The sea surface temperature (SST) data used are from the NOAA Optimum Interpolation (OI) Sea Surface Temperature (SST) V2. NOAA_OI_SST_V2 dataset provided by the NOAA/OAR/ESRL PSD, Boulder, Colorado, USA, from their Web site at https://www.esrl.noaa.gov/psd/. The OISST analysis is constructed by combining observations from satellites, ships, and buoys on a regular global grid, and interpolating to fill in gaps.

Time series plots of winter (January-March) and spring (April-June) sea surface temperature anomalies in the Labrador Basin (55-60°N, 50.0-52.5°W) show positive anomalies of 0.5-1.0 SD and 0.5 SD in winter and spring, respectively (Figure 3), meaning that the seasonal sea surface temperature values were 0.5 SD to 1.0 SD above-normal in both winter and spring in the Labrador Basin.

Winter and spring maps of sea surface temperature anomalies (Figure 5) show positive anomalies in the northern Labrador Sea, similar to the air temperature anomalies. However, unlike air temperature anomalies, minimum SST anomalies areas are limited by the freezing point of seawater.

SEA ICE OBSERVATIONS

Sea ice concentrations derived from satellite passive microwave data since late 1978 are obtained from the U.S. National Snow and Ice Data Center. These data were used instead of Canadian Ice Service (CIS) data because they extend farther east, so that they cover the Greenland shelf (comparisons conducted in support of this report show that the anomalies computed from each dataset for the same area agree very closely).

Monthly sea ice concentration data are used for 1978-2020 (Cavalieri et al., 1996; Fetterer et al., 2002). Ice extent is defined as the area in which ice concentration is at least 15%, and is computed for three latitude bands in the Labrador Sea region: 63-68°N (Davis Strait), 58-63°N (Northern Labrador Sea), and 53-58°N (Labrador Shelf). Sea ice observations for the Labrador Shelf region based on CIS ice chart data are presented in Cyr et al. (2021).

Winter and spring time series of sea ice extent anomalies for these three regions are shown in Figure 6, with the locations of the regions shown in Figure 7 (bottom panel). The 2020 winter and spring ice extent anomalies were negative in all regions.

Figure 7 shows monthly maps of sea ice concentration anomalies (top panel) and extent (middle panel) in January to March 2020, using data from the US National Snow and Ice Data Center. The magenta lines in the lower panel show the median limit of ice extent. In all three regions, negative ice concentration anomalies prevailed in 2020, and the ice extent was lower than normal, in agreement with winter air temperature and sea surface temperature anomalies.

IN-SITU OCEANOGRAPHIC OBSERVATIONS

SHIP SURVEY DATA

Since 2004, the AR7W line has been occupied in May, except for June-July in 2012, June in 2019 and July-August in 2020. Each AR7W occupation comprises at least 30 oceanographic stations running from Misery Point (Labrador) to Cape Desolation (Greenland). On each station, the key seawater properties, such as temperature, conductivity, salinity, density, dissolved oxygen, fluorescence and pH are recorded from surface to bottom using conductivity-temperature-depth/pressure (CTD) profiling system. All key sensors are doubled up – e.g., paired temperature, conductivity, oxygen and fluorescence sensors. The number of sensor types installed on the CTD mainframe (also known as a CTD Rosette) connected to the same system increases over time, adding pressure to collection of water samples needed to calibrate both standard and experimental sensors. The standard set of water samples on a typical oceanographic station includes samples for determination of salinity, dissolved oxygen, nutrients and transient tracers.

During the period of 1990-2019, the pressure, temperature, conductivity, salinity, and dissolved oxygen data sets have been quality controlled and calibrated to meet WOCE standards. This was achieved by using sufficient quantities of accurately determined water sample salinity and dissolved oxygen concentration values with the Autosal and Winkler titration systems, respectively; massive 0.001°C accurate SBE35 temperature recorder readouts obtained at all water sampling depths and laboratory sensor calibration data.

However, the vertical distribution and quality of the salinity and oxygen water sample measurements on the AR7W line in 2020, were not sufficient for calibrating the CTD conductivity and oxygen sensors to the accuracy achieved in the past (1990-2019) occupations of the line. As an additional support for the calibration and validation of the 2020 CTD data, the properties (temperature, salinity, dissolved oxygen concentration) of the least temporally

modified part of the Labrador Seawater column – the core of the Northeast Atlantic Deep Water – have been extrapolated to 2020 to improve and validate the present calibrations. These "oceanographically" calibrated data are used in the full-water-depth annual profile compilations and 2020 water column state indices provided in the report.

The historical and recent shipboard oceanographic observations, including, for example, water sample data and CTD profiles, have been quality controlled and processed using multistep critical data analysis procedure, comprising the data editing and processing methods similar to those briefly described by Yashayaev and Seidov (2015).

Argo float temperature and salinity profiles, available since 2002, and rapidly growing in quantity, but not necessarily in quality, have been quality controlled through comparisons with vessel CTD and water sample data and comparisons between floats, and by performing critical analyses of spatial and temporal deviations.

The BIO-led Labrador Sea survey data were enhanced with temperature and salinity observations archived by other programs and national and international data centers (e.g., Kieke and Yashayaev, 2015).

ARGO PROFILING FLOAT DATA

Argo is an international network of profiling floats collecting high-quality temperature and salinity profiles from the upper 2000 m of the ice-free global ocean, and through float displacements, currents from intermediate depths. For most of a typical 10-day cycle a battery-powered autonomous float freely drifts at a "parking depth" of usually 1000 m, where its position is stabilized through buoyancy adjustment. Once the float is released from its parking depth, it descents to approximately 2000 m and then ascents to the surface, while profiling temperature, salinity and other variables, if additional sensors are installed. When the surface is reached, the acquired data are transmitted, and the float sinks back to its parking depth. Since 2002, the near real-time temperature and salinity Argo float data collectively draw a large-scale picture of the oceanographic structure and circulation of the Labrador Sea. The array is typically used to reconstruct the seasonal and interannual variability of the physical characteristics and dissolved oxygen in the upper 2000 m water column. The value of the Argo floats is even more significant in winter, when they serve as the only means of providing information about real-time development of winter convection, and when there are no shipboard measurements available.

Overall, the network of profiling Argo floats provided temperature and salinity data to 2000 m used for monitoring of year-round variability of the oceanographic conditions in the Labrador Sea. However, the number of the floats within the Labrador Sea during 2020 was again just marginally sufficient to resolve sub-monthly variability.

SYNTHESIS OF MULTIPLATFORM DATA SETS

Temperature and salinity data in the Labrador Sea from various sources are compiled and seasonally adjusted to provide individual time series. Our primary data sources include *(i)* full-depth temperature, salinity, and dissolved oxygen profiles collected on the AR7W line across the Labrador Sea that has been occupied by BIO since 1990, *(ii)* water sample and discrete SBE35 temperature data used to calibrate the instrument sensors, *(iii)* temperature and salinity profiles over the upper 2000 m in the Labrador Sea region from the International Argo float program, *(iv)* publically available observed-level temperature and salinity data from other programs and national and international data centers (e.g., Kieke and Yashayaev, 2015), and *(v)* a near-bottom moored temperature time series from a long-term mooring maintained by the BIO on the Labrador continental slope – a respective 30-year series follows the same pattern of

interannual temperature changes as the intermediate-depth layer in the central Labrador Sea (Figure 5 in Yashayaev and Loder, 2016).

Following Yashayaev and Loder (2009, 2016 and 2017), but now including all available Argo float data up to May 2021 and ship survey data up to August 2020 (Figure 1), time-depth series of spatially averaged potential temperature, salinity, and potential density with weekly-to-monthly (dependent on Argo and ship survey data coverage) resolution have been computed for an area of ~60,000 km^2 in the central Labrador Sea. To provide for this, all individual CTD, water sample and Argo float profiles of an analyzed variable selected within the central Labrador Sea contour defined in our earlier studies (e.g., Yashayaev and Loder, 2016), which encompasses the profile locations indicated in Figure 1 with the scattered pink dots, were vertically interpolated and aggregated into time series for each depth level included in a chosen layer.

As shown in the figures discussed here, in the next section and in the **Appendix 1**, the seasonal cycle dominates the upper layer variability and extends to the intermediate layer. Therefore, any analysis of multiyear data should begin with a thorough assessment and, if required, a correction of seasonal biases. Specifically, at least one of the following requirements must be met to be able to investigate longer-term variability in presence of strong seasonality: (1) the contribution of the seasonal cycle to the total variance is less than the contribution of longer-term signals, (2) the seasonal cycle can be effectively removed from analyzed measurements, and (3) the temporal resolution and seasonal coverage of analyzed data is sufficient and consistent through a study period. This requirement is backed up by the analyses of regular (the Appendix 1) and single-year-based (Figures 8 and 9) seasonalities presented in this report. The **Appendix 1** includes seasonal cycles of temperature and salinity (Figure A1), associated seasonal changes encountered over overlapping 30-day periods (Figure A2), and seasonal changes referenced or relative to the 15th of May (Figure A3), standard deviations of multiyear anomalies computed in 10-day bins (Figure A4), and contributions of seasonal cycles to total variances (Figure A5). A careful contemplation of the material on oceanic seasonality leads to the conclusion that the shipboard data collected on the AR7W line over 30 years cannot be used to map interannual variability in both physical and biochemical variables in the top 100 m. The largest seasonal temperature changes are observed in April-June, at the time of the fastest increase in the solar irradiance. The noted seasonal changes exceed the reported interannual variability. To address this issue, the measurements of all physical variables (temperature, salinity and density) have been corrected, depth by depth, for seasonality by using an iterative procedure obtaining a harmonic representation of the seasonal cycle and removing data outliers. The resulting series have been low-pass-filtered, and the filtered values have been averaged annually to obtain the annual variable values since 1948, depending on data availability (Figures 10, 11, 12 and 13).

Further, to quantitatively place the recent variability in a historical context, we use annual time series of temperature, salinity, and density averaged over the 15-100 and 200-2000 m vertical intervals in the central Labrador Sea back to 1948 as long-term indices of these variables over its upper and intermediate-depth waters (Figure 13). These were derived from time series for selected depths like those discussed above and previously reported.

ADEQUACIES AND LIMITATIONS OF IN-SITU OBSERVATIONS FOR MONITORING INTERANNUAL CHANGES IN THE LABRADOR SEA

It should be noted that there are certain limitations in the AR7W shipboard observations restricting the range of tasks that can be effectively solved with the annual survey data used alone. The major limitation of the shipboard data used exclusively for both ocean state

assessments and process/variability studies is attributed to the dominance of seasonality in the upper layer property changes. Indeed, the seasonal spread of the AR7W oceanographic observations was not randomly distributed throughout the entire period, adding a systematic bias to estimates of long-term changes in seawater properties based on the shipboard measurements in the upper (e.g., top 200 m) layer. Since 1990, the mid-point date of the AR7W survey has occurred between early May and early August, with relatively earlier, including the earliest, dates tending to occur in the period of 2014-2018, and later, including the latest, dates occurring before 2004, and in 2012, 2019 and 2020. These sampling limitations make the changes that occur in the upper layer on seasonal, interannual and longer time scales unresolvable with the annual ship survey data, as discussed in **Synthesis of Multiplatform Data Sets**. However, the scatter in the survey dates helped determining the seasonal cycles in different regions of the sea (Fragoso et al., 2016). As shown in the **Appendix 1**, for physical variables, the variability in survey date has a significant effect near the surface (0-100 m), exceeding standard deviation of anomalies, but little effect at depths greater than 200 m. In order to report the interannual and longer-term variability of the physical variables throughout the entire water column, surface-to-bottom, the regular (i.e., based on entire records) seasonal cycle has been removed from all data depth-by-depth. This operation, *namely, data de-seasoning through successive iterations*, makes interannual signals a dominant source of variability at all depth, up to the sea surface.

Each reporting period, such as a particular calendar year, comes with its own unique seasonal cycles in all oceanographic variables. The magnitudes, shapes and phases of these cycles vary with location and depth, and are subject to interannual and longer-term modulations. There are also various physical mechanisms (such as incoming solar radiation) and state variables (such as vertical stratification) responsible for spatiotemporal variability of the related parameters. The processes generating seasonal signals in the ocean, shaping their appearance and governing their time-varying dynamics are part of our ongoing investigation. In the next paragraph, we discuss a new method for tracking the joint result of the seasonally-active physical processes and mapping seasonal anomalies evolving within a relatively short time, e.g., a year, allowing us to follow the seasonal signal timing and magnitude changes during 2018 to 2020. The seasonal anomalies showing in the same years can then be evaluated by subtracting the climatological seasonal cycle (also known as normal or regular, e.g., Yashayaev and Zveryaev, 2001; Yashayaev and Seidov, 2015) from the year-specific (irregular) seasonal cycles. The climatological seasonal cycle is typically based on a 30-year or longer time period of sufficiently frequent observations. Considering that the time scale of prominent changes in the deep ocean often exceeds a decade (as also shown in this report), it is more advantageous from the research standpoint to build a deep-sea climatology using a more prolonged sequence of observations than that spanning 30 years. Another advantage of choosing a longer normal period is directly related to improving statistical uniformity in multiyear seasonal data distribution. The seasonal pattern and annual number of observations in the Labrador Sea have changed considerably since the early 1990s. The interannual changes in data distribution may add systematic biases and random errors to the sought climatological normals. The biases and errors associated with the long-term changes in sampling content tend to reduce as the length of the time period chosen to construct the normals increases.

The careful evaluation and cause analysis of all irregularities or anomalous features detectable in individual year-specific seasonal cycles is important for a much broader ocean state analysis. This assertion is underlined by the fact that an entire range of seasonal signals or features, regardless of their duration, massively contribute to the seasonal, annual and longer-term anomalies contained in each record. The seasonal anomalies can be evaluated in the following way. All data points identified within a continuous 365-day period, e.g., a year of interest, are

approximated with the harmonic functions of annual and nested periods. The procedure associated with this step includes testing of temporal data coverage over the chosen period for an adequate representation of seasonal cycle, and the iterative outlier control and removal. The resulting seasonal cycle (only for the period of interest) is then compared to the regular climatological cycle constructed for the period of 1948-2021. The seasonal cycle anomalies are then evaluated for each day by subtracting the regular cycle from the cycle representing the chosen period. The outlined approach can be effectively visualized by displaying both regular climatological and single-year seasonal cycles for a chosen depth with all quality controlled observations used to evaluate these seasonal cycles layered behind the continuous curves. In particular, Figures 8 and 9 show day-by-day progressions of seasonal signals for particular years, and how these signals compare to the climatological normal (defined as the continuous regular seasonal cycle). These figures show four seasonal cycles of temperature and salinity for the depths of 15 m and 50 m, respectively. The black lines in these figures represent the regular climatological seasonal cycle that was defined using all observations in the central Labrador Sea for the period of 1948-2021 (pink markers in Figure 1). The blue, green and red lines in Figures 8 and 9 represent irregular (or year-specific) seasonal cycles defined individually for the years – 2018, 2019 and 2020. The observations used to compute the four seasonal cycles (climatology, 2018, 2019 and 2020) are also shown in these figures with markers coloured in accordance with the seasonal cycle lines.

The absolute (Figures A1-A3) and relative (Figure A5) effects of the regular (climatological) seasonality on the key sea state variables, such as temperature (left) and salinity (right), are further quantified and illustrated in the **Appendix 1**. The regular seasonal cycle is capable of contributing to any observations randomly taken within seasonally-matching 30-day periods of different years as much as the period's range of the seasonal values. This range is estimated by taking the start and end (or all) values in a given 30-day time frame. The same calculation is performed for all yeardays (i.e., days elapsed from the start of January). This approach is valid for every sea state variable. E.g., Figure A2 shows regular seasonal changes of temperature and salinity over respective 30-day periods, day-by-day. The magnitudes of the seasonal changes that occur over such overlapping 30-day periods is the highest at the sea surface and reduces with depth. This analysis convincingly shows that any uncorrected seasonal bias entering both annual and seasonal sea state estimates with measurements randomly taken within a targeted 30-day seasonal time frame, especially if occurring in spring or fall, is likely to exceeds the magnitude of interannual changes in the upper 100 m layer (e.g., standard deviation shown in Figure A4). The issue is further complicated by the fact that the seasonal occurrence of the AR7W surveys during 1990-2020 spans 100 days, May-to-August, making the seasonal bias considerably larger than incurred in a single month frame.

The major error in the sea state estimates arises from neglecting the rapid warming of the upper water column occurring between May and June, obvious in Figures A1-A5. Figures 8 and 9 reveal another aspect of the problem. There are year-to-year changes in both phase (e.g., time shifts in the end of cooling and start of warming, like in 2018) and shape of the seasonal cycle. The vertical magenta dotted lines in Figures 8 and 9 confine the calendar day range of May 15 – June 15, and the changes during this period are obviously much larger than the differences between the annual spring average values. It is also apparent in these figures that averaging the daily anomalies over a week, its associated month, season and year may likely give significantly different results. Consequently, the near-surface seasonal anomalies (with the regular seasonal cycle removed) averaged over a short-term interval in spring (e.g., a five-day survey in early May) may not be representative of an entire season (e.g., mid-April to mid-June). Therefore, both the high rate of seawater property changes in the regular or climatological seasonal cycles, and the multiscale irregularity in the year-specific seasonal cycles need to be

taken into consideration every time a statement about seasonal, interannual, decadal and longer-term changes is made. This rule was closely followed when compiling, processing and analyzing the shipboard, profiling float and moored observations for the present report.

The measurements of dissolved oxygen, CFC-11, CFC-12, silicate, nitrate and phosphate concentrations collected on the AR7W line during a 30-year time period, 1990-2019, were extracted from different data sources, cleaned from outliers, analyzed for instrumental inner- and inter- cruise shifts and drifts, corrected respectively and used to assemble annual composite profiles presented and discussed in this report. Multiyear progressions of the annual seawater property profiles, constructed using the cleaned water sample data before applying any time-dependent correction, are shown in Figures A6 and A7, and discussed in the **Appendix 2**. Multiyear progressions of the analogous annual profiles, only this time with the time-dependent corrections applied to the original data, are shown in Figures 11 and 12, and discussed with respect to long-term changes in convective mixing and ventilation. The climatological normals of dissolved oxygen, CFC-11, CFC-12, silicate, nitrate and phosphate concentrations on the AR7W line for the period of 1990-2019 are shown in Figure 22.

In addition to irregular seasonal coverage, there are limitations imposed on interpretations of oceanographic data collected in the shelf and even slope segments of the AR7W line by insufficient spatial coverage due to moderate-to-heavy sea-ice conditions in some years. As a result, the near-coastal stations cannot always be reached, making the shelves and, in a number of cases, the continental slopes more limited in data coverage than the deeper regions, thereby creating spatial shifts in data distribution in high-horizontal-gradient boundary regions.

WINTER CONVECTION AND HYDROGRAPHIC CONDITIONS IN THE CENTRAL LABRADOR SEA

LONG-TERM CHANGES IN KEY WATER MASSES

Multidecadal time-depth distributions of annual temperature, salinity and density (referenced to a pressure of 1000 dbar) values in the central Labrador Sea since 1948 at depths of 200-3500 m are shown in Figure 10. A combination of averaging on constant density and constant pressure surfaces or levels was used in the computational procedure to achieve best representation of annual seawater characteristics.

Multiyear evolutions of dissolved oxygen, CFC-11 and CFC-12 concentrations assembled from the respective vertical annual profiles, which were in turn composed from the shipboard observations on the AR7W line confined to the central Labrador Sea spanning the period of 1990-2019 are shown in Figure 11. Chlorofluorocarbons (CFCs), also known as Freons (industrial definition of the CFCs), are the anthropogenic gases that are commonly used as tracers of convectively-formed water masses in the ocean. Together with dissolved oxygen, CFC-11 and CFC-12 measurements complement the physical variables in the studies of ventilation and rejuvenation of the Labrador Sea water column. Constructed similarly to the temporal progressions of the annual profiles shown in Figure 11, the annual composite profiles of silicate, nitrate and phosphate concentrations in the central region of the Labrador Sea for the depth range of 200-3500 m and the time period of 1990-2019 are arranged chronologically in Figure 12. The processing steps that were followed to create these figures are summarized in the next paragraph.

Prior to assembling the annual profiles and building their multiyear progressions, all unedited profiles of the studied seawater characteristics without any omission were thoroughly checked for outliers. All outliers were then excluded from the original data and initial collections of annual

composite profiles created for all variables. The **Appendix 2** briefly outlines the procedure used to construct the annual profiles and discusses the 1990-2019 progressions of these profiles (Figures A6 and A7). Note that at this point there was no additional time-dependent correction applied to the initial data. However, certain massively sampled chemical variables, particularly, nitrate and phosphate concentrations, are known to be sensitive to varying standard quality and calibration methods causing drifts or rather shifts both during and between sea missions. Among possible reasons of such drifts and shifts are inaccurate standards, missing or biased calibrations and other instrumental errors. Whenever the case, a time or cruise based correction was designed and used to correct detectable systematic errors. Cleaned from random outliers and corrected for time-based or cruise-based shifts or drifts, the observed data profiles were interpolated to both depth (5 m) and seawater density grids, and then averaged annually on both constant density and pressure surfaces, respectively. The resulting annual profiles were then assembled in the multiyear progressions and interpreted with reference to the physical variables. Figures 11 and 12 show annual composite profiles with cruise-specific corrections applied in order to reduce the mentioned instrumental biases caused by inadequate standardization and calibration. Before applying these corrections, the instrumental biases dominated some chemical data obscuring the natural variability that is detectable in the corrected data. Comparing Figures A6 and A7 with Figures 11 and 12, respectively, shows the difference.

In 2020, the AR7W water sample measurements of dissolved oxygen did not meet the quality requirement for extending the analysis of interannual variability, but the CTD data were used to construct a vertical section plot discussed below. The 2020 CFC-11 and nutrient data were not available at the time of figure preparation.

Time series plots of annual and spring (April-June) mean temperature and salinity values averaged over the 15-100 m and 200-2000 m depth ranges are presented in Figure 13.

The hydrographic data transmitted by profiling Argo floats since 2002 resolve sub-monthly to decadal variability in the top two kilometers of the ocean and in the recent years even deeper. Time-depth distributions of temperature, salinity and density (referenced to a pressure of 1000 dbar) observations from the sea surface to a depth of 2000 m averaged over 10-day intervals since 2002 are presented in Figure 14. Time series of temperature, salinity and density multiplatform (i.e., ship, float and mooring) observations at 1000 m and 1500 m depths and overaged over the intermediate layer (500-1850 m) before and after time bin averaging are shown in Figure 15. This figure also shows a side-by-side comparison of the heat content reductions that occurred in the top 1800 m layer over 19 consecutive cooling seasons, from 2002-2003 to 2020-2021, and the surface heat losses integrated over the periods of prevailed surface cooling, from 1986-1987 to 2020-2021.

The intermediate, deep and abyssal or bottom water masses found in the Labrador Sea are LSW, Northeast Atlantic Deep Water (NEADW, 2500-3000 m), and Denmark Strait Overflow Water (DSOW, defined as a 200 m thick bottommost layer at the water depths exceeding 3000 m). Similarly to DSOW, NEADW is also derived from the Iceland-Scotland Overflow Water, but undergoes a longer and more substantial mixing, transformation and modification along its path (Yashayaev and Dickson, 2008). While the temporal changes within NEADW are comparably slow, typically spanning a few decades, and appear to be vertically-uniform (note how NEADW salinity changed from 1975 to 2001 and from 2001 to present in Figure 10), both LSW and DSOW exhibit strong variations on decadal and shorter time scales.

The fact that the temporal changes in the core of NEADW are comparably small, slow, temporarily persistent and vertically uniform allowed the development of an objective method for

correcting systematic instrumental and methodological drifts and shifts during and between DFO and international. The dissolved oxygen, CFC-11 and CFC-12 concentrations, and the silicate, nitrate and phosphate concentrations used to construct Figures 11 and 12, respectively, include time-dependent corrections based on the multivariate analysis in the core of NEADW. The climatological normals of these variables on the AR7W line for the period of 1990-2019 (Figure 22) are also presented here for the first time.

Recurring warm and saline, and cold and fresh events spread in the upper 2000 m layer mainly occupied by LSW. In over 90 years of direct oceanographic observations (Figures 10 and 13, earlier years are not included in these figures), the intermediate, 200-2000 m, layer of the Labrador Sea experienced three periods of sustained multiyear cooling of the entire layer, reaching their coldest points in the 1950s, 1990s and 2010s, separated by two periods of warming. The first cooling event took place in the 1950s, followed by a warming and salinification trend through the early 1970s, bringing the sea to its record warm and saline state. Dismissing some relatively short cooling cycles, like the one centered over 1977-1978, the intermediate layer had been steadily cooling since then. This trend continued until 1994 as the layer reached its all-time cold point. The length, persistence and magnitude of this massive cooling radically altered the entire water structure and heat content of the sea. Indeed, the lowest sea-average temperature and salinity values were those achieved with cooling and freshening of LSW culminating in the late 1980s to mid-1990s. This period was characterized by deep winter convection that filled the upper 2000-2500 m layer of the Labrador Sea with cold, dense and relatively fresh water.

This predominantly steady warming trend, boosted by the sea recovering from its record deep convection, cold and dense state achieved in 1994, lasted until the second temperature record high in 2010 and 2011 in the upper (15-100 m) and intermediate (200-2000 m) layers, respectively.

The positive temperature and negative density trends established in the intermediate (200-2000 m) layer of the sea, and its upper (200-1000 m) and lower (1000-2000 m) sublayers, following the cessation of extreme convection in the mid-1990s were repeatedly interrupted by episodic moderately-deep winter mixing and cooling events, especially, in 2000, 2002 (Figure 10), 2008 and 2012 (Figures 10 and 14). Some of these events were strong (or powerful) enough to disrupt and even reverse the warming trend for a year or two, but none lasted long enough to alter the overall water-column temperature growth rate, which kept reestablishing itself after each severe winter event. The moderately-deep to deep convection of 2008, for instance, clearly evident in both the temperature and salinity fields and time series, was followed by much shallower convection in 2009, which depth was partly reduced because of massive surface freshening in the preceding summer and fall.

Similarly to the high-temperature high-salinity state that the intermediate (200-2000 m) layer of the Labrador Sea acquired in the second half of the 1960s to retain until the early 1970s, the warm and salty state reached by this layer in the early 2010s also did not last long. Similarly to the earlier two periods (in the 1950s and 1990s) of sustained cooling of the intermediate layer, the cooling that followed the second warming period (spanning 1994-2011) came as a direct result of persistently deepening winter convection during the time period of 2012-2018.

The upper (15-100 m) and intermediate-depth (200-2000 m) layers cooled during the periods of 2010-2018 and 2011-2017 reaching their 2002-2020 and 2001-2020 temperature lows in 2018 and 2017, respectively (Figure 13). Both layers then warmed in 2019, and slightly cooled in 2020. The recent (2019-2020) cessation of the multiyear cooling of the upper and intermediate layers, with very possible transition to warming in the coming years, is a direct consequence of

the 2019 cumulative winter surface heat loss being the lowest since 2013. Despite the winter NAO index and surface heat loss being high next year (2020), deep convection and water column cooling did not occur in 2020 as well. If the reason for the deep convection that occurred in 2018 was the water column preconditioning caused by convective mixing and intermediate layer cooling in the previous years, the situation was opposite in 2020. The lack of necessary preconditioning due to the reduced heat loss and shallowed convection in the winter of 2019 followed by the warming of the upper and intermediate layers of the Labrador Sea did not help with development of convection in the winter of 2020.

It should also be noted that temperature and salinity do not always follow similar patterns of interannual changes. In particular, while the intermediate layer of the Labrador Sea continued to cool until 2017, or even 2018, remaining nearly unchanged since then, the freshening of the newly-formed or newly-ventilated LSW occurring in 2012, 2014 and 2015 was followed by a salinity increase in 2017 after a short hiatus in 2016, leading by one or two years the cooling trend disruption and thus making the LSW formed in 2017 and 2018 the densest since the mid-1990s (owing to combined effects of cooling and salinity increase on density). Over the past three years, 2018-2020, the annually averaged intermediate layer salinity values experienced a downward trend (200-2000 m salinity; Figure 13), finally making this layer the freshest since 2002.

With respect to the upper 200 m layer, and particularly its uppermost half (15-100 m salinity; Figure 13) and quarter (50 m), the annually averaged 2012 and 2013 de-seasoned upper layer salinity values were the lowest since 2001. Following the 2013 low, the annual upper layer salinity values first increased to meet their 2006-2020 high in 2017, then reduced the next year, and remained nearly unchanged during the 2018-2020 period.

The mechanisms responsible for these warm-to-cold and cold-to-warm transitions in the Labrador Sea can be better understood by analyzing the winter NAO index and integrated over individual cooling seasons surface heat flux shown in Figure 13. As the region loses heat over each winter, the integrated heat flux is referred to as "cumulative heat loss", although the latter is opposite in sign to the former. Both winter NAO index and cumulative surface heat loss were low-pass filtered to evaluate the net contribution of both present and past atmospheric forcing, (e.g., NAO, wind stress and surface heat loss) values on the present oceanic heat content and convection depth. The weights of the respective low-pass filter were designed in such way that the oceanic conditions in any given year could be seen as a sum of responses on the atmospheric forcing in that year, weighted as 1.0, and in the four preceding years, weighted as 0.8, 0.6, 0.4 and 0.2 in the reversed time order. In other words, the weights of this filter are the highest at the locations matching its output data points, linearly reduce to zero over the preceding points and are zero at all subsequent points. The low-pass filtered series of the NAO index and cumulative surface heat loss produced using this data weighting scheme are shown in Figure 13 in front of the respective unfiltered series. From the process viewpoint, these filtered time series capture the combined effects of the present-year winter forcing and the thermal and convective conditioning of the water column partially retained from the previous years, hence convective preconditioning, on the present winter mixing and heat content in the Labrador Sea (e.g., convection depth and 200-2000 m average temperature shown in Figure 13).

The long-term changes in seawater temperature, salinity and density are complemented by the results of cleaning, correction and synthesis of chemical data presented in Figures 11 and 12. The three most prominent classes of LSW developed in the early 1990s, early 2000s and mid-2010s can be clearly identified in the temporal progression of annual dissolved oxygen profiles. The normalized dissolved oxygen indices for the intermediate, 200-2000 m, and deep, 2000-

2500 m, layers are now included in the Labrador Sea scorecard (Figure 27). The 2000-2500 m layer oxygen lags by a few years the intermediate layer values. Both CFC-11 and CFC-12 show a major increase in their concentrations in the mid-1990s (Figure 11), CFC-12 (CFC-11 was not sampled after 2011), similarly to dissolved oxygen, follows deepening of winter convection and the associated mixed layer during 2014-2018. The effect of winter convection in the Labrador Sea on uptake of the anthropogenic gases by the North Atlantic is discussed by Rhein et al. (2013).

The nitrate and phosphate concentrations, without any bulk cruise-by-cruise correction, exhibit strong uncorrelated year-to-year variations below 200 m (Figures A7) of undoubtedly instrumental, standardization or calibration nature as the ratio of these quantities is expected to remain relatively uniform within any deep water mass showing uniform distribution of physical properties. Such inconsistency in the sampled chemical properties disallows their analysis and interpretation in both subsurface and deep layers. Applying the time-dependent corrections apparently improved the situation with these nutrients, making the nutrient ratios more stable over time, and, for the first time, allowing to see a sensible signal correlated with the reported developments of winter convection in the Labrador Sea. Indeed, comparing the silicate, nitrate and phosphate trends in the 500-1000 m depth range in Figures 11 and A7, we note that the concentrations of these properties are significantly higher in 1990-1998 and 2014-2019 with respect to their long-term average values. The increased nutrient concentrations in these two periods are likely associated with the progressive deepening of vertical mixing during the periods of 1987-1994 and 2012-2018, when recurrent winter convection established a steady flux of nutrients from the nutrient-rich deep intermediate (1000-2000 m) and deep (2000-2500 m) layers to the nutrient-depleted upper intermediate (500-1000 m) and upper layers. Reversely, the nutrient concentration averaged over the deep intermediate layer tends to decline with developing of deep winter convection, signaling the downward flux of the upper waters.

THE RECENT DEVELOPMENT AND CESSATION OF RECURRING DEEP CONVECTION

As it was just reported for the intermediate layer (200-2000 m) of the Labrador Sea, its characteristic positive temperature and negative density trends that originated in the mid-1990s and went on for about two decades (Figures 10, 13, 14) were remarkably persistent resuming their general rates, with insignificant variations, soon after each interruption. These trends came to their final pre-reversal point in 2011 completing the most recent multiyear warming period. The general sea conditions in that year, including extremely limited extent of winter convection not exceeding 800 m in vertical mixing, were similar to those in the previous year, 2010. However, immediately after 2011, convection started picking up in response to the increased NAO index and surface heat loss in the following winter. Spreading over the most of the Labrador Basin and reaching and exceeding 1400 m in depth, the winter convection of 2012 had once again reversed the directions of interannual changes (except for 2013) and longer-term (more than five-year long) trends in both temperature and density from positive to negative and negative to positive, respectively. Mid-depth winter convection also occurred in 2013, but being mostly limited to the top 1000 m, it was not as deep, and the mixed layer was not as cold as in the previous year. However, this single-year rebound to milder winter conditions did not leave a noticeable trace in the subsequent hydrographic developments. The deepening of winter mixing and cooling of the intermediate layer that occurred in 2012 events were precursors of another set of sustained multiyear trends – positive in convection depth, negative in temperature and positive in density.

The situation changed again in the winter of 2014, when surface cooling triggered convective mixing, homogenizing the top 1600 m (and probably even deeper) layer in the central Labrador Sea. Deep convection has deepened progressively over each of the five consecutive winters – from 2014 to 2018. During this period, each convective development produced a colder denser and deeper LSW than the preceding event. As result, the convectively formed water mass, LSW, was getting colder and denser as convection kept getting deeper. Overall, the progressive cooling of the top 2000 m, and deep and intense winter mixing during the five consecutive winters of 2014-to-2018 (or seven, if starting with the cold winter of 2012) have irreversibly interrupted the general warming and stratification-building trend that has persisted in the intermediate waters of the Labrador Sea since the mid-1990s. Winter convection continuously progressed over this period, deepening and making the top 2000 m layer colder and denser with each successive cooling cycle. In the last of these winters, convection reached and exceeded the depth of 2000 m.

The persistent temperature (negative), density (positive) and convection depth (positive), trends spanning the 2011-2018 period (Figures 10, 13, 14) were brought by a multiyear recurrence of relatively strong, but not necessarily extreme, winter cooling, normally coinciding with moderate-to-high positive NAO. Specifically, when convective mixing events of comparable strengths recur in consecutive winters, the layer that gets repeatedly and persistently (systematically) cooled and homogenized by convection does not only get thicker and deeper with each event, but becomes more capable of retaining reduced vertical density gradients or weakened stratification of the intermediate layer for longer (e.g., until next winter convection). The ability of a semi-enclosed deep basin to partially retain density stratification imposed on it by a recurring convection leads to convective preconditioning discussed in the previous section from the standpoint of the atmospheric forcing. Therefore, the Labrador Sea thoroughly preconditioned by convective events of preceding winters is likely to experience further cooling and mixed-layer deepening even under a reduced winter-cooling scenario.

The 2018 winter situation offers a good and presently last example of how a preconditioning of a deep basin reservoir in preceding years may affect convection in a current year, further supporting the hypothesis by Yashayaev and Loder (2017). As in the previous two winters, in the winter of 2018, the subpolar North Atlantic basins lost considerably lesser amounts of heat to surface cooling than in the winter of 2015 (the latter demonstrated the highest cumulative surface heat loss in more than two decades). With the exception of the winter of 2019, the cumulative 2018 winter heat loss was also the lowest in the Labrador Sea since the winter of 2014. However, despite the continual reduction in winter cooling, the steady increase in the depth of winter convection since 2015 has resulted in the development of the most significant, in terms of volume, depth and density, class of LSW since 1994.

So far we looked at all most significant developments of winter convection in the Labrador Sea with all annual means in view and without analyzing how a certain event or a group of events progressed during their respective cooling seasons. This approach is suitable for analyzing and understanding long-term variability, decadal and multidecadal convective cycles and trends. However, in order to reveal and diagnose long-term water-column preconditioning situations such as the one presented in the previous paragraph, continuous year-round measurements of temperature and salinity measurements are required. Indeed, even though the successive deepening of winter mixing during the 2012-2018 period is distinctly obvious in the longer-term compilations of annual mean values (Figures 10 and 13), its true origin as well as vertical and temporal developments can only be fully mapped and analyzed using quality-controlled high-resolution vertical temperature, salinity and density profiles averaged in 10-day long overlapping temporal bins (e.g., with 50% overlap, i.e., with a 5-day increment) from all available profiling

float and research vessel observations, and presented in Figure 14 (2002-2020). This figure depicts the temporal progression of the 10-day composite seawater property profiles, effectively capturing the progressive development of convective mixing responsible for the production of the most recent voluminous LSW class, and the subsequent cessation and reversal of this development. In particular, Figure 14 shows that the winter mixed layer and hence convection in the central Labrador Sea reached and even exceeded 2000 m in March of 2018, ending the sustained positive trend in convection depth spanning the winters of 2012 and 2018 except for 2013. The last three winters in this sequence have demonstrated that certain extreme properties, such as low temperature, weak vertical stability and weak overall stratification, imposed on the water column by a stronger-than-usual convective mixing in the previous years, may assist further development of deep convection. The cold dense vintages of new LSW continued reaching deeper and deeper annually (Figure 14) until 2019 – the year when this trend reversed. Each of the freshly-made deepened and densified LSW vintages was in part preserved in the deep basin until the next winter. This figure also illustrates the essence of water column preconditioning by winter convection – retaining or "memorizing" the previous year conditions throughout the intermediate depths (200-2000 m) in the region where deep convection is expected to occur. The last two years, 2019 and 2020, added to the record enrich our understanding of switchovers between recurrent intensification and relaxation of winter convection in the Labrador Sea.

Focusing on the changes at the intermediate depths (500-1850 m, the layer that captures the subpolar climate signal transmitted to the other North Atlantic basins) and their causes, the processed and vertically interpolated ship (the central Labrador Sea), Argo float (the central Labrador Sea) and Hamilton Bank mooring (the upper Labrador slope near-bottom, ~1000 m) measurements of temperature, salinity and density are shown in Figure 15 for two depths, 1000 m and 1500 m (upper panel), and for the intermediate, 500-1850 m, depth layer (lower panel). In addition to the winter NAO index and the net surface heat flux integrated over individually-defined continuous periods with the cumulative heat flux being exclusively directed from sea to air, i.e., heat loss, from 1986-1987 to 2020-2021, previously shown in Figure 13, Figure 15 adds another dimension to the atmospheric forcing – oceanic response analysis, that is the amount of heat lost by the water column of the central Labrador Sea over each individually-defined water column cooling period. The water column heat content losses were computed for all individual cooling seasons from 2002-2003 to 2020-2021, i.e., mostly owing to the Argo float data. A high correlation (R~0.88) of the cumulative surface heat loss and the seasonal ocean cooling means that the wintertime atmospheric forcing is the lead driver of the oceanic heat content changes in the region (responding on key changes in the atmospheric dynamics), which can be predicted as far ahead in time as a reliable atmospheric forecast can possibly reach.

The central Labrador Sea shipboard and float observations are indicated in the upper panel of Figure 15 with dots, while the annually averaged values are connected with grey lines placed in the background. The actual observations at the two chosen depths shown in this panel provide a clear view of the depth-selectivity of winter convection during the Argo period, 2002-2021, supporting our earlier statements (e.g., Figure 14). In particular, the vertical mixing reached 1000 m in 13 winters out of 20, cooling this level throughout most of the domain. The frequency of major (spanning the domain) convective occurrences reduces by almost a half just 500 m deeper – 1500 m was reached by winter convection only in 7 cases, or in 35% of all winters with sufficient number of Argo float profiles. 6 out of these 7 cases fall on the past 7 years, while only once winter convection reached the depth of 1500 m during the 2002-2013 time period, which was in 2008 (Yashayaev and Loder, 2009).

The phenomenon of convective preconditioning discussed earlier is complemented by the actual observations shown in Figure 15 (upper panel). Following the temporal changes in the temperature and density values observed at 1000 m one should notice that the cooling and respective density increase in some winters (e.g., 2012, 2014-2016) were not fully compensated by subsequent warming and density decrease during the post-convection restratification periods. This means that at the start of the next winters the water at the same depth was colder and denser than a year ago. These residual cooling and densification preconditioned the layer making a deeper penetration of winter convection more likely with an even lesser surface heat loss than before as a lesser cooling would be required to overcome the underlying density barrier.

The cumulative winter heat loss was in 2019 only slightly lower in magnitude than in the previous year. However, despite the comparable surface heat losses, convection in the winter of 2019 was much weaker and shallower than in the winter of 2018, breaking the tendency of recurrent convective deepening that was on for the straight five preceding years. This situation helps with both understanding and forecasting of the degree to which a current winter convection is likely to be facilitated/enforced/empowered/enhanced by the water column preconditioning, e.g., through weakening of the vertical density stratification, by convective mixing of the preceding winters. This statement gets further supported and strengthened with the observations of winter atmospheric conditions and Labrador Sea convection in 2020, i.e., in the reporting year. The 2020 winter NAO index reached one of its historic highs, and the surface heat losses were greater than those in 2018. Nevertheless, the 2020 winter convection, even though slightly deeper than in the previous year, was at least 400 m shallower than in 2018, and the main factor making the two outcomes so different is the amount of preconditioning.

Overall, the switchovers from progressive deepening to shallowing of winter convection also add to our understanding of the recurrent nature of deep convection and its similarity with a typical stochastically-forced climate system, i.e., containing a memory of past states. These critical switchover points mark the moments when the past-winter preconditioning of the water column loses its significance for development of convection in present and future winters. Indeed, while convection continued to exceed 1500 m and even deepen over the three years first after the surface heat losses started to decline (since the winter of 2015), it happened only on the fourth year when the intensity and depth of winter convection picked the trend in the surface heat loss. It was not the first time when a deep-water preconditioning had a prolonged effect on convection in the Labrador Sea. A similar situation was observed in the 1987-1996 time period. Despite a decline in atmospheric forcing from the previous winter, the Labrador Sea experienced deep convection (>2000 m) in the winter of 1995, whereas there was no deep convection observed in the same basin in the following winter (1996).

Further, we compare the seasonal and interannual signals in the central region of the Labrador Sea and over its western continental slope, this time including temperature measurements from the Labrador slope mooring. The near-bottom (~1000 m) temperature measurements at the Hamilton Bank mooring location (Figure 1) show a pattern of interannual variability strikingly similar to the changes at 1000 m in the central Labrador Sea (Figure 15, upper panel; unlike the shipboard and float observations the mooring data values shown in this figure were obtained by low-pass filtering the original series) implying that either the changes in winter forcing extend far beyond the central region changing gyre circulation and, thereby, orientation of isothermal surfaces, or when the convective processes, when intensified "deform" the peripheral zone of the Labrador Sea changing the relative contributions of warmer saltier and colder fresher waters in the boundary flow (the Hamilton Bank mooring is aligned with the Deep Labrador Current). The other important phenomenon of the bottom layer at the 1000 m isobath is the presence of

strong seasonal variations in all years regardless of the strengths of winter cooling and convection. The average amplitude of the seasonal changes at this location is much higher than at the same depth in the central Labrador Sea. Both of these Hamilton Bank phenomena, high coherence with the central region on the interannual scales and, strong and persistent seasonality, are yet to be explained!

The lower panel in Figure 15 further support the point made with more recent measurements concerning the similarity of interannual variability at the intermediate depths across the entire sea (the observations over the Greenland Slope were studied separately). In this case the low-pass filtered Hamilton Bank 1000 m temperature series is compared with temperature, salinity and density averaged over the 500-1850 m depth range (the intermediate layer) and then annually. The Hamilton Bank mooring series starts in the first year with available data, 1979, and the position of this mooring and its design changed a few times over the past four decades, yet the long-term cycles depicted from both mooring and hydrographic data look similar across the sea.

In addition to surface heat flux, another factor that could potentially change convection is surface freshening due to accelerated melting of the Greenland Ice Sheet. However, a recent study by Dukhovskoy et al. (2019) indicates that the effect of the Greenland freshwater flux anomaly brought by the observed acceleration of Greenland Ice Sheet melt is not sufficient to fully explain the present changes in water column salinity and convective activity. In fact, there is no significant negative trend present in surface salinity in the Labrador Basin in the last decade.

CLIMATOLOGICAL NORMALS AND TRENDS OF OCEANOGRAPHIC CHARACTERISTICS ON THE AR7W LINE

This section presents vertical sections of the key seawater properties (temperature, salinity, density) on the AR7W repeat hydrography in some years of interest (e.g., high and low convection years) and the results of synthesis of all international occupations of AR7W conducted during the period of 1990-2020, including climatological normals, decadal anomalies and multidecadal trends. The recent changes in the Labrador Sea convection, discussed in this report earlier, are now shown in their full extent across the entire basin.

Distance-depth plots of temperature, salinity, density and oxygen from the survey data in 1994, 2008, 2011, 2012, 2015, 2018, 2019 and 2020 are presented in Figures 16, 17, 18. An extensive reservoir filled with a newly ventilated, 2000 m deep, cold, dense, fresh, atmospheric gas loaded vintage of LSW is clearly evident in the AR7W seawater property section based on the 2018 May shipboard CTD data. The 2018 vintage of LSW is associated with low temperature (< 3.3°C) and low salinity (< 34.86) between 1000 and 2000 m. The winter convection in the recent time period, 2015-2018, especially in the winter of 2018, is arguably the deepest since the record-deep cooling that reached 2400 m in the winter of 1994. The LSW year class is one of the largest ever observed outside of the early 1990s.

The sections plots (Figures 16, 17, 18) further confirm that winter convection lost its strength in the winter of 2019, reaching the depth of 1400-1500 m in the western part of the Labrador Basin, and only about 1000 m in the central and eastern parts. In the following year (2020) convection slightly intensified, being able to reach 1600 m, still affecting the distributions of freshwater (salinity) and gases (dissolved oxygen) in the intermediate layer across the Labrador Sea, but not as deep as in the years preceding 2019.

Combining oceanographic data from all occupations of the Atlantic Repeat hydrography line 7-West (AR7W) carried by both DFO and international institutes a set of annual seawater property

sections was constructed for the entire period of observations, 1990-2020. The AR7W spatially-gridded annual composite section collections were averaged to obtain full 31-year climatological normals for the key seawater properties (or oceanographic variables), including temperature, salinity and density, presented in Figure 20, and dissolved oxygen, silicate, phosphate and nitrate. The rate of change (linear trend slope) over the 1990-2020 period and contribution of the trend to the total variance are also shown in in Figure 20. The trends largest in both magnitude and their contribution to the total variance of temperature and salinity spread across the basin within the depth range of 1500-2200 m. The origin of these phenomenal trends is related to the extremely strong and deep convection spanning the early 1990s that produced large volumes of record cold fresh and dense water successively filling the lower part of the deep intermediate layer across the Labrador Sea and eventually the subpolar North Atlantic. Even though during the period of 2014-2018 moderately-deep to deep convection penetrated to the depth of 2000 m, if not deeper, the effect of the latter was not the same as of the convection at the beginning of the studied 31-year long period. The recent convective event although fairly deep was not able to produce a water mass as cold fresh and dense as the most voluminous coldest freshest and densest LSW class in the entire observational record.

The pattern seen in the 1990-2020 density trend in the intermediate layer (200-2000 m), namely, a uniform negative trend, reveals the dominance of the contribution of long-term temperature changes to density over the contribution of salinity changes (Figure 20, right column). However, the deeper waters (2200-3200 m), e.g., NEADW, feature density increase on constant pressure (depth) levels (surfaces) during the same period.

Annual anomalies of all studied variables were computed with respect to their climatological normals (Figure 20, upper row) at each point of the AR7W line. The annual anomalies were analyzed individually, and were also grouped and averaged over all pentads and decades covered by the period of observations on the AR7W line. In particular, Figure 21 presents decadal anomalies of temperature, salinity and density on the line with AR7W computed in such way. The decadal anomalies support and strengthen our interpretation of the linear trends presented here earlier. The decade of the 1990s is characterized by low average temperatures and salinities and high average densities over the entire 50-2000 m layer. Following the cessation of the extremely deep convection of the 1990s, the sea began to accumulate heat and salt in this layer, which clearly shows in the respective anomalies averaged over each of the two first decades of the current century. Indeed, the winters in the 2000s were generally milder than the winters of the first half of the 1990s, resulting in more limited amounts of shallower LSW produced, which, along with the disconnected from the atmosphere and the upper ocean layer, and irreversibly aging deep dense LSW (Yashayaev, 2007a), have gradually become warmer, saltier, and less dense than in the previous decade (Figure 21). Even though the regional winter convection intensified, cooling the intermediate layer of the Labrador Sea and recurrently replenishing it with newly formed LSW through most of the 2010s, when comparing the multiyear average state conditions of the three decades, the decade of the 2010s still shows much warmer, saltier and less dense than the decade of the 1990s, and even somewhat warmer and saltier than the decade of the 2000s. A closer look at the processes that played essential roles in forming these anomalies is given earlier in the report.

NUMERICAL MODEL RESULTS

In this report, an ocean model hindcast from the Bedford Institute of Oceanography North Atlantic Model (BNAM, Brickman et al., 2016; Wang et al., 2016; Brickman et al., 2018; Wang et al., 2018) is used to report changes of the Labrador Current and the Atlantic meridional overturning circulation (AMOC).

The BNAM is based on the NEMO 2.3 (Nucleus for European Modelling of the Ocean) model. It includes an ocean component OPA and a sea ice module LIM (Louvain-la-Neuve Sea Ice Model). Its domain was selected to include the North Atlantic Ocean (7ºN – 75ºN and 100ºW – 25ºE) with a nominal resolution of 1/12º. The model has a maximum of 50 levels in the vertical, with level thickness increasing from 1 m at the surface to 200 m at a depth of 1250 m and reaching the maximum value of 460 m at the bottom of the deep basins. The maximum depth represented in the model is 5730 m.

Open boundary data are from the GLORYS reanalysis product (Global Ocean ReanalYses and Simulations). The model surface forcing is taken from a combination of CORE (Coordinated Ocean-ice Reference Experiments) and NCEP/NCAR reanalysis forcing. Model forcing variables include air temperature, wind velocities and humidity; daily short- and long-wave radiation, and total precipitation (rain plus snow). No surface restoring to sea surface temperature is applied. However, the model's sea surface salinity is restored to its monthly climatology with a 60-day restoring time scale.

The model was spun-up for 10 years using the CORE normal year forcing. The 10-year spin-up simulation is initialized with a January climatology of temperature and salinity (T-S). The T-S climatology combines the Polar Science Center Hydrographic Climatology (PHC2.1) at high latitudes with the T-S climatology of WOA5 at middle and low latitudes.

The hindcast period is from 1990 to 2020. The barotropic transport is used to represent the strength of the Labrador current. Wang et al. [2016] discovered that the Labrador Current on the shelf break can be partitioned into two portions, and we report the changes of the two branches as well. For the purposes of the present report the transports were calculated based on modelled flows through the western segment of the AR7W transect.

The AMOC is a climatically important circulation, and it can impact climate at both local and global scales. The BNAM has a decent skill in representing the AMOC (Wang et al., 2019), which allows us to use BNAM to present the variations of the AMOC in this report.

VARIATIONS OF THE LABRADOR CURRENT

The variations of the Labrador Current (LC) can be seen as an indicator for the changes in the subpolar North Atlantic circulation. The variations of the LC are often connected to the variations of the AMOC. Here we present the variations of barotropic transports of the LC.

An EOF analysis of the model output by Wang et al. (2016) presented in Figure 23 suggests that the variability in the Labrador Current can be partitioned into a western Labrador Current (WLC; from the 300-2500 m isobaths), and an eastern Labrador Current (ELC; from the 2500-3300 m isobaths). Following the definition of the WLC and ELC, we calculated the transports of ELC and WLC, and also those of the LC (the summation of the ECL and WLC).

The averaged transport over the 1990-2019 period is 45.3 Sv for LC, 19.6 Sv for WLC, 25.7 Sv for ELC. Figure 24 shows the transport anomalies for the LC, ELC and WLC. The WLC in 2020 was ~0.5 Sv weaker than in 2019, about 1.6 Sv above the 1990-2020 mean, as it has been since 2002

A declining trend of the ELC began in 1996, coinciding with a significant drop in the winter NAO index in the same year. The trend reversed in 2014, and the ELC was ~0.3 Sv weaker in 2020 than in 2018, and it became 0.4 Sv below the 1990-2020 average.

VARIATIONS OF THE ATLANTIC MERIDIONAL OVERTURNING CIRCULATION

The AMOC can be analyzed in two coordinate systems. In the first coordinate system, the AMOC is sliced by the isobaric surfaces (constant pressure or depth levels) and is consequently projected onto the vertical or depth axis, while in the other approach, the AMOC, mapped on the isopycnic (constant density) surfaces, is projected onto the density axis (Wang et al., 2019). The AMOC reported here is calculated in the depth space. Wang et al. [2019] investigated the variability of the AMOC from the BNAM solution by using EOF approach. Their study proposed the AMOC PC1 as the AMOC index. The AMOC PC1 was found to be representative of the general low frequency changes of the AMOC, and a general weakening trend was found in the 1990-2015 period. The AMOC PC2 represented the wind-driven Ekman transport portion of the AMOC, which has high frequency variability and has no obvious trend.

Figure 25 shows a time-latitude plot of the variations of the AMOC from 10°N to 60°N using the monthly mean output from 1990 to 2020, and the seasonal cycle was removed in this calculation A general weakening tendency can be seen in Figure 26. Following the approach in Wang et al. [2019], we applied the EOF approach to the annual mean (de-seasoned) AMOC to compute the EOF patterns and their associated PCs. The EOF1 represents 75% of the total variance, and the EOF2 represents 10%. The EOF patterns are consistent with those in Wang et al. [2019]. The AMOC PC1 clearly shows the continuing weakening trend after 2011. No clear trend is shown in the Ekman portion of the AMOC shown in the AMOC PC2. The Labrador Current had been strengthening in recent years until 2020 when it was weaker than that in 2019, as shown above, and the AMOC solution from BNAM still presents the existing weakening trend. The weakening trend of the AMOC in recent years is consistent with Smeed et al. [2018], who used observational data of the AMOC from the RAPID line at 26°N and other observations in their study. The AMOC PC1 shows that the 2019 AMOC is the weakest in the 1990-2019 period, and in 2020, the AMOC strengthened, though it was still in its weak regime.

SUMMARY

The DFO-led annual oceanographic survey of the Labrador Sea provides observations of variability in the key ocean climate and ventilation variables. The changes observed in the region are closely linked to the dynamics of the planetary climate system as a whole and affect the regional climate and ecosystems off Atlantic Canada. In July-August of 2020, the AR7W line was occupied by the Bedford Institute of Oceanography for the 33rd time since 1990. Additionally, the network of profiling Argo floats providing temperature and salinity data in the upper 2000 m layer of the ocean in real-time was used to monitor year-round variability of the oceanographic conditions in the Labrador Sea and make more accurate estimates of annual state variables not only at the intermediate depths, but in the upper layer, which would be unachievable with shipboard data alone. The Argo float profiles are also used to construct virtual oceanographic transects (e.g., AR7W) allowing to compensate for any omission in annual survey sequences (as, for example, happened in 2017 and 2021). Overall, the syntheses of the shipboard and Argo float observations presented in this report offers a DFO client an in-depth diagnosis and assessment of coast-to-coast full-depth environmental conditions in one of the most critical locations of the world ocean, which are essential in both operational forecast and climate prediction.

BNAM model results were used to present changes in the Labrador Current (shelf break segment) and the AMOC.

Key characteristics of the past and recent environmental conditions in the Labrador Sea are summarized in the scorecard shown in Figure 27, and are listed below:

1. While the winter (Dec–Mar) NAO index in 2020 was above-normal and the highest since 2015, the sea level pressure pattern was not associated with strong westerly winds along the Labrador coast. This led to, respectively, near-normal and above-normal winter and spring air temperatures in the Labrador Basin domain. Both winter and spring sea surface temperatures in the Labrador Basin were above-normal.

2. Winter sea ice extent was below-normal in the Davis Strait, Northern Labrador Shelf and Labrador Shelf regions. Spring sea ice extent was also below-normal in all three regions.

3. In the Labrador Basin (the deep central part of the Labrador Sea), surface heat losses in winter result in the formation of dense waters, which consequently spread across the ocean ventilating its deep layers and essentially driving the global ocean overturning circulation. In the winter of 2015, the Labrador Sea incurred the highest heat loss in more than two decades. However, the four following winters showed a significant reduction in the respective net surface heat losses, which remained above-normal in 2016 and 2017, but then declined to near-normal in 2018, and remained near-normal in both 2019 and 2020.

4. In the Labrador Basin, the 2020 average temperatures with subtracted climatological seasonal cycle remained above-normal for the second year in a row in the 15-100 m layer, and near-normal for the fifth straight year in the 200-2000 m layer, essentially ending, if not reversing the negative temperature trends seen in these layers since 2010 and 2011, respectively. The preceding cooling of the deeper layer was mainly caused by deepening of winter convection, while the ongoing stabilization of the 200-2000 m layer heat content and its possible increase owe to the facts that because of reduced surface cooling the 2019 winter convection was notably shallower than in the previous years, and that prior to the winter of 2020, the water column was not preconditioned well enough for the 2020 convection to develop to a greater depth.

5. Despite the persistent decline in the surface cooling since 2015, the water column preconditioned by a series of deep convection events eased the formation of a new Labrador Sea Water (LSW) that is seen as the most significant, in terms of volume and depth, since the mid-1990s. However, this tendency in LSW formation changed over the past two years, 2019 and 2020.

6. During the winter of 2020, Labrador Sea convection reached as deep as 1600 m and possibly deeper, exceeding the depths of convective mixing observed in 2019 by at least 100 m. The deepening of convection and slight cooling of the deep mixed layer in 2020 concur with the reported increases in the North Atlantic Oscillation index and net surface cooling relative to the previous winter. However, despite a high winter NAO index (the highest since 2015), the 2020 winter mixing depths were much shallower than during the entire period of 2015-2018, by the end of which winter convection reached and possibly exceeded 2000 m, making it the deepest since record-deep 2500 m convection in 1994. Therefore, we regard the LSW year class developed during the pentad preceding 2019 as one of the largest LSW classes formed outside of the first pentad of the 1990s. This recent progressive development of convection declined in 2019, featuring patchy and irregular winter mixing to the depths ranging from 1000 to 1500 m. Convection reached 100 m or so deeper in the following year (2020), while remaining shallower than in 2018. However, with the 2019 and 2020 winter convection depths showing as near-normal, these years continued to add to gas (dissolved oxygen, anthropogenic gases, and carbon dioxide) uptake and consequently respective gas concentrations in the Labrador Sea in the upper 1500 m layer.

7. Model results suggest that the transport of the Labrador Current decreased between 1995 and 2014, but since then increased slightly until 2020, and the current weakened in 2020.

A weakening trend of the AMOC since mid-1990s is obtained in this model hindcast. Using PC1 of the AMOC as an AMOC strength index, the BNAM solution shows that weak AMOC has been consistent for the years after early 2000s, and the weakest AMOC was in 2019. It started to strengthen in 2020, though the Labrador Current weakened in this year.

ACKNOWLEDGEMENTS

APPENDIX 1: SEASONAL CYCLE AS A SOURCE OF ERROR IN OCEAN STATE ASSESSMENTS

Figures A1-A5 show the regular seasonal cycles of temperature and salinity (A1), the associated seasonal changes encountered in 30 days (A2) and seasonal changes measured from May 15 (A3), standard deviations of anomalies in 10-day bins (A4) and contributions of the seasonal cycles to the total variances (A5). The estimates included in these figures are based on iterative evaluation of seasonal cycle using irregular data analysis routines (Yashayaev and Zveryaev, 2001). The seasonal warming that occurs over a 30-day May period, coinciding with May, is much larger than the standard deviation of temperature anomalies, meaning that the seasonally-imposed scatter would be large, if a time series was constructed for the upper 100 m layer without applying a seasonal correction. Furthermore, the trend in survey date would lead to a systematic seasonal bias in a long time series forming an artificial trend, if the seasonal was not properly removed from the observations.

APPENDIX 2: CONSTRUCTING DISSOLVED OXYGEN, CFC-11, CFC-12, SILICATE, NITRATE AND PHOSPHATE ANNUAL COMPOSITE PROFILES

Extensive quality control and data outlier detection and cleaning were routinely performed on all vertical profiles of the named chemical components comprising original measurements. The cleaned (despiked) chemical measurements were then, one by one, vertically interpolated over the entire depth range, on condition that at least one accepted measurement is present within a certain depth range on the either side of a given grid point, this allows for some vertical profiles not being completely filled with interpolated values. The distance range restricting the size of allowable vertical gaps in initial measurements depends on a type of observed variable (e.g., physical, chemical, biochemical), location and depth. Respectively, the maximum vertical distance between two adjacent measurements allowing vertical interpolate on the segment of a vertical profile between these points is expressed as a function of analyzed variable, geographic location and depth. This function, organized as a Matlab script, is available from Dr. Yashayaev.

To construct a composite vertical profile based on all profiles selected in a given (e.g., annual) survey within the boundaries of the central Labrador Sea, three approaches to spatial averaging of oceanographic data were followed and their results compared. These averaging techniques, their combinations and hybrids are also discussed in the chapter introducing the syntheses of the research ship and profiling float data within a spatial domain or along a vertical section.

The first type of averaging is isobaric averaging. It allows to produce a composite profile without importing any additional external information to the selected vertical profiles before averaging these profiles at respective vertical (pressure or depth) grid points. However, this approach does not account for vertical displacement in the important water masses and may produce properties substantially differing from those in the original profiles.

The second type of averaging of vertical profiles is isopycnic averaging (used in most cases when the shipboard observations are involved). It requires merging the high-resolution high-accuracy CTD profiles with the vertically interpolated chemical property profiles, which allows interpolation on density surfaces or along density contours. This method was mainly used to construct the annual composite profiles included in both Figures 11 and 12, and Figures A6 and A7.

The third type is used exclusively for interpolation along the seafloor. It is mainly used in addition to one of the first two interpolation techniques. The results of two methods (the third one bound with either first or second) were blended together to achieve the best representation of important oceanographic features.

The resulting annual composite profiles were then merged together to analyze temporal evolutions of the studied variables. Figures A6 and A7 show annual composite profiles of dissolved oxygen, CFC-11, CFC-12, silicate, nitrate and phosphate concentrations in the central region of the Labrador Sea for the depth range of 200-3500 m and the time period of 1990-2019. From an examination of these figures, it becomes obvious that the chemical measurements are subject to significant cruise-to-cruise variations, either in form of an abrupt jump or a drift. Such jumps and drifts in the annual values are particularly strong in the nitrate and phosphate concentrations, and make identification of Labrador Sea Water, Northeast Atlantic Deep Water and Denmark Strait Overflow Water, and analysis of temporal variability in these water masses impossible. Furthermore, the large uncorrelated interannual exertions of different nutrient components contradict the earlier repeatedly reported constancy or temporal stability or persistence of the nutrient ratios in water masses. Therefore, time-dependent corrections are required for achieving at least marginal progress in utilization of the chemical variables, especially nutrients, in the Labrador Sea oceanography. The steps of obtaining these corrections are outlined in the report. Figures 11 and 12 were constructed with the time-dependent corrections applied to the respective chemical measurements in addition to (and actually before) the data processing steps outlined above, data quality assessment and overall cruise-to-cruise performance check.

The time-dependent corrections constructed and applied individually to each variable improved temporal stability of the nutrient ratios.

APPENDIX 3: THE CALCULATION OF AMOC

The AMOC is defined by:

$$\Psi(z) = \int\limits_{x_w}^{x_e} \int\limits_{-H}^{z} v(x,z)dzdx,$$

where x_w and x_e denotes the western and eastern boundaries, respectively. H denotes the bottom depth. z denotes the vertical coordinate. $v(x,z)$ is the meridional velocity at vertical location z.

REFERENCES

Bindoff, N. L., Willebrand, J., Artale, V., Cazenave, A., Gregory, J., Gulev, S., Hanawa, K., Le Quéré, C., Levitus, S., Nojiri, Y., Shum, C. K., Talley, L. D. and Unnikrishnan A. 2007. Chapter 5. Observations: Oceanic Climate Change and Sea Level, Climate Change 2007: The Physical Science Basis, Contribution of Working Group I to the Fourth Assessment Report of the Intergovernmental Panel on Climate Change, [Solomon, S., D. Qin, M. Manning, Z. Chen, M. Marquis, K.B. Averyt, M. Tignor and H.L. Miller (eds.)], Cambridge University Press, Cambridge, United Kingdom and New York, NY, USA.

Barnston, A. G., and Livezey, R. E. 1987. Classification, seasonality and persistence of low-frequency atmospheric circulation patterns. Mon. Wea. Rev., 115, 1083-1126.

Brickman, D., Wang, Z., and Detracy, B. 2016. Variability of Current Streams in Atlantic Canadian Waters: A Model Study. Atmosphere-Ocean, 54:3, 218-229, DOI: 10.1080/07055900.2015.1094026

Brickman, D., Hebert, D., and Wang, Z. 2018. Mechanism for the recent ocean warming events on the Scotian Shelf of eastern Canada. Cont. Shelf Res. 156, 11-22 https://doi.org/10.1016/j.csr.2018.01.001.

Castelao, R. M., Luo, H., Oliver, H., Rennermalm, A. K., Tedesco, M., Bracco, A., Yager, P. L., Mote, T. L., & Medeiros, P. M. (2019). Controls on the transport of meltwater from the southern Greenland ice sheet in the Labrador Sea. *Journal of Geophysical Research: Oceans*, **124**, 3551– 3560. https://doi.org/10.1029/2019JC015159.

Cavalieri, D. J., Parkinson, C.L., Gloersen, P., and Zwally, H.J. 1996. updated yearly. *Sea Ice Concentrations from Nimbus-7 SMMR and DMSP SSM/I-SSMIS Passive Microwave Data, Version 1*. [north/monthly]. Boulder, Colorado USA. NASA National Snow and Ice Data Center Distributed Active Archive Center. doi: https://doi.org/10.5067/8GQ8LZQVL0VL. [Accessed 08 Mar 2021]

Curry, R., R.R. Dickson, and I. Yashayaev, 2003. A change in the freshwater balance of the Atlantic Ocean over the past four decades, Nature, 426, 826 – 829.

Cyr, F., Colbourne, E., Galbraith, P.S., Gibb, O., Snook, S., Bishop, C., Chen, N., Han, G., and D. Senciall. 2021. Physical Oceanographic Conditions on the Newfoundland and Labrador Shelf during 2019. DFO Can. Sci. Advis. Sec. Res. Doc. 2021/xx + xx p.

DFO, 2020. Oceanographic conditions in the Atlantic zone in 2019. DFO Can. Sci. Advis . Sec. Sci. Advis. Rep. 2020/028.

Dickson, R.R., I. Yashayaev, J. Meincke, W.R. Turrell, S.R. Dye, and J. Holfort, 2002. Rapid freshening of the deep North Atlantic Ocean over the past four decades. Nature, 416, 832–837.

Dickson, R.R., Meincke, J., and Rhines, P. (Eds.). 2008. Arctic-Subarctic Ocean Fluxes: Defining the Role of the Northern Seas in Climate. 2008, Springer Science & Business Media, March 4, 2008, 736 pages.

Dukhovskoy D. S., I. Yashayaev, A. Proshutinsky, J. L. Bamber, I. L. Bashmachnikov, E. P. Chassignet, C. M. Lee and A. J. Tedstone, 2019, Role of Greenland Freshwater Anomaly in the Recent Freshening of the Subpolar North Atlantic, Journal of Geophysical Research: Oceans, Volume 124, Issue 5, Pages 3333-3360, https://doi.org/10.1029/2018JC014686.

Fetterer, F., Knowles, K., Meier, W. and Savoie, M. 2002. Updated 2011. Sea ice index. Boulder, CO: National Snow and Ice Data Center. Digital media.

Fragoso, G.M., Poulton, A.J., Yashayaev, I., Head, E.J.H., Stinchcombe, M., and Purdie, D.A. 2016. Biogeographical patterns and environmental controls of phytoplankton communities from contrasting hydrographical zones of the Labrador Sea, Progress in Oceanography, V.141, 212–226.

Fröb, F., Olsen, A., Våge, K., Moore, K., Yashayaev, I., Jeansson, E., and Rajasakaren, B. 2016. Irminger Sea deep convection injects oxygen and anthropogenic carbon to the ocean interior, Nature Communications, 13244, doi: 10.1038/ncomms13244.

González-Pola, C., Larsen, K. M. H., Fratantoni, P., and Beszczynska-Möller, A. (Eds.). 2020. ICES Report on Ocean Climate 2019. ICES Cooperative Research Reports No. 350. 136 pp. https://doi.org/10.17895/ices.pub.7537.

Hauser, T., Demirov, E., Zhu, J., and Yashayaev, I. 2015. North Atlantic atmospheric and ocean inter-annual variability over the past fifty years – Dominant patterns and decadal shifts. Progress in Oceanography, Volume 132, March 2015, Pages 197–219.

Holliday, N.P., Bersch, M., Berx, B. et al. Ocean circulation causes the largest freshening event for 120 years in eastern subpolar North Atlantic. Nature Communications 11, 585 (2020). https://doi.org/10.1038/s41467-020-14474-y.

Hurrell, J.W. 1995. Decadal trends in the North Atlantic Oscillation: Regional temperatures and precipitation. Science, 269, 676-679.

Hurrell, J. W. and National Center for Atmospheric Research Staff Eds. (Last modified 04 Aug 2018), "The Climate Data Guide: Hurrell North Atlantic Oscillation (NAO) Index (station-based)." Retrieved from https://climatedataguide.ucar.edu/climate-data/hurrell-north-atlantic-oscillation-nao-index-station-based.

Kalnay, E., Kanamitsu, M., Kistler, R., Collins, W., Deaven, D., Gandin, L., Iredell, M., Saha, S., White, G., Woollen, J., Zhu, Y., Chelliah, M., Ebisuzaki, W., Higgins, W., Janowiak, J., Mo, K.C., Ropelewski, C., Wang, J., Leetmaa, A., Reynolds, R., Jenne, R., and Joseph, D. 1996. The NCEP/NCAR 40-Year Reanalysis Project., Bull. Amer. Meteor. Soc., 77, No. 3, 437-470.

Kieke, D., and Yashayaev, I. 2015. Studies of Labrador Sea Water formation and variability in the subpolar North Atlantic in the light of international partnership and collaboration, Progress in Oceanography, doi:10.1016/j.pocean.2014.12.010.

Lazier, J. R. N., Hendry, R. M., Clarke, R. A., Yashayaev, I., and Rhines, P. 2002. Convection and restratification in the Labrador Sea, 1990– 2000, Deep Sea Res., Part A, 49, 1819–1835. https://doi.org/10.1016/S0967 - 0637(02)00064 - X

Lozier, M.S., et al., 2019. A sea change in our view of overturning in the subpolar North Atlantic, Science, Vol. 363, Issue 6426, pp. 516-521, DOI: 10.1126/science.aau6592.

Luo, H., Castelao, R., Rennermalm, A., Tedesco, M., Bracco, A., Yager, P. L., Mote, T. L. 2016. Oceanic transport of surface meltwater from the southern Greenland ice sheet. *Nature Geosci* **9,** 528–532. https://doi.org/10.1038/ngeo2708.

Meier, W. N., Fetterer, F., and Windnagel, A. K. 2017. *Near-Real-Time NOAA/NSIDC Climate Data Record of Passive Microwave Sea Ice Concentration, Version 1.* [north/daily]. doi: https://doi.org/10.7265/N5FF3QJ6.

Progress in Oceanography, 2007, Observing and Modelling Ocean Heat and Freshwater Budgets and Transports, Edited by Igor Yashayaev, Vol. 73, 3-4, May-June 2007, Pages 203-426.

Progress in Oceanography, 2015, Oceanography of the Arctic and North Atlantic Basins, Edited by Igor Yashayaev, Dan Seidov, Entcho Demirov, Vol. 132, March 2015, Pages 1-352.

Rhein, M., S.R. Rintoul, S. Aoki, E. Campos, D. Chambers, R.A. Feely, S. Gulev, G.C. Johnson, S.A. Josey, A. Kostianoy, C. Mauritzen, D. Roemmich, L.D. Talley and F. Wang. 2013. Observations: Ocean. In: Climate Change 2013: The Physical Science Basis. Contribution of Working Group I to the Fifth Assessment Report of the Intergovernmental Panel on Climate Change [Stocker, T.F., D. Qin, G.-K. Plattner, M. Tignor, S.K. Allen, J. Boschung, A. Nauels, Y. Xia, V. Bex and P.M. Midgley (eds.)]. Cambridge University Press, Cambridge, United Kingdom and New York, NY, USA.

Rhein, M, Steinfeldt, R, Kieke, D, Stendardo, I and Yashayaev, I. 2017. Ventilation variability of Labrador Sea Water and its impact on oxygen and anthropogenic carbon: a review. Philosophical Transactions of the Royal Society A: Mathematical, Physical and Engineering Sciences, 375(2102). 20160321. doi:10.1098/rsta.2016.0321

Smeed, D. A., Josey, S. A., Beaulieu, C., Johns, W. E., Moat, B. I., Frajka-Williams, E., et al. 2018. The North Atlantic Ocean is in a state of reduced overturning. Geophysical Research Letters, 45, 1527–1533. https://doi.org/10.1002/2017GL076350

Thornalley, D.J.R., Oppo, D.W., Ortega, P., Robson, J.I., Brierley, C.M., Davis, R., Hall, I.R., Moffa-Sanchez, P., Rose, N.L., Spooner, P.T., Yashayaev, I., Keigwin., L.D. 2018, Anomalously weak Labrador Sea convection and Atlantic overturning during the past 150 years. Nature, 2018; 556 (7700): 227 DOI: 10.1038/s41586-018-0007-4

Visbeck, M.H., Hurrell, J.W., Polvani, L., and Cullen, H.M. 2001. The North Atlantic Oscillation: Past, Present and Future. Proc. Nat. Acad. Sci., 98, 12876-12877 doi: 10.1073/pnas.231391598.

Wang, Z., Brickman, D., Greenan, B., and Yashayaev, I. 2016. An abrupt shift in the Labrador Current System in relation to winter NAO events. Journal of Geophysical Research: Oceans. DOI: 10.1002/2016JC011721.

Wang, Z., Lu, Y., Greenan, B., Brickman, D., and DeTracey, B. 2018. BNAM: An eddy-resolving North Atlantic Ocean model to support ocean monitoring. Can. Tech. Rep. Hydrogr. Ocean. Sci. 327: vii + 18p.

Wang, Z., Brickman, D., and Greenan, B. 2019. Characteristic evolution of the Atlantic Meridional Overturning Circulation from 1990 to 2015: An eddy-resolving ocean model study. Deep Sea Research Part I, https://doi.org/10.1016/j.dsr.2019.06.002.

Yashayaev, I., and Zveryaev, I. 2001. Climate of the seasonal cycle in the North Pacific and the North Atlantic Oceans. Int. J. Climatol., 21, 401-417, https://doi.org/10.1002/joc.585.

Yashayaev, I. 2007a. Hydrographic changes in the Labrador Sea, 1960-2005, Progress in Oceanography, 73, 242-276.

Yashayaev, I. (Ed.). 2007b. Observing and Modelling Ocean Heat and Freshwater Budgets and Transports. Progress in Oceanography. 73 (3–4): 203-426.

Yashayaev, I., and Dickson, R. R. 2008. Chapter 21. Transformation and Fate of Overflows in the northern North Atlantic, Arctic-Subarctic Ocean Fluxes: Defining the Role of the

Northern Seas in Climate, R.R.Dickson, J.Meincke, P.Rhines (Eds.), Springer (www.springer.com), ISBN: 978-1-4020-6773-0.

Yashayaev, I., and Loder, J.W. 2009. Enhanced production of Labrador Sea Water in 2008. Geophys. Res. Lett., 36: L01606, doi:10.1029/2008GL036162.

Yashayaev, I., Seidov, D., and Demirov, E. 2015a. A new collective view of oceanography of the Arctic and North Atlantic basins, Progress in Oceanography. 132: 1-21, doi:10.1016/j.pocean.2014.12.012.

Yashayaev, I., Seidov, D., and Demirov, E. (Eds.). 2015b. Oceanography of the Arctic and North Atlantic Basins. Progress in Oceanography. 132: 1-352.

Yashayaev, I., and Seidov, D. 2015. The role of the Atlantic Water in multidecadal ocean variability in the Nordic and Barents Seas. Progress in Oceanography, doi:10.1016/j.pocean.2014.11.009.

Yashayaev, I., and Loder, J.W. 2016. Recurrent replenishment of Labrador Sea Water and associated decadal-scale variability. Journal of Geophys. Res.: Oceans, 121, 11, DOI: 10.1002/2016JC012046.

Yashayaev, I., and Loder, J.W. 2017. Further intensification of deep convection in the Labrador Sea in 2016. Geophysical Research Letters, 44, 3, DOI: 10.1002/2016GL071668.

Yashayaev, I., Peterson, I., and Wang, Z. 2020. Meteorological, Sea Ice, and Physical Oceanographic Conditions in the Labrador Sea during 2019. NAFO SCR Doc.20/037, N7085.
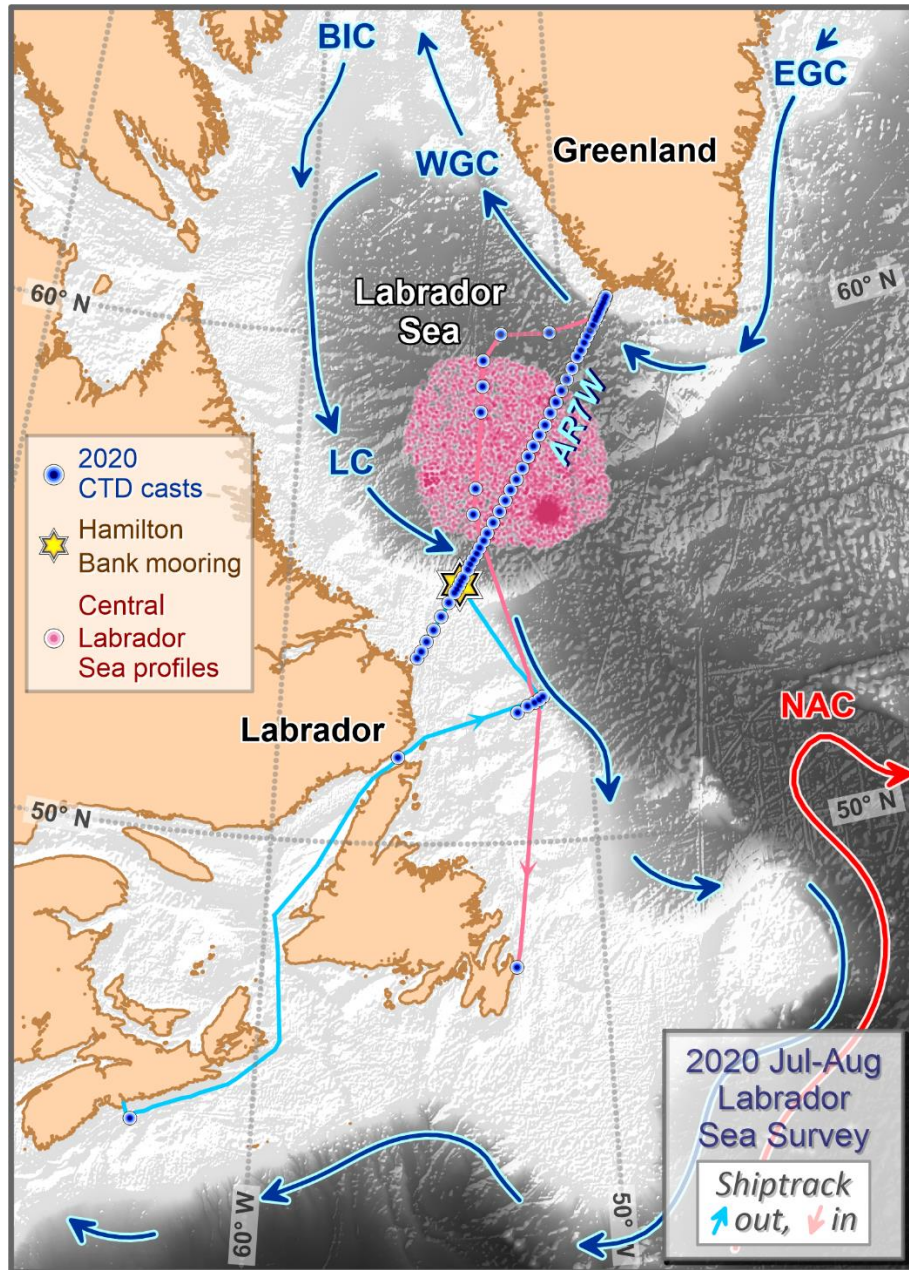
Figure 1. Topographic features and major deep-water currents in the Labrador Sea and adjacent regions of the North Atlantic. The 2020 July-August Labrador Sea mission CTD stations, the Hamilton Bank mooring and the location of temperature and salinity profiles within the central Labrador Sea domain.
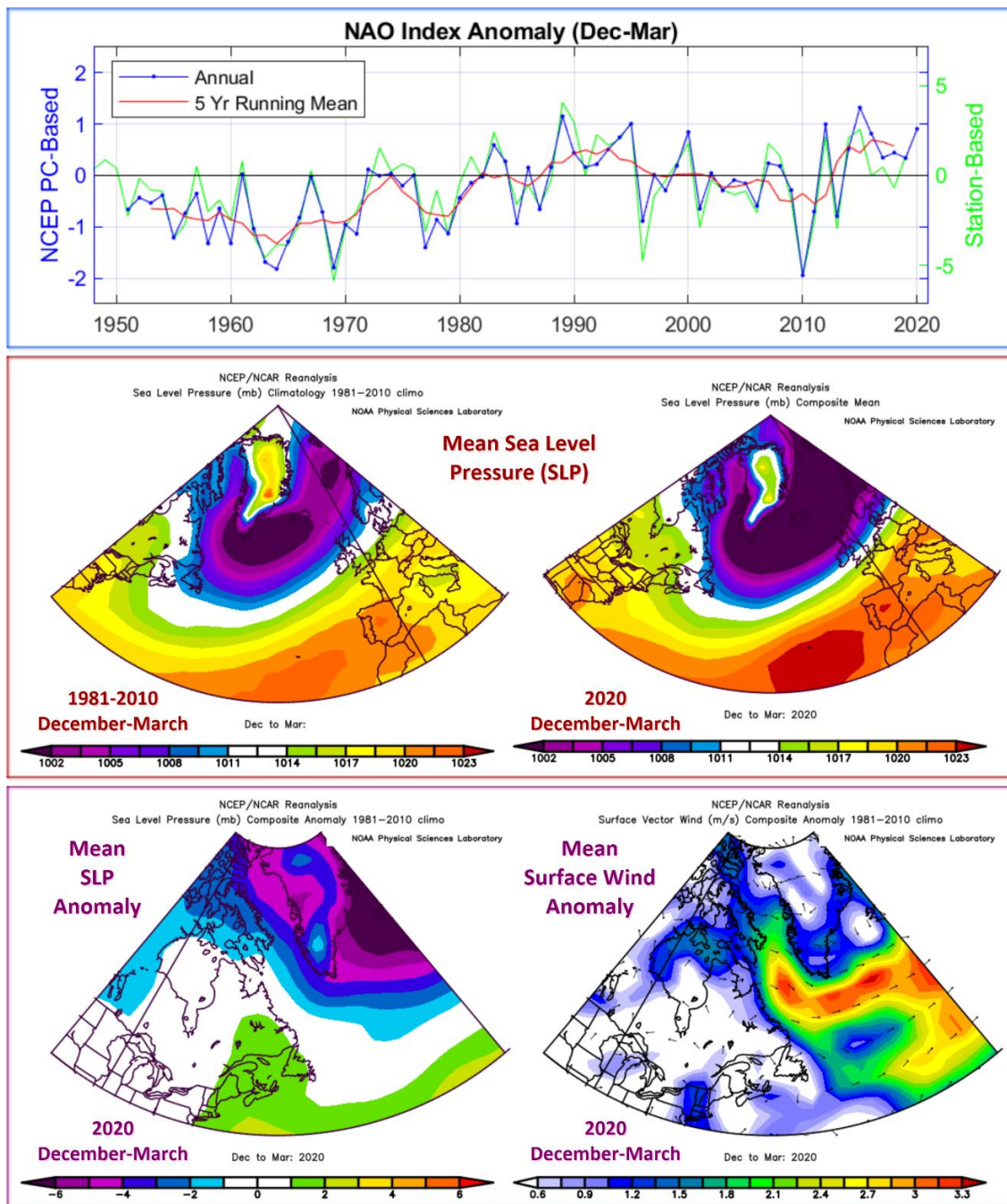
Figure 2. Anomalies of the North Atlantic Oscillation (NAO) index, relative to the 1981-2010 mean. The station-based NAO index (green) is defined as the winter (December, January, February, March) sea level pressure difference between the Azores and Iceland; data were obtained from https://climatedataguide.ucar.edu/climate-data/hurrell-north-atlantic-oscillation-nao-index-station-based (Hurrell et al. 2018). The PC-based NAO index (blue) is associated with the first empirical orthogonal function (EOF) of standardized monthly 500-mb height anomaly fields for the Northern Hemisphere; data were obtained from https://www.cpc.ncep.noaa.gov/data/teledoc/nao.shtml. The middle panels show the 1981-2010 December-March mean (middle left panel) and 2020 December-March sea level pressure (middle right panel) over the North Atlantic. The lower panels show the 2020 December-March SLP anomaly (lower left panel) and the 2020 December-March surface vector wind anomaly (lower right panel).
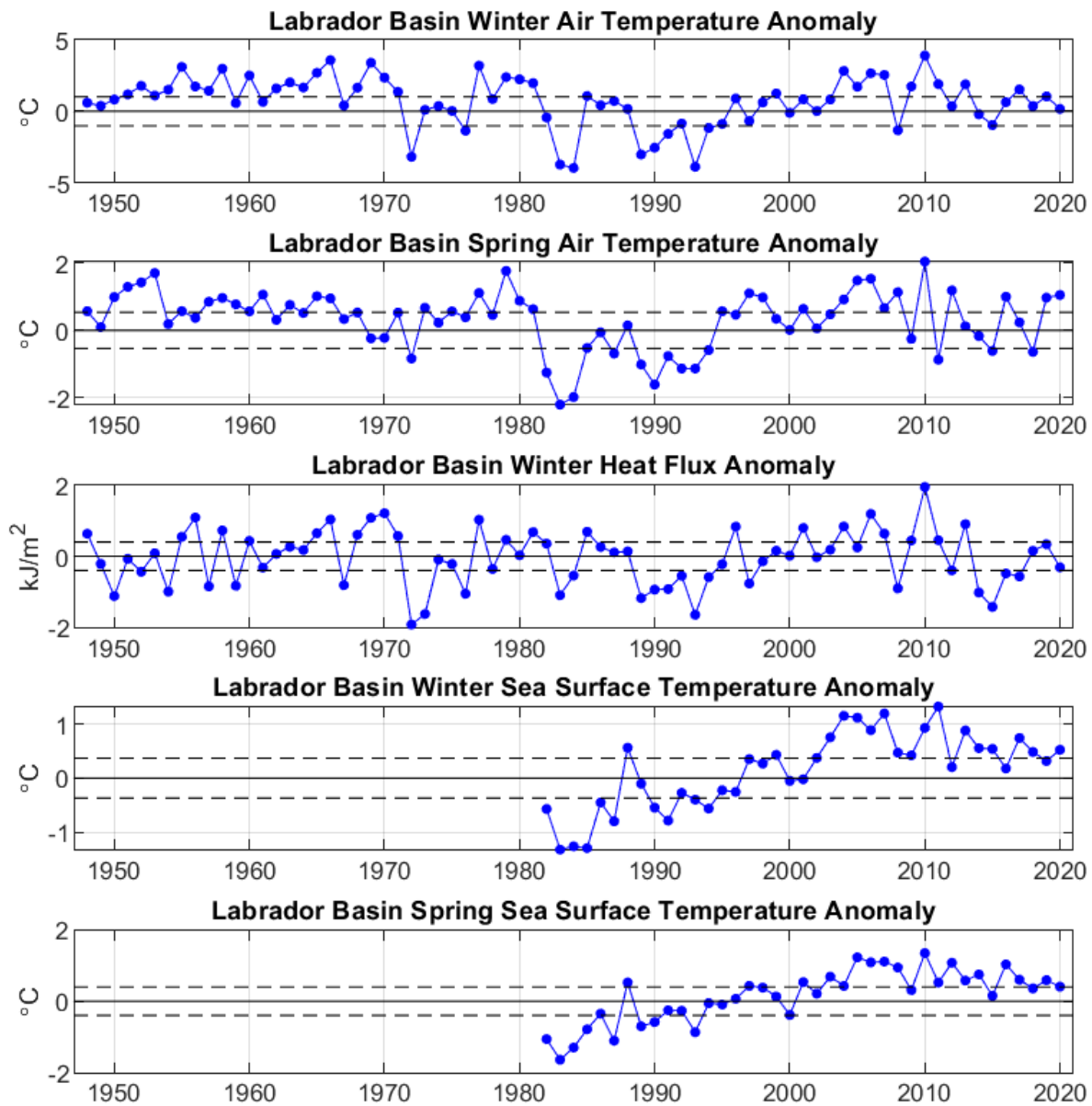
Figure 3. Anomalies of Labrador Basin winter and spring air temperature, cumulative winter surface heat flux, and winter and spring sea surface temperature (SST), relative to the 1981-2010 mean. Horizontal solid black lines represent the respective mean for the 1981-2010 period. Horizontal dashed lines represent 0.5 standard deviations from the mean. SST data were extracted from the OISST dataset. The other series shown in the figure are based on the NCEP/NCAR Reanalysis dataset. Both datasets were provided by NOAA (https://www.esrl.noaa.gov/psd/).
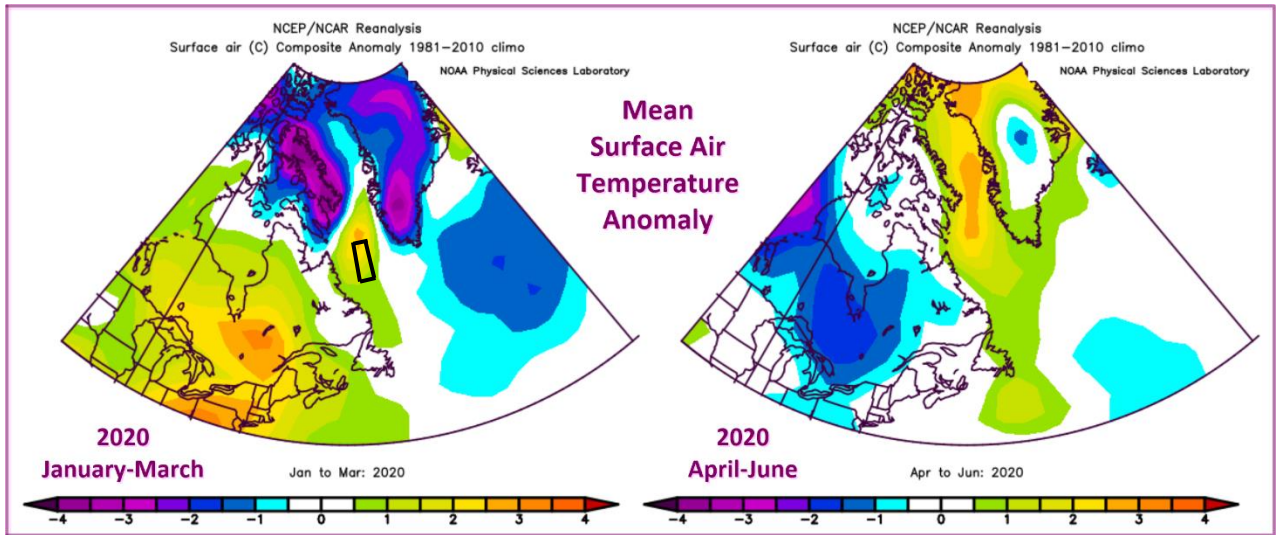
Figure 4. Winter and spring air temperature anomalies (ºC) over the Northwest Atlantic relative to the 1981-2010 means; data were obtained from NOAA Internet site (accessed 04 Feb 2020).
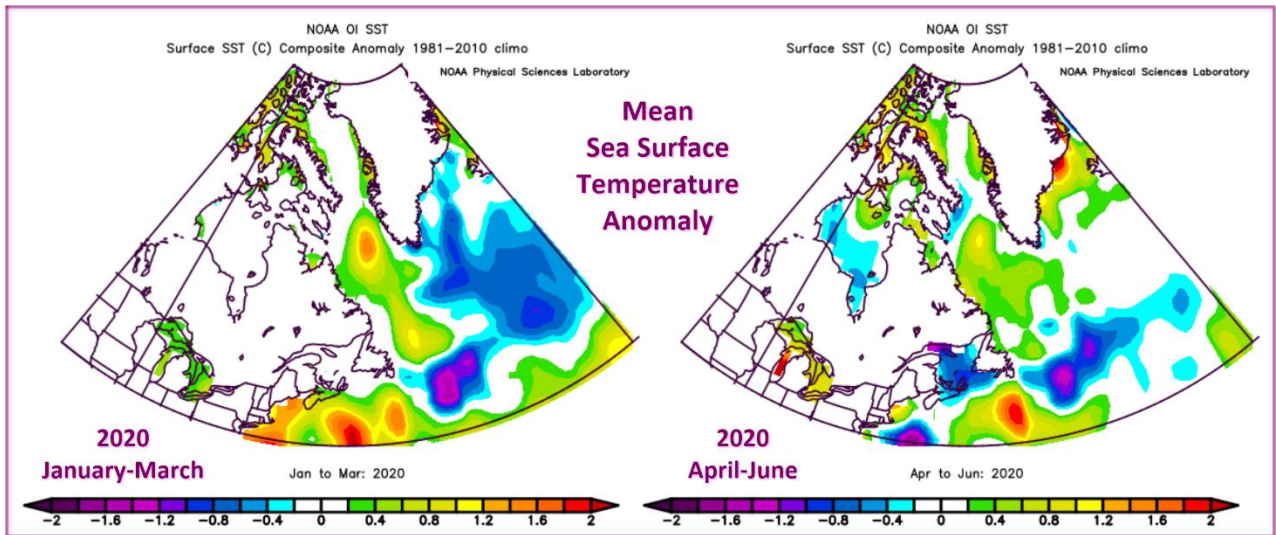
Figure 5. Winter and spring sea surface temperature anomalies (ºC) over the Northwest Atlantic relative to the 1981-2010 means; data were obtained from NOAA Internet site (accessed 04 Feb 2020).
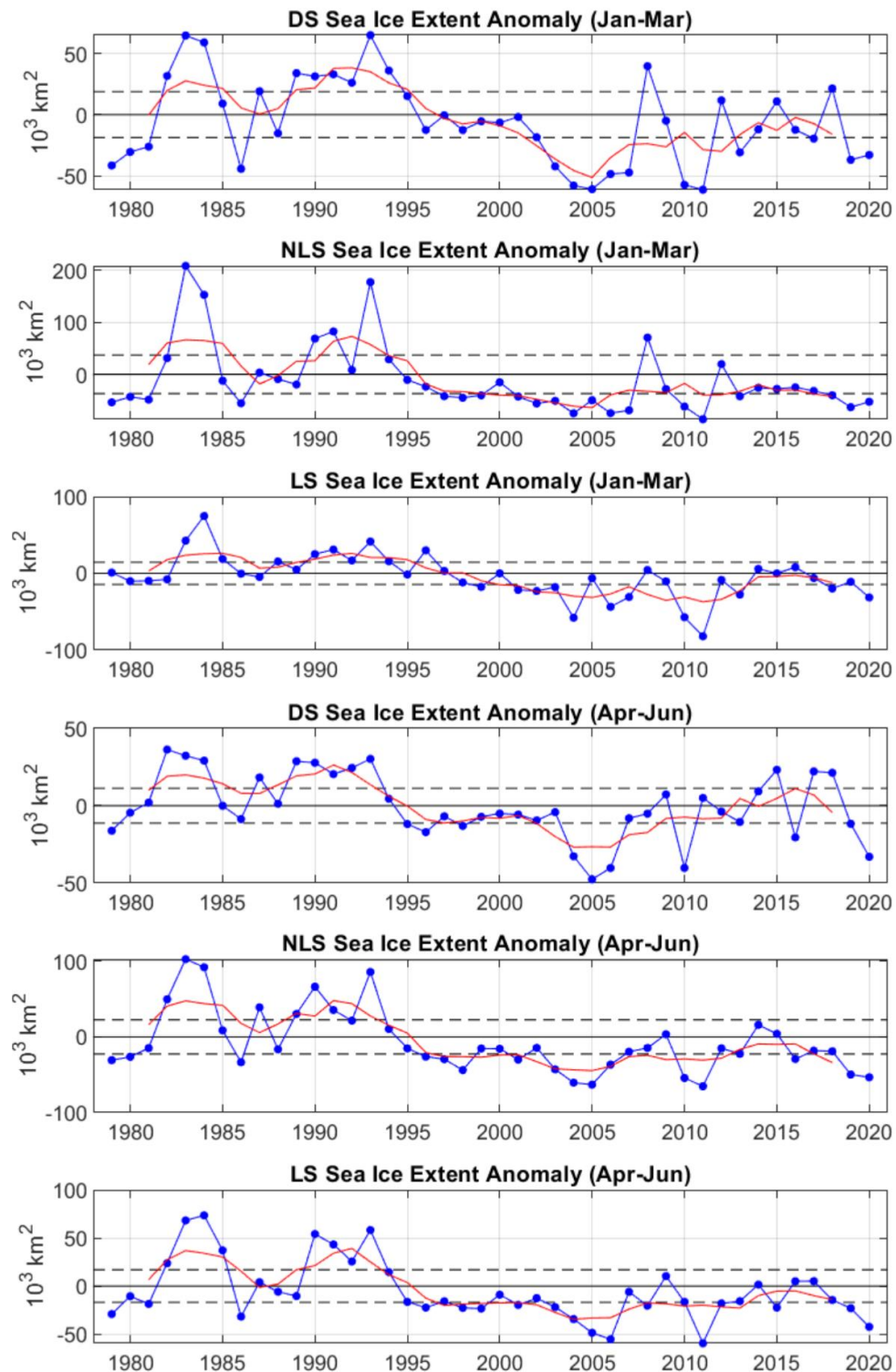
Figure 6. Winter and spring sea ice extent anomalies (blue) and their five year running means (red) for: (1) Davis Strait (63-68°N), (2) the Northern Labrador Sea (58-63°N), and (3) Labrador Shelf (53-58°N), based on the US National Snow and Ice Data Center dataset (http://nsidc.org/). Horizontal solid black lines represent the respective mean for the 1981-2010 period. Horizontal dashed lines represent 0.5 standard deviations from the mean.
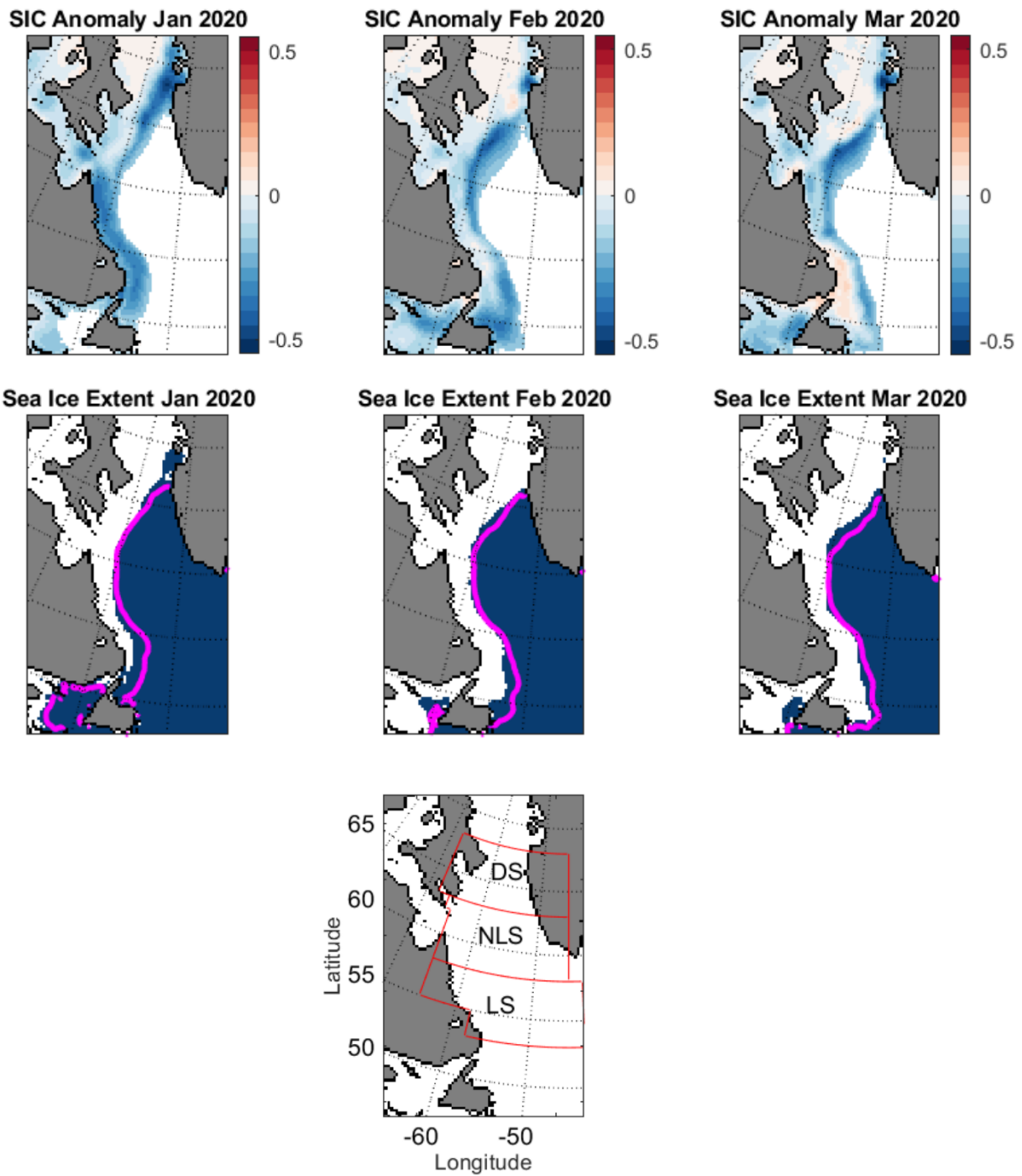
Figure 7. Sea ice concentration anomalies (top) and sea ice extent (middle) for the January-March period of 2020 as derived by the US National Snow and Ice Data Center (reference period 1979-2000) http://nsidc.org/. The magenta lines show the median ice edge for 1981-2010.
Davis Strait (DS), Northern Labrador Sea (NLS), and Labrador Shelf (LS) regions (bottom panel).
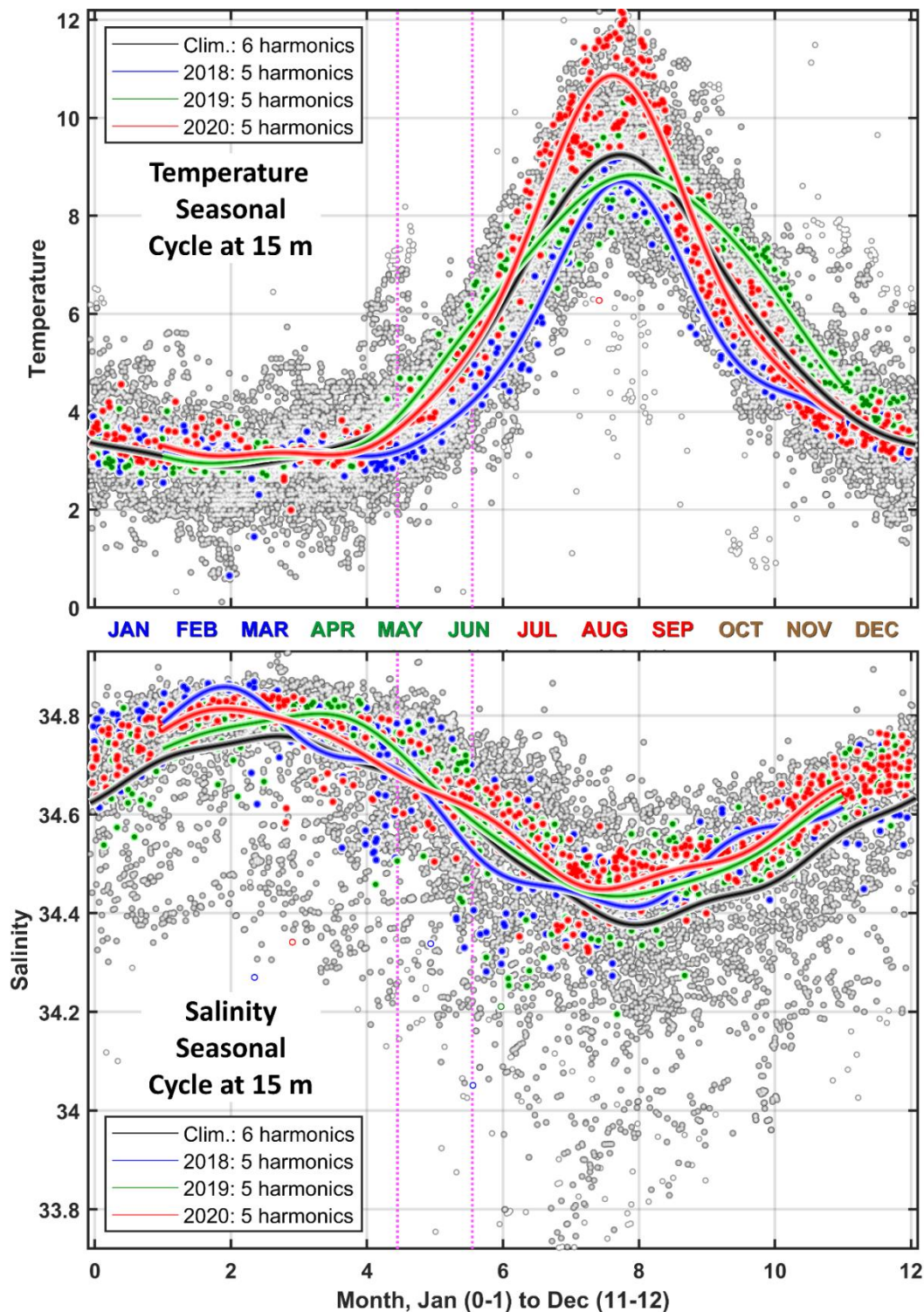
Figure 8. (a) Temperature (upper panel) and salinity (lower panel) measurements at 15 m in the central Labrador Sea for the period of 1948-2021 (Figure 1). The 2018, 2019 and 2020 data values are shown in blue, green and red, respectively. The black line represents the all-data climatological, regular or normal seasonal cycle; the blue, green and red lines represent the 2018, 2019 and 2020 seasonal cycles, respectively. The vertical magenta dotted lines confine the time period from May 15 to June 15.
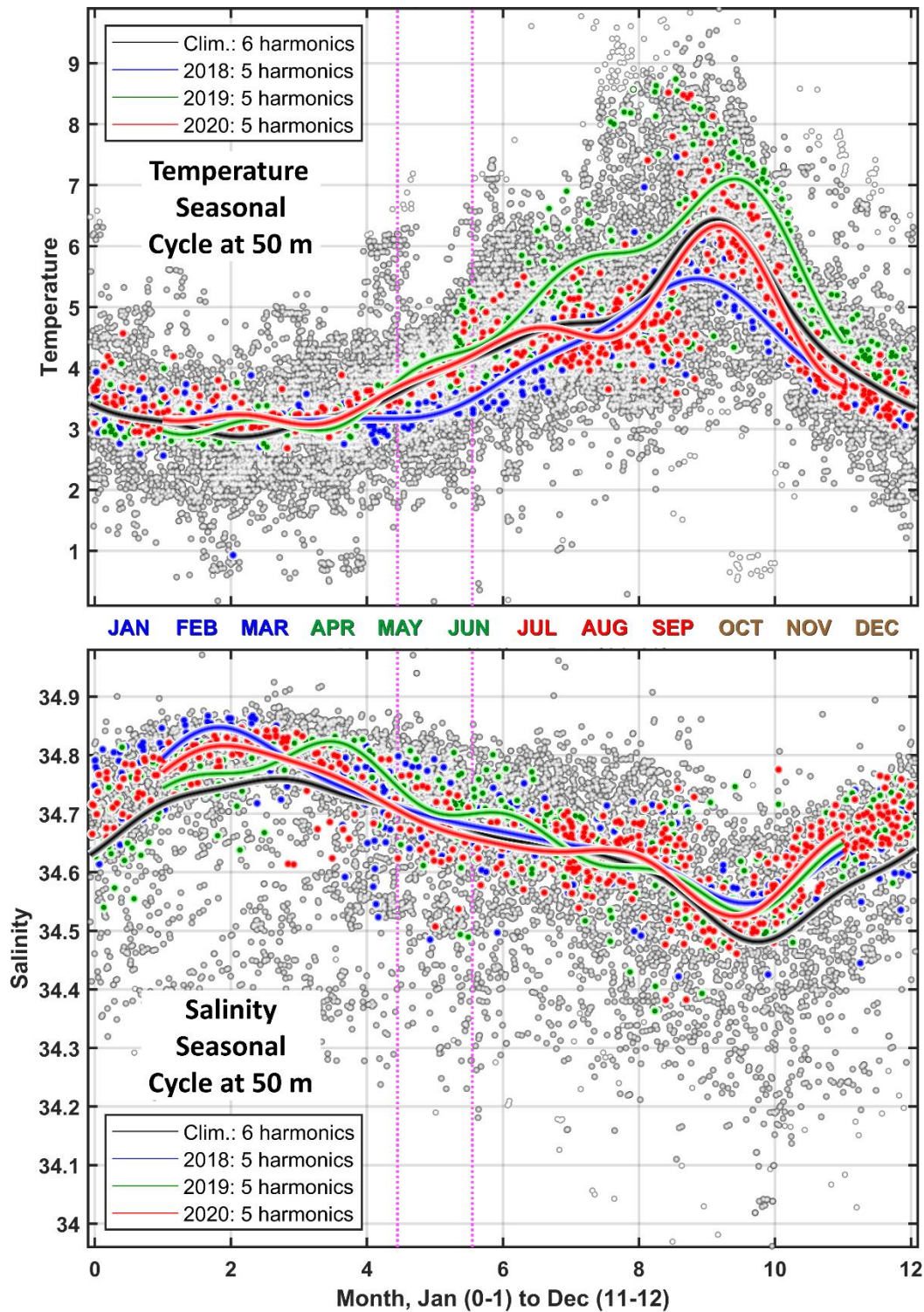
Figure 9. (a) Temperature (upper panel) and salinity (lower panel) measurements at 50 m in the central Labrador Sea for the period of 1948-2021 (Figure 1). The 2018, 2019 and 2020 data values are shown in blue, green and red, respectively. The black, blue, green and red lines represent the all-data climatological (regular or normal), 2018, 2019 and 2020 seasonal cycles, respectively (note phase shift from 15 m). The vertical magenta dotted lines confine the period from May 15 to June 15.
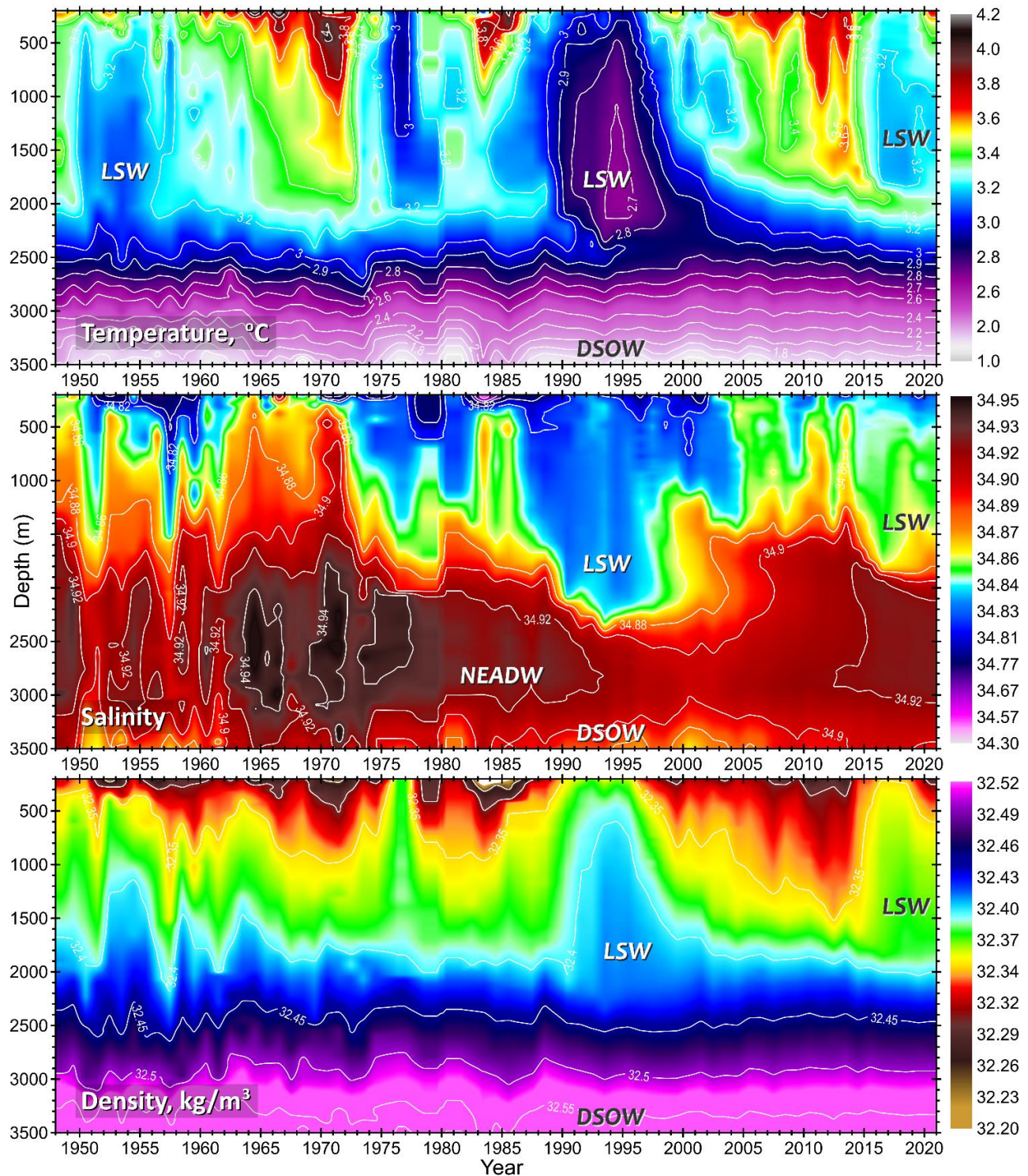
Figure 10. Annual temperature (upper panel), salinity (middle panel) and density (referenced to 1000 dbar pressure, lower panel) profiles in the central region of the Labrador Sea (time period: 1948-2020, depth range: 200-3500 m). The quality controlled observations were averaged annually for 1948-1987, in two steps: first, locally isobarically, and then, regionally isopycnally. For 1987-2020, the shipboard data were averaged mainly isopycnally, while Argo in the two-step process. LSW, NEADW and DSOW indicate Labrador Sea Water, Northeast Atlantic Deep Water and Denmark Strait Overflow Water, respectively.
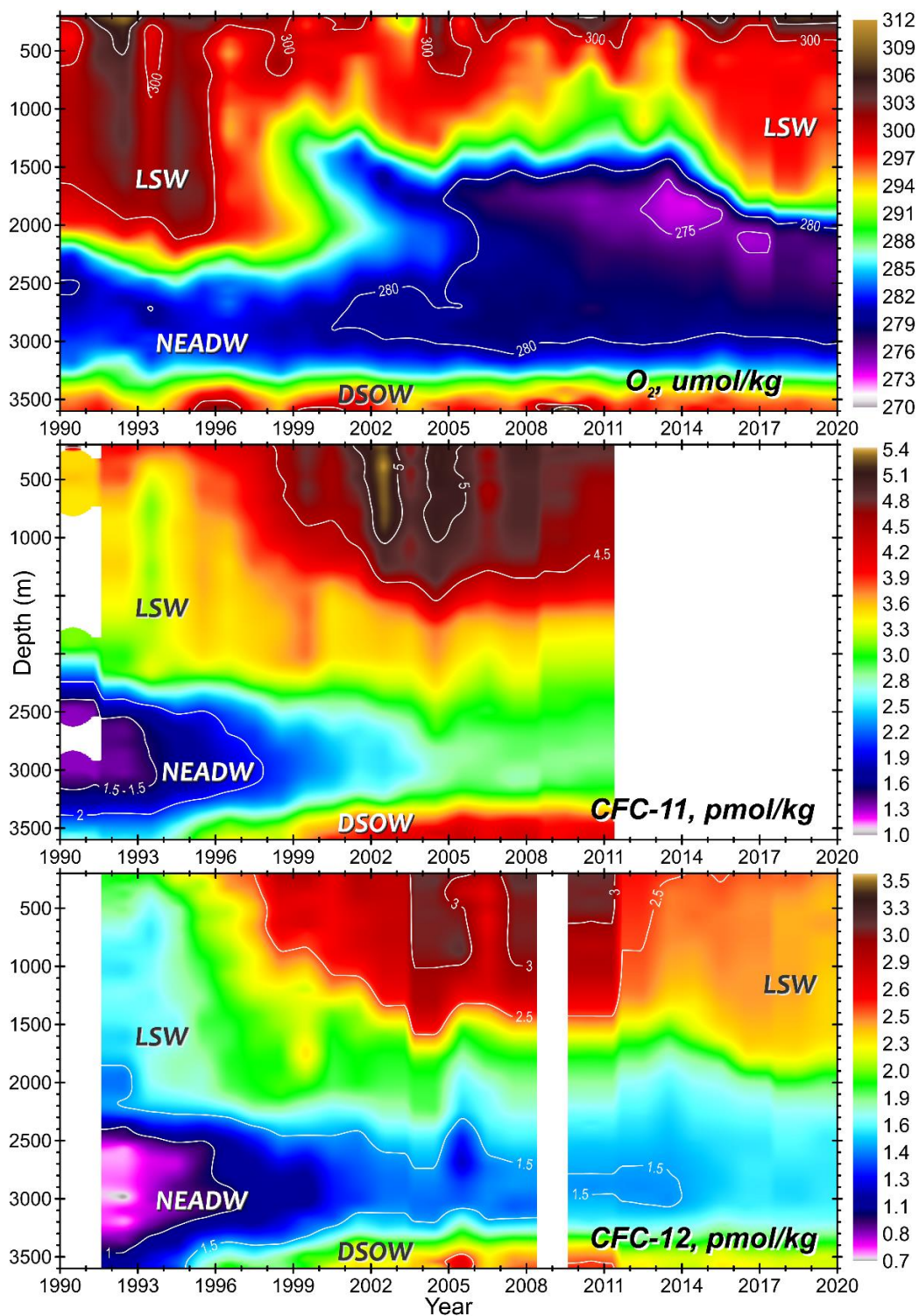
Figure 11. Annual composite profiles of dissolved oxygen, CFC-11 and CFC-12 (upper, middle and lower panels, respectively) in the central region of the Labrador Sea (time period: 1990-2019, depth range: 200-3500 m). LSW, NEADW and DSOW indicate Labrador Sea Water, Northeast Atlantic Deep Water and Denmark Strait Overflow Water, respectively. Extensive quality control and time-dependent corrections, based on multivariate analysis of oceanographic data (e.g., in near-stagnant or slow-evolving water mass layers such as the NEADW core) were applied to the data sets before averaging.
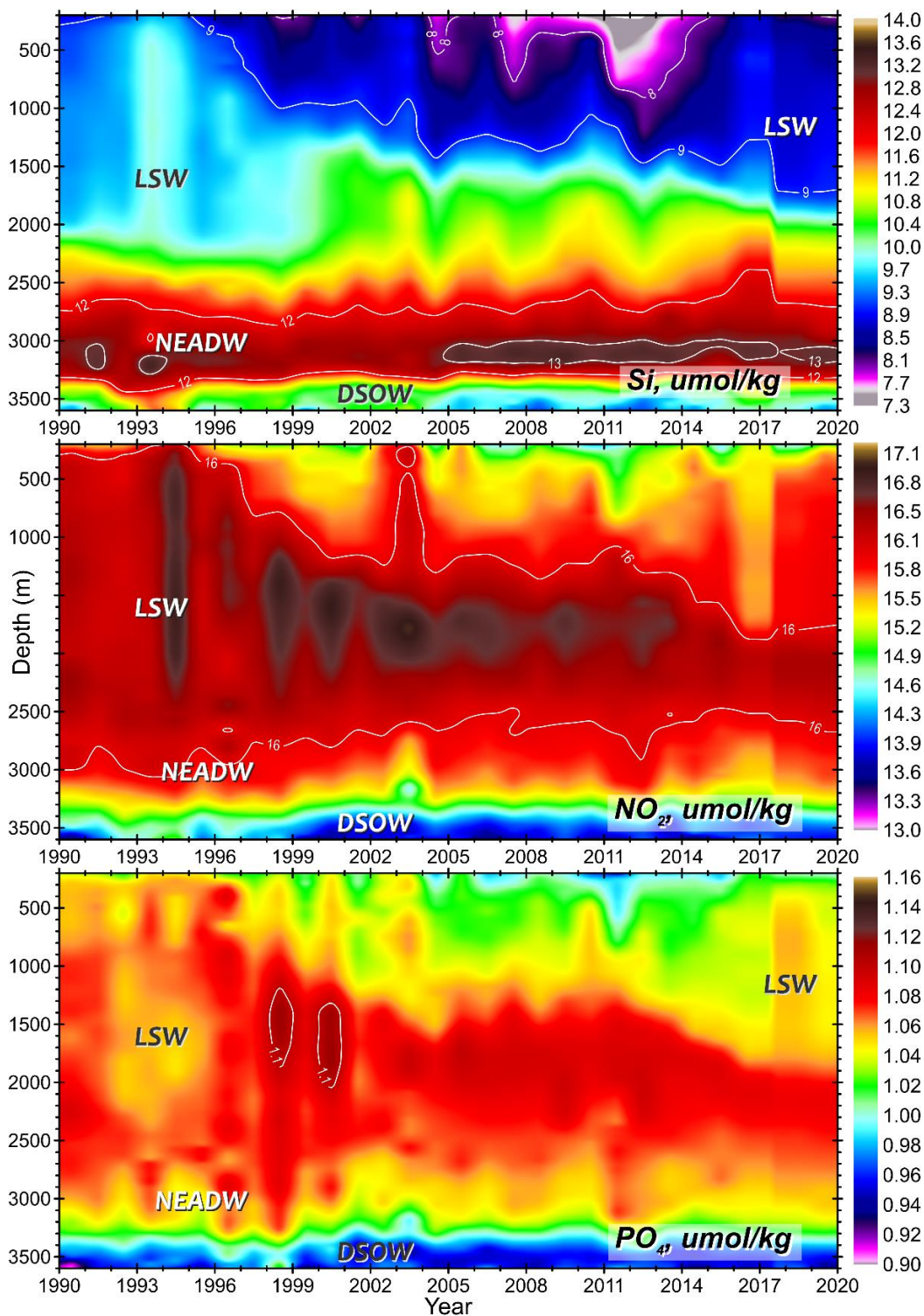
Figure 12. Annual composite profiles of dissolved silicate, nitrate and phosphate concentrations (upper, middle and lower panels) in the central region of the Labrador Sea (time period: 1990-2019, depth range: 200-3500 m). LSW, NEADW and DSOW indicate Labrador Sea Water, Northeast Atlantic Deep Water and Denmark Strait Overflow Water, respectively. Extensive quality control and time-dependent corrections, based on multivariate analysis of oceanographic data (e.g., in near-stagnant or slow-evolving water mass layers such as the NEADW core) were applied to the data sets before averaging.
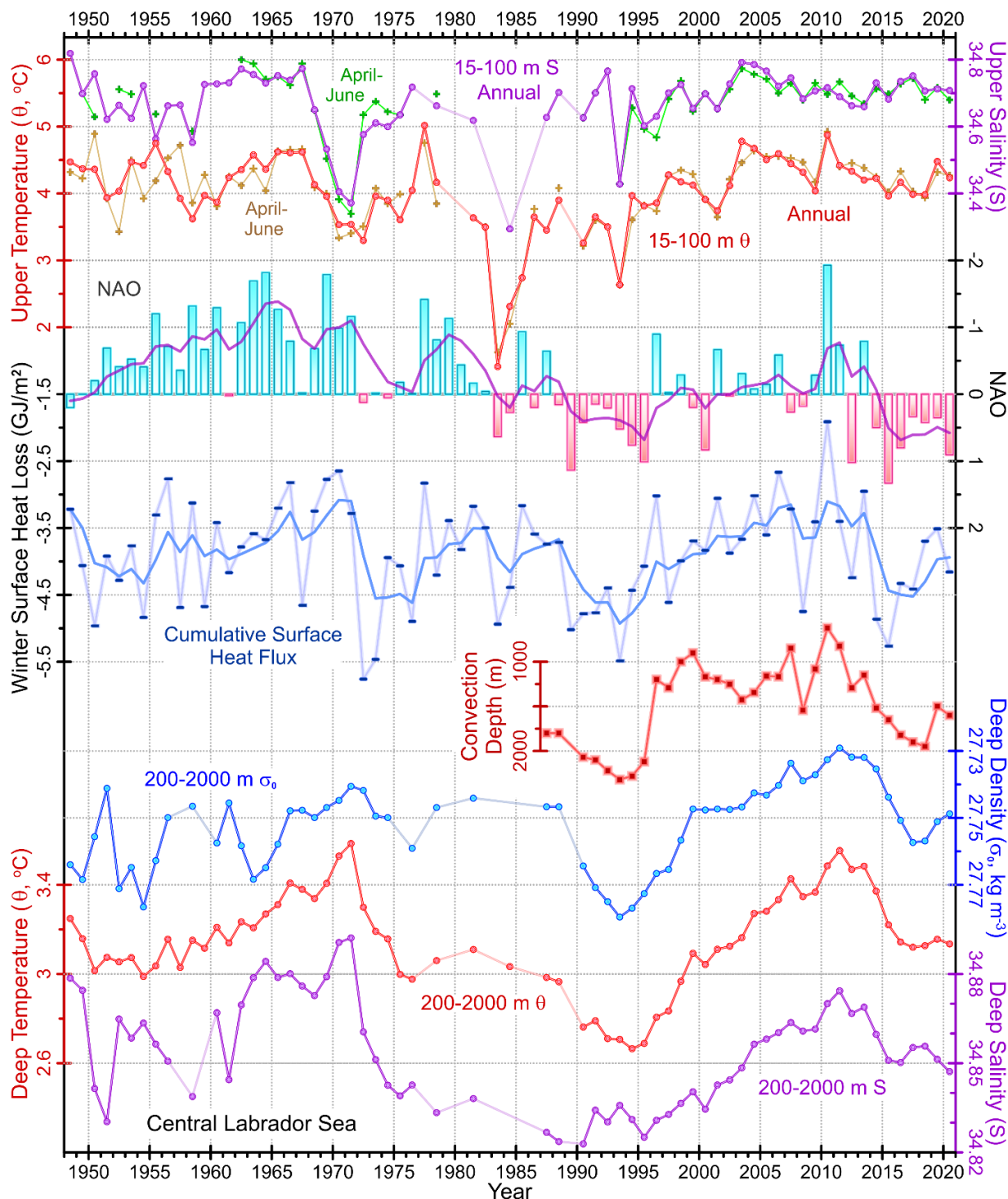
Figure 13. Key central Labrador Sea environmental state variables since 1948. From top down: annual and spring mean salinity (S) and temperature (θ) averaged over the 15-100 m depth range; the normalized winter NAO index (bar graph, inverted scale); the NCEP reanalysis-based cumulative surface heat flux computed for the central Labrador Sea over individually-defined annual cooling seasons (blue); the two solid lines overlaying the NAO and heat flux graphs show five-back-point filtered series; annual mean seawater density (σ₀, referenced to 0 dbar), θ and S averaged over the 200–2000 m depth range in the central Labrador Sea.

40
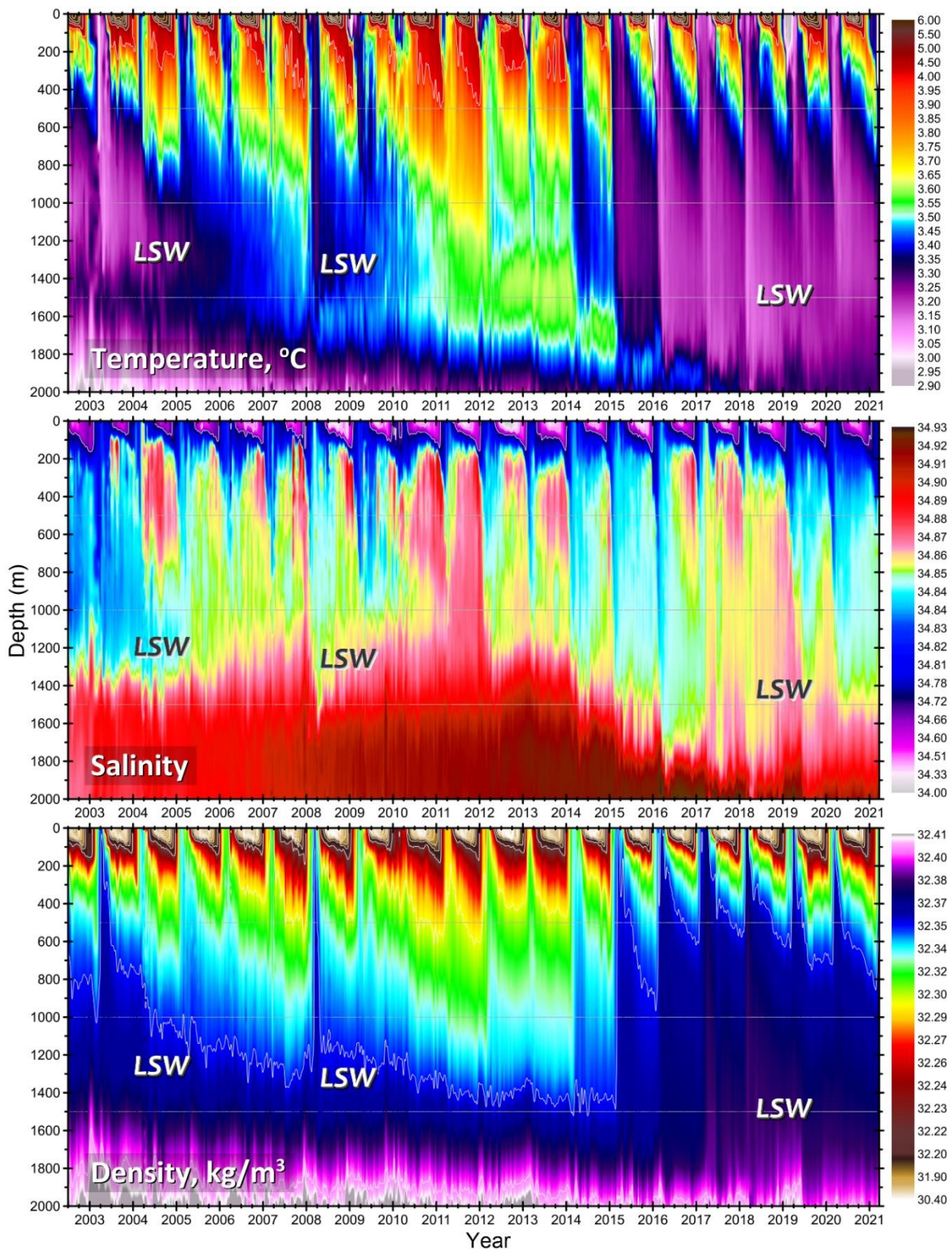
Figure 14. Temperature (upper), salinity (middle) and density (ref. to 1000 dbar; lower) in the central Labrador Sea created by averaging of the cleaned and corrected Argo float and shipboard data in 10-day-long overlapping time bins starting at 5-day steps over 2002-2021 year and 0-2000 m depth ranges.
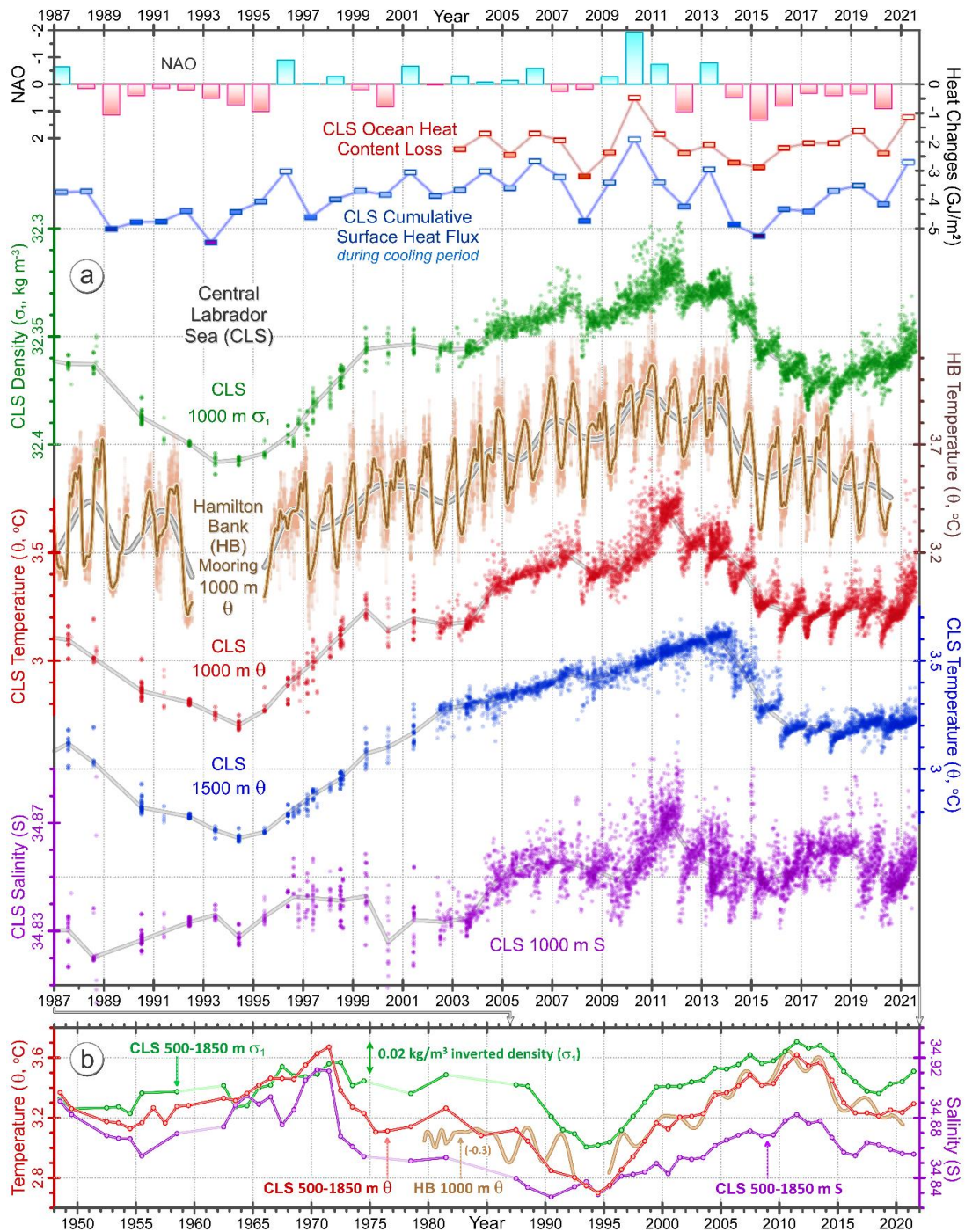
Figure 15. Upper panel: the normalized winter NAO index (inverted); the annual heat loss of the 15-2000 m water layer in the central Labrador Sea (CLS) defined over individual ocean cooling periods (red); the CLS net surface heat flux integrated over individual cooling seasons (blue); unordered CLS seawater density (σ₁, green), temperature (θ, red) and salinity (S, purple) at 1000 m and θ (blue) at 1500 m from ship and Argo profiles and respective annual averages (grey); low-pass filtered Hamilton Bank (HB) mooring bottom (~1000 m) θ (brown). Lower panel: annual averages of σ₁ (green), θ (red) and S (purple) averaged over the 500-1850 m depth range of the CLS profiles; low-pass filtered HB bottom θ (brown).
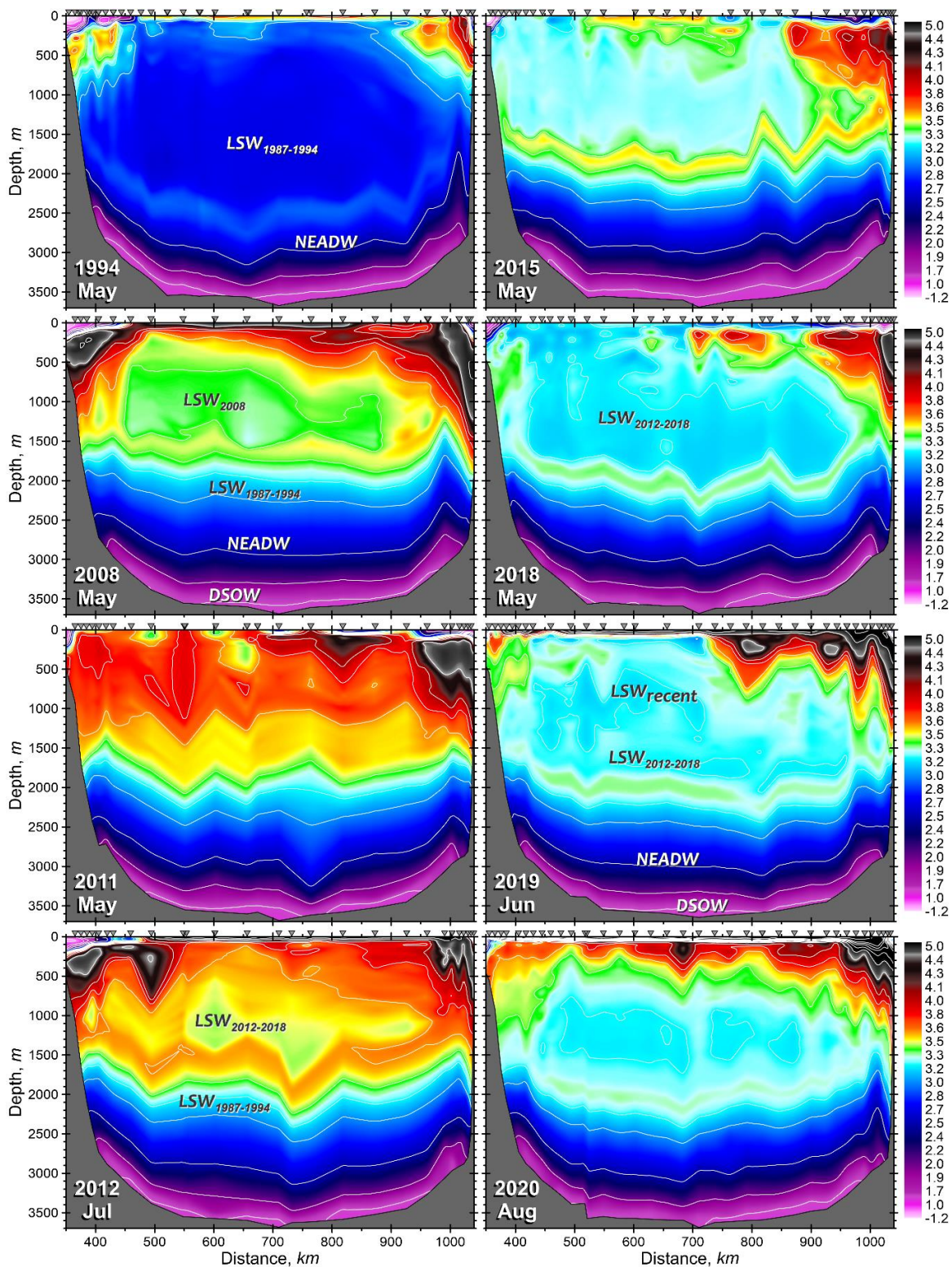
Figure 16. Distributions of potential temperature (°C) on the AR7W line across the Labrador Sea from annual spring-summer surveys in 1994, 2008, 2011, 2012, 2015, 2018, 2019 and 2020. Inverted triangles along the top of each panel indicate station locations. LSW, NEADW and DSOW indicate Labrador Sea Water, Northeast Atlantic Deep Water and Denmark Strait Overflow Water, respectively.

43
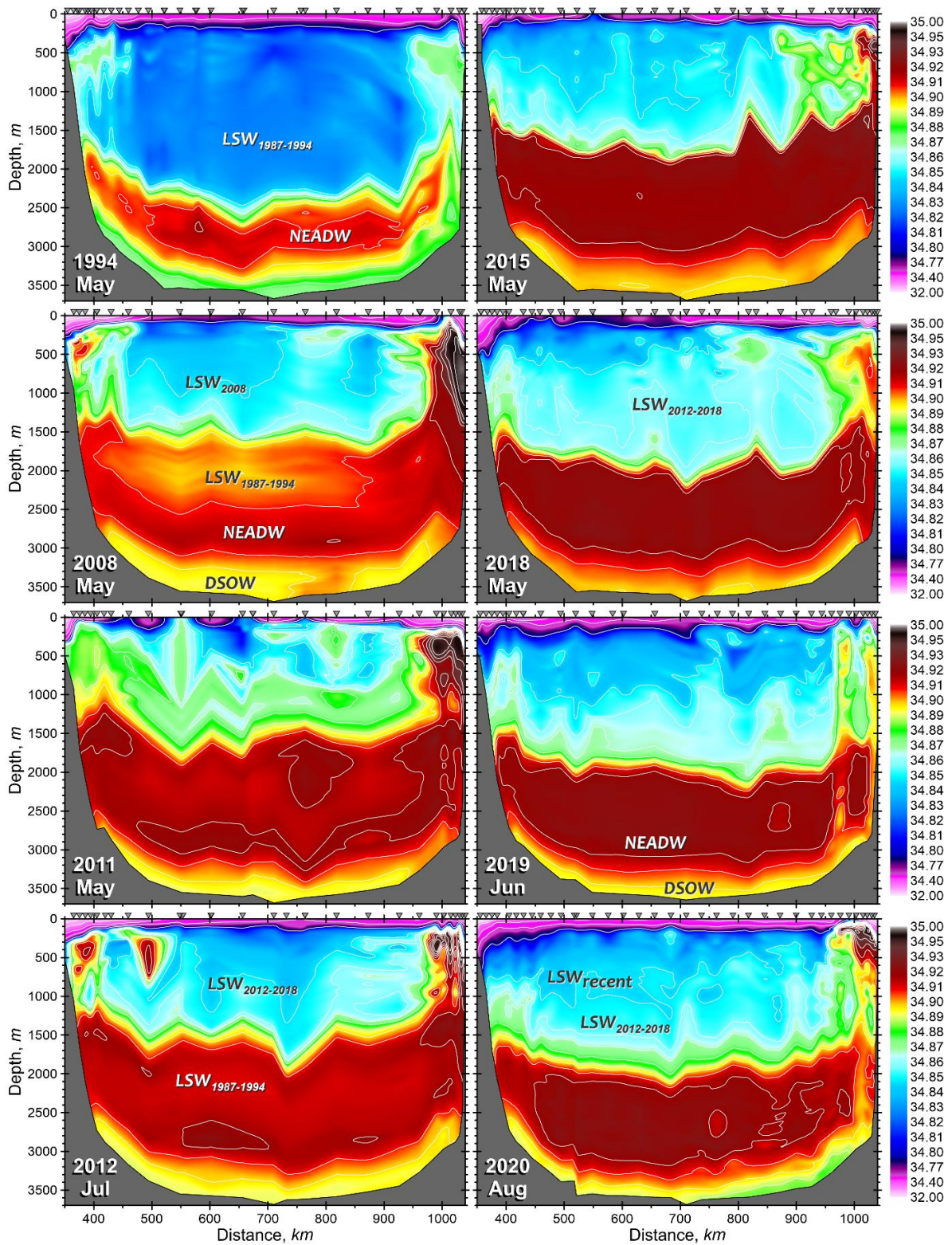
Figure 17. Distributions of salinity on the AR7W line across the Labrador Sea from annual spring-summer surveys in 1994, 2008, 2011, 2012, 2015, 2018, 2019 and 2020. Inverted triangles along the top of each panel indicate station locations. LSW, NEADW and DSOW indicate Labrador Sea Water, Northeast Atlantic Deep Water and Denmark Strait Overflow Water, respectively.
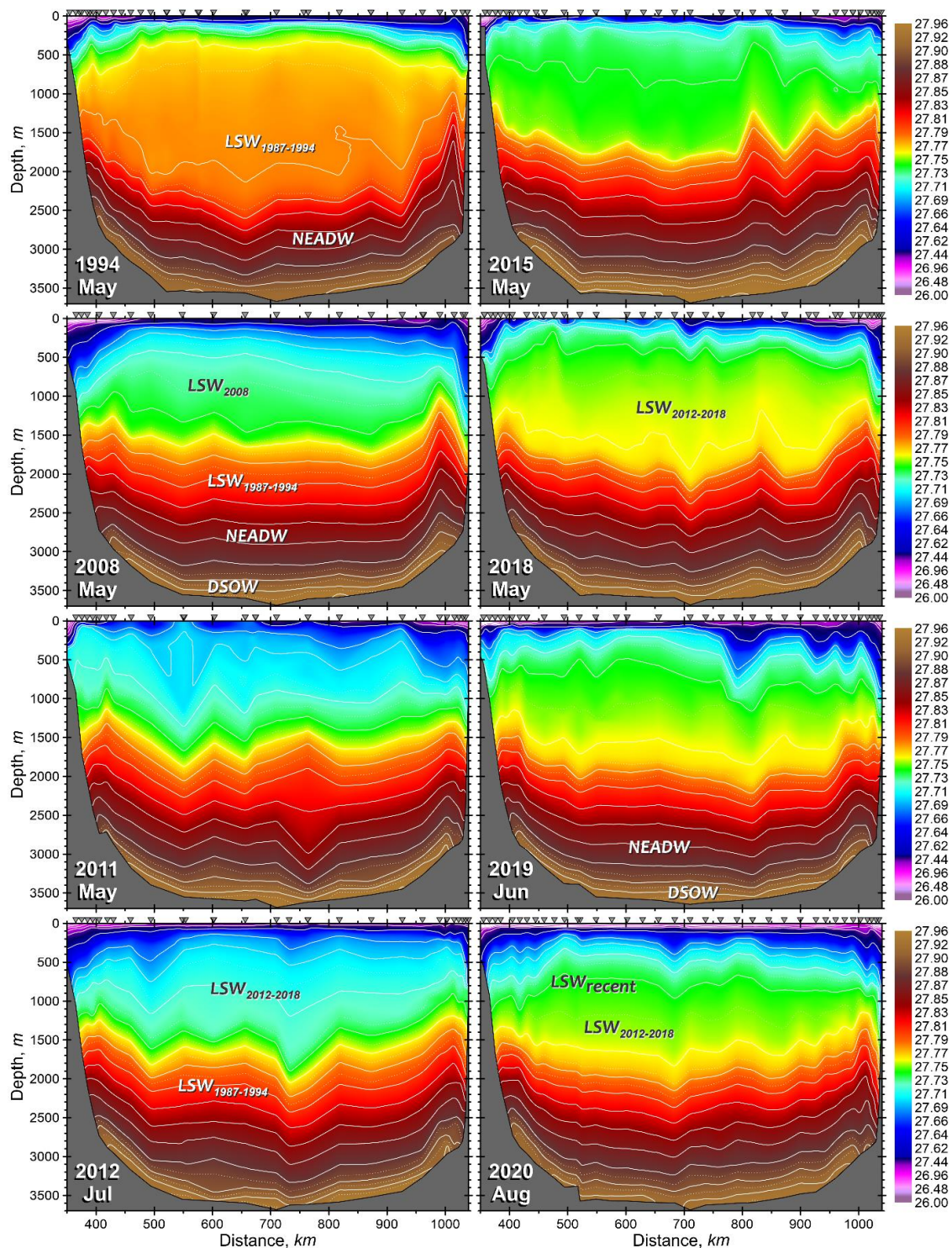
Figure 18. Distributions of potential density (referenced to the sea surface, kg/m³) on the AR7W line across the Labrador Sea from annual spring-summer surveys in 1994, 2008, 2011, 2012, 2015, 2018, 2019 and 2020. Inverted triangles indicate station locations. LSW, NEADW and DSOW indicate Labrador Sea Water, Northeast Atlantic Deep Water and Denmark Strait Overflow Water, respectively.
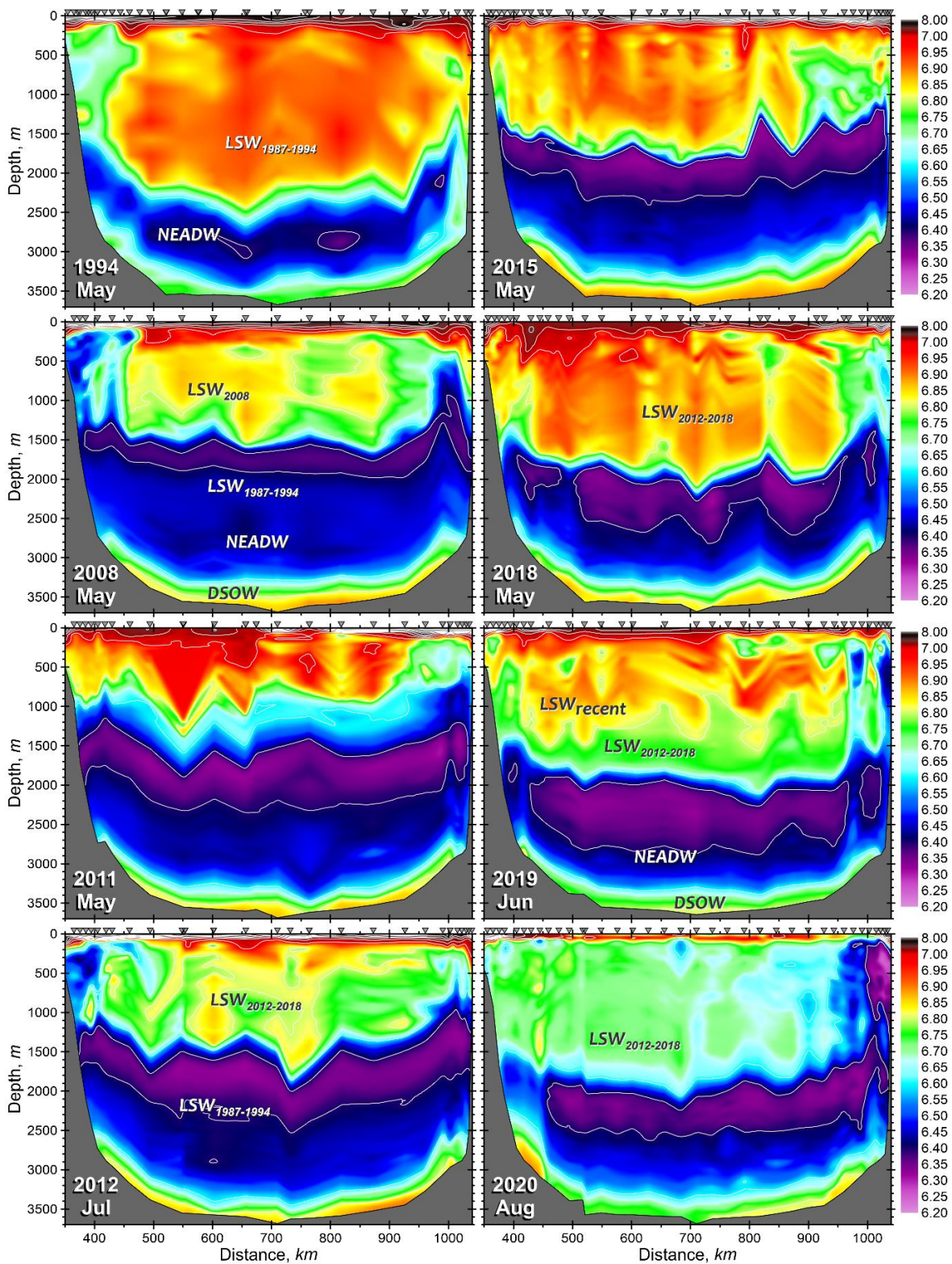
Figure 19. Distributions of dissolved oxygen concentration (ml/l) on the AR7W line across the Labrador Sea from annual spring-summer surveys in 1994, 2008, 2011, 2012, 2015, 2018, 2019 and 2020. Inverted triangles indicate station locations. LSW, NEADW and DSOW indicate Labrador Sea Water, Northeast Atlantic Deep Water and Denmark Strait Overflow Water, respectively.
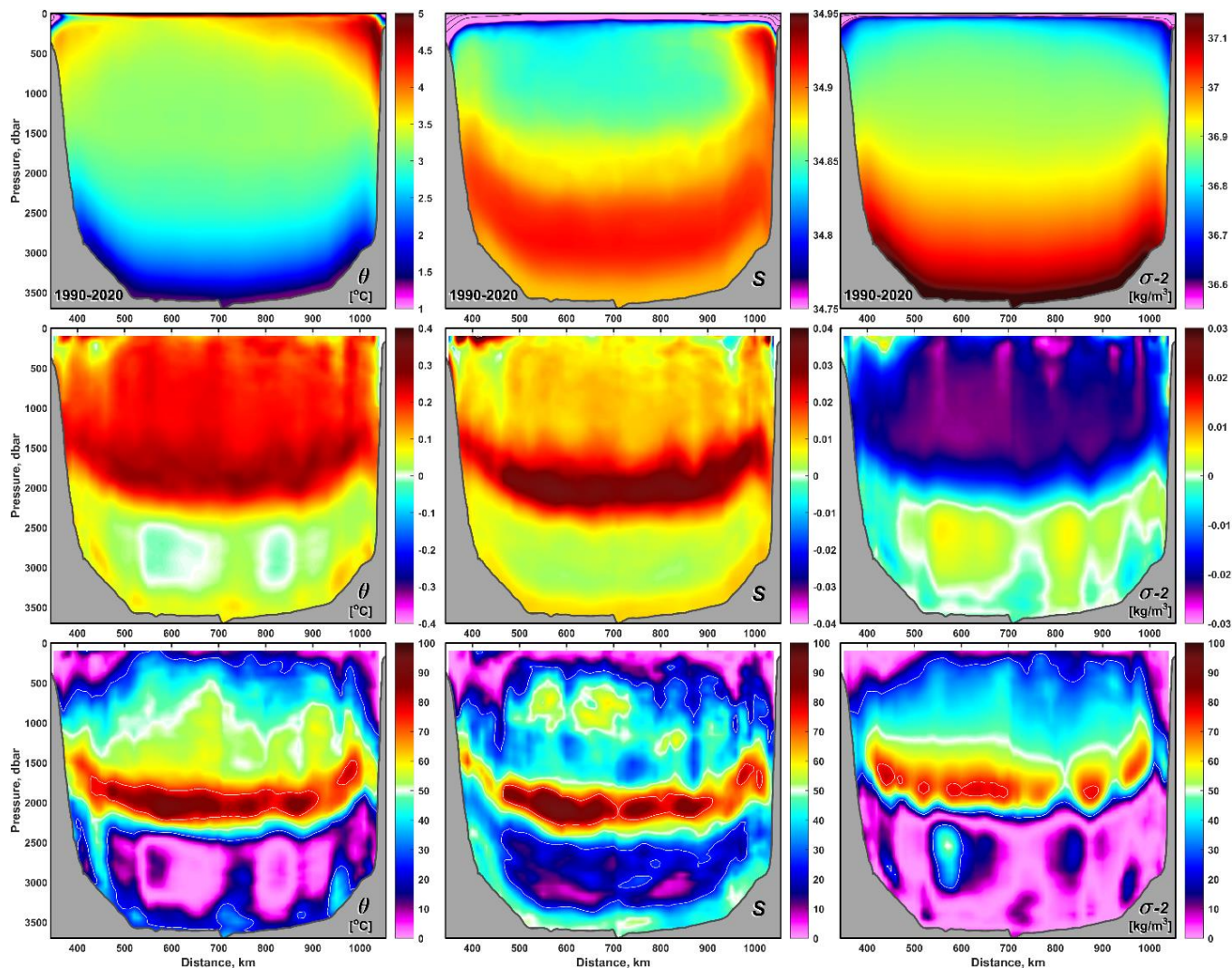
Figure 20. Temperature (left), salinity (central column) and density (right) climatological normals (top); the average rate of change over the 1990-2020 period, obtained by fitting linear trends the respective 31-year long time series constructed for each depth/pressure-distance bin within the active AR7W section plane and rated as a changes over ten years (middle row); and the contributions, in percent, of the linear trend to the total variance (lower). The shown estimates are based on the entire collection of both Canadian and international Labrador Sea oceanographic survey data on the AR7W line for the period of 1990-2020.
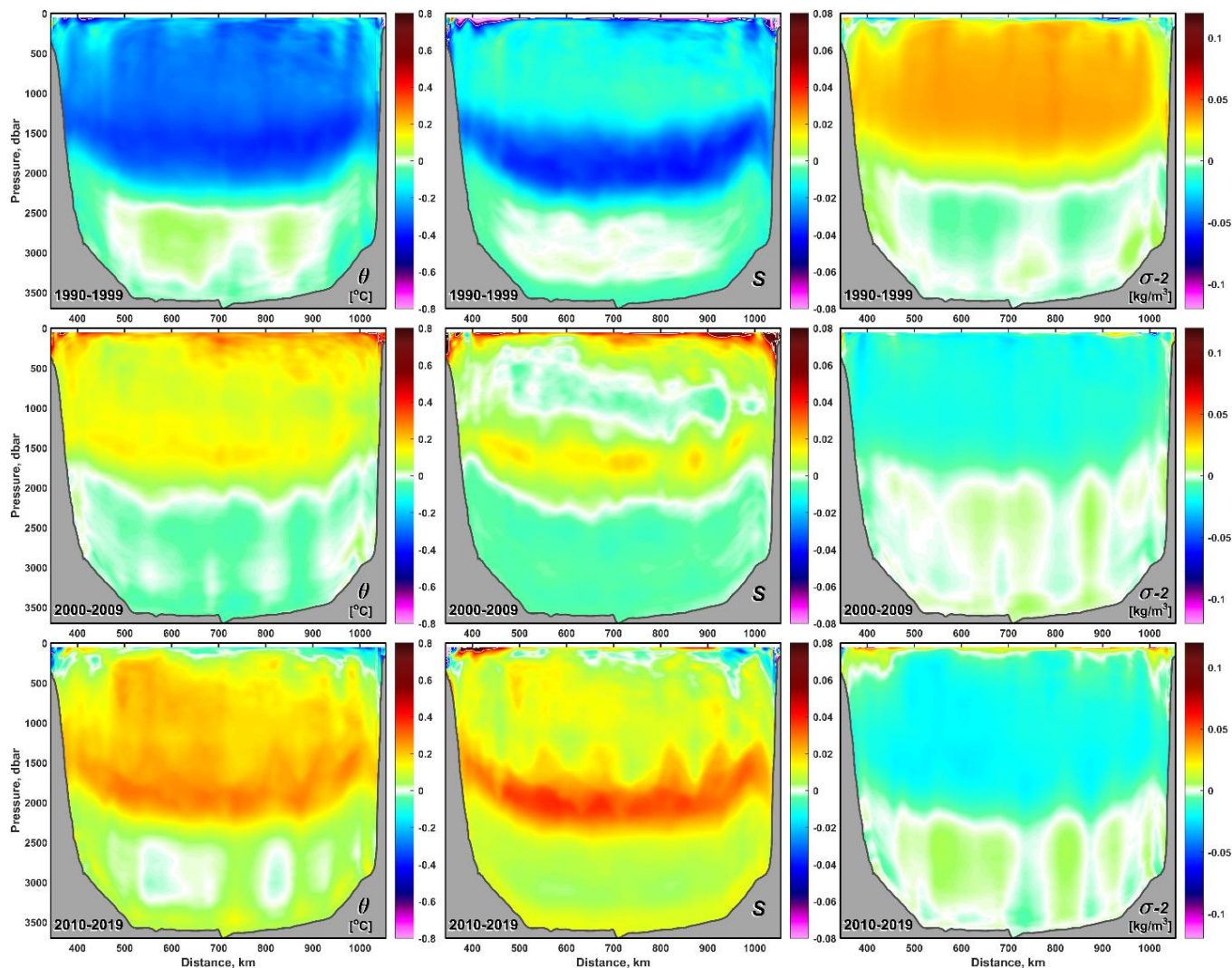
Figure 21. Average decadal 1990-1999 (upper row), 2000-2009 (middle row) and 2010-2019 (lower row) anomalies of temperature (left column), salinity (central column) and density (right column) on the AR7W line, based on the entire collection of both Canadian and international Labrador Sea oceanographic survey data. The decadal anomalies are based on averaging of annual anomalies referenced to the 1990-2020 climatological normal presented in Figure 20.
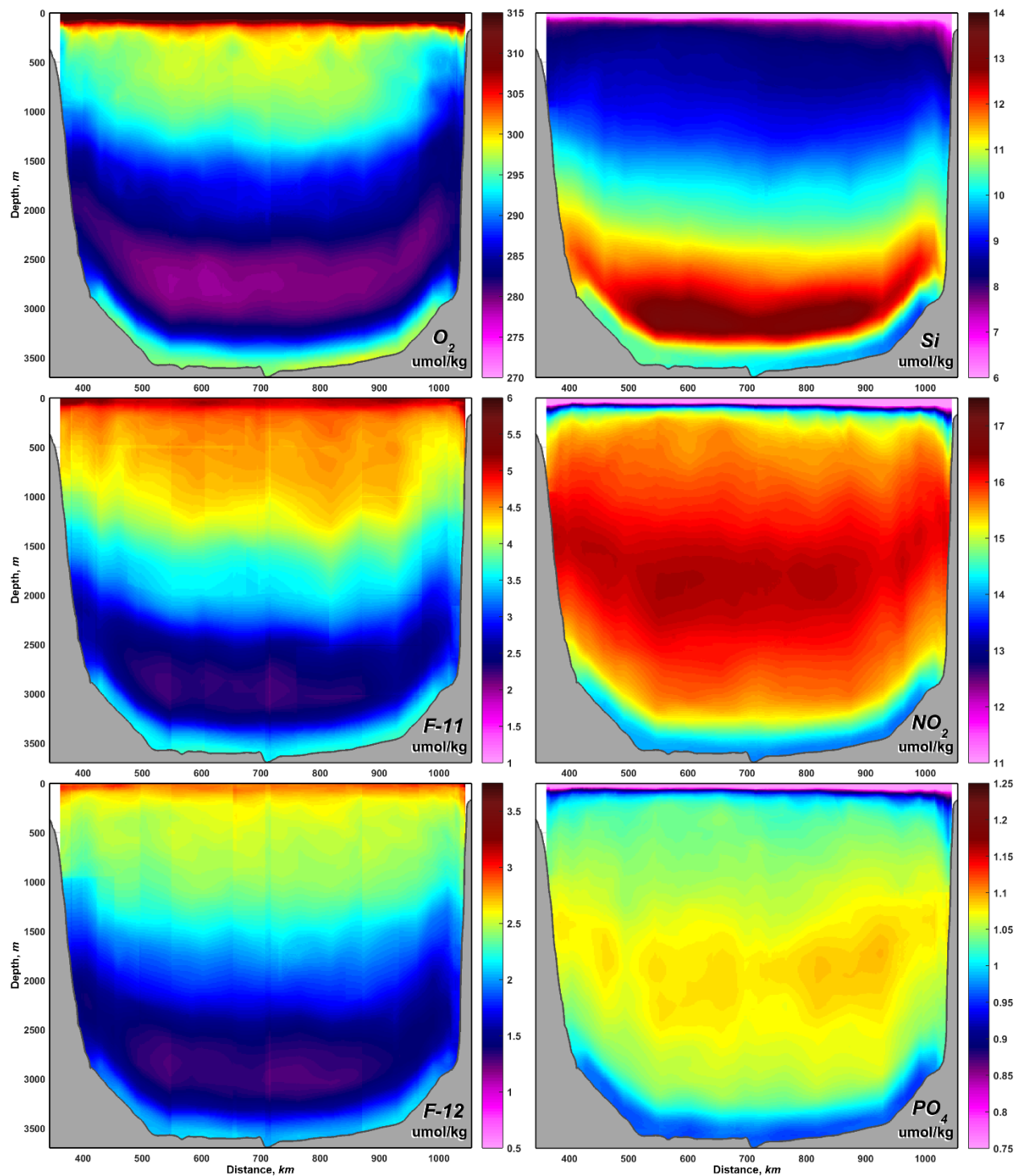
Figure 22. Climatological normals of dissolved oxygen, CFC-11 and CFC-12 (upper, middle and lower left panels, respectively), and silicate, nitrate and phosphate (upper, middle and lower right panels, respectively) concentrations on the AR7W line for the period of 1990-2019. The water sample chemical property values from all 1990-2019 DFO occupations of this line were checked in conjunction with other physical and chemical variables, consequently cleaned from data outliers, then annually interpolated on isopycnic surface (excepting horizontal distance gaps exceeding a certain distance-dependent threshold), and averaged over the entire period.
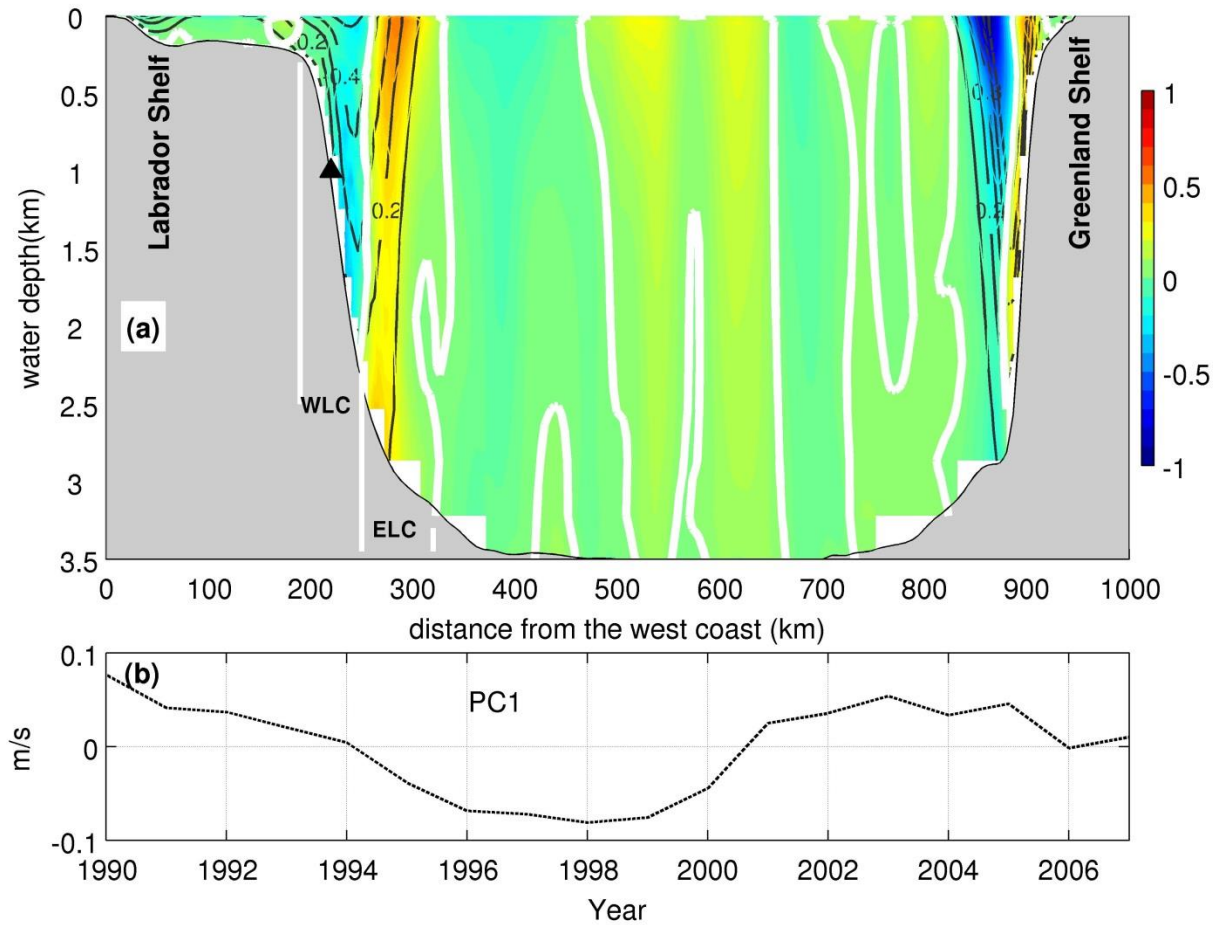
Figure 23. (a) EOF1 pattern of the normal velocities along AR7W (based on results from 1990 to 2007). The shaded areas represent the EOF pattern, bold white lines are zeros contours of the EOF pattern, the black labeled lines are the mean normal velocities (in m/s). Note: positive direction is northward. The black triangle indicates the location of the mooring referred to in the text. (b) Corresponding PC1.
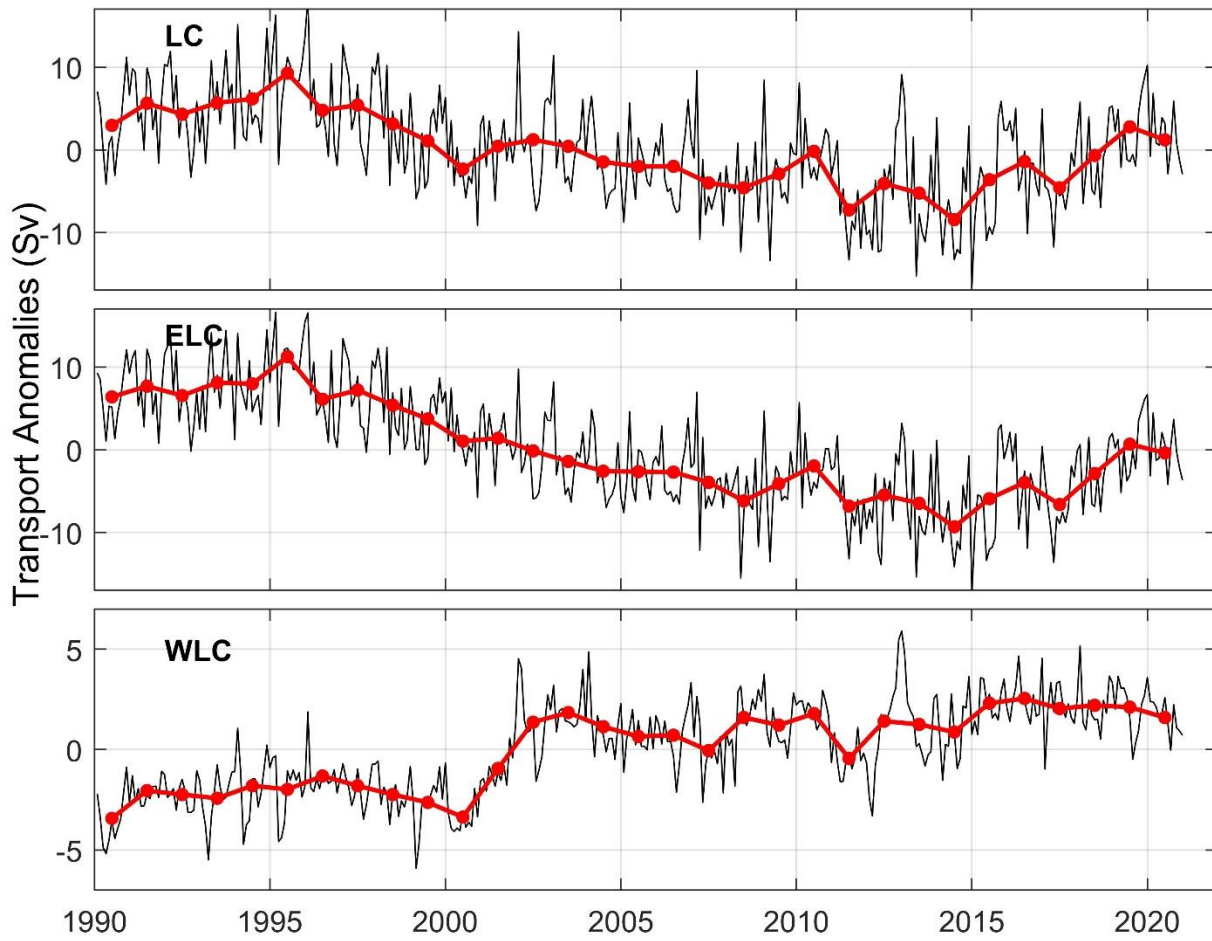
Figure 24. Transport anomalies of the LC, ELC, and WLC from 1990 to 2019.
Note: black lines are from the monthly data, and red lines and dots are from the annual means.
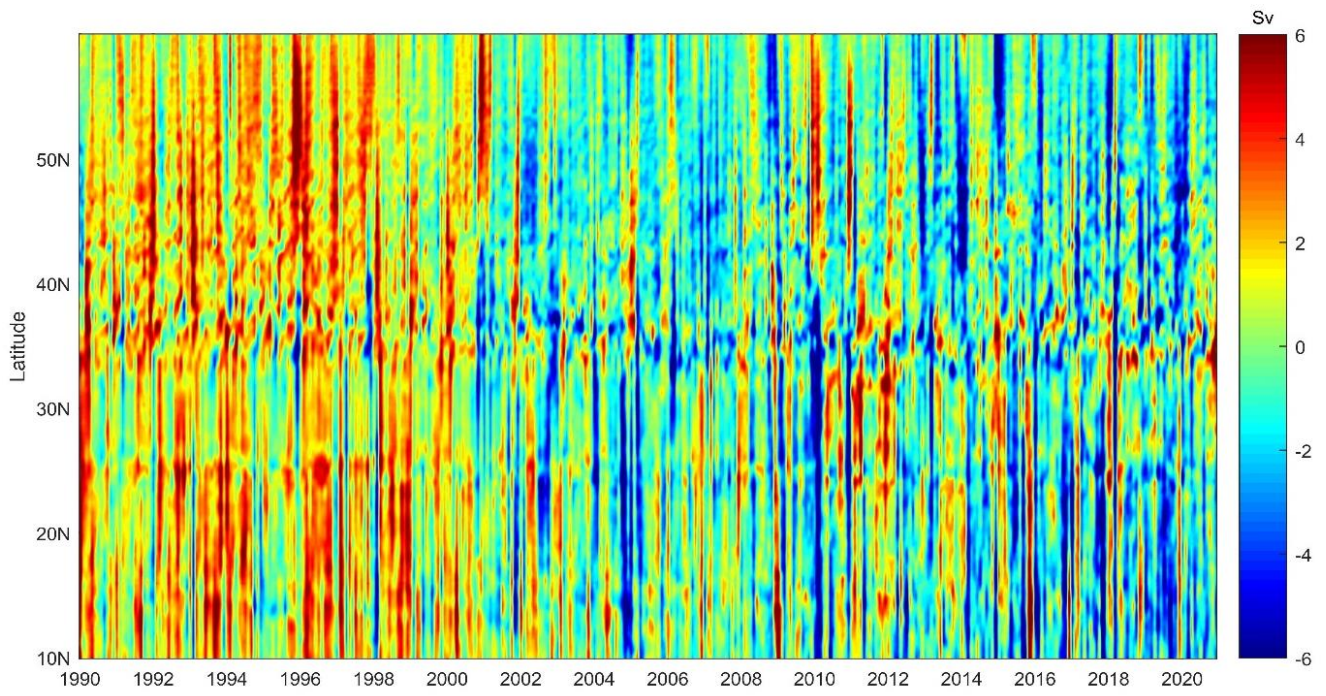
Figure 25. The AMOC anomalies at different latitudes with the seasonal cycles removed, but without detrending.
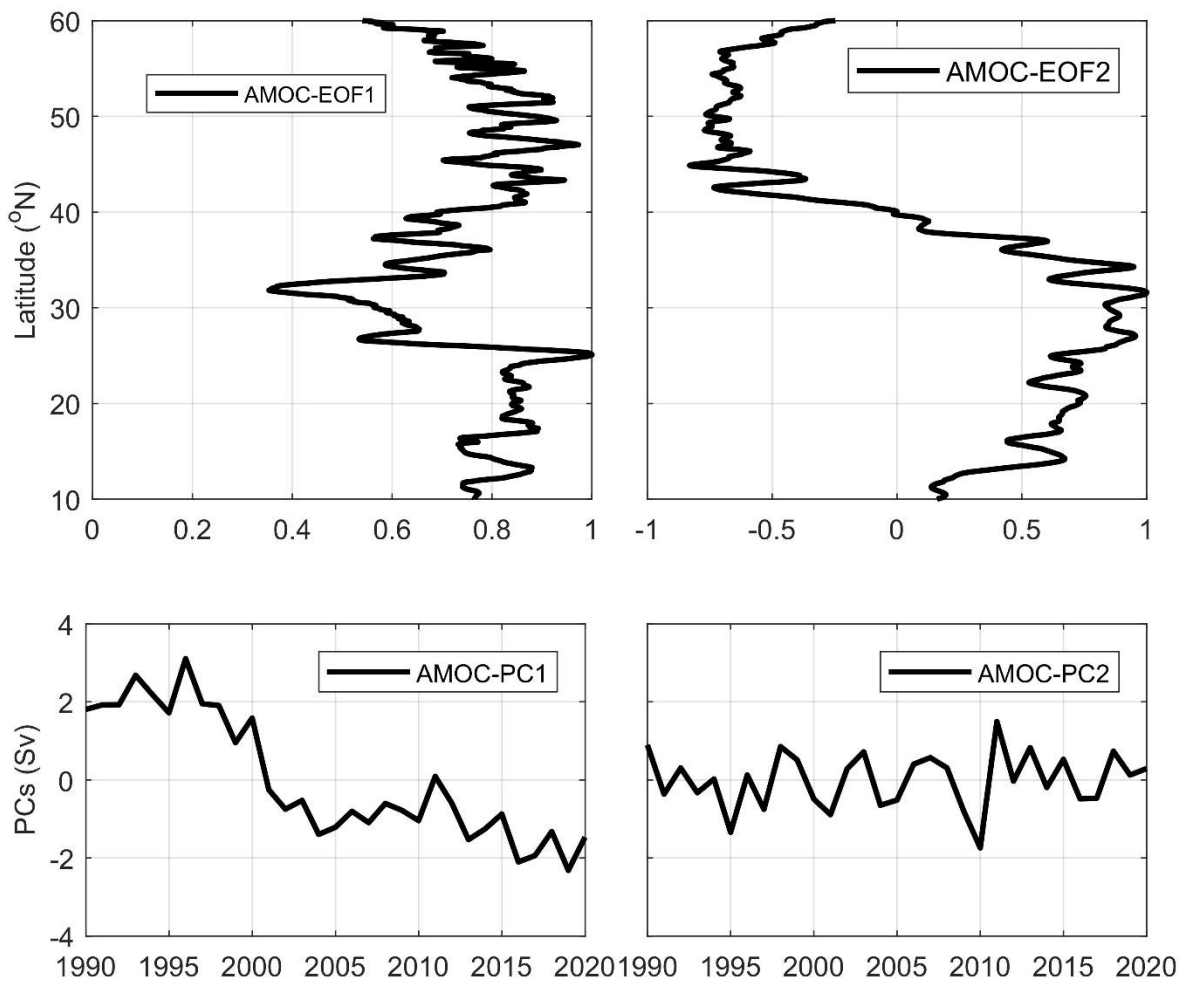
Figure 26. EOF patterns of AMOC (top panel) and associated PCs of these EOFs (bottom panel).
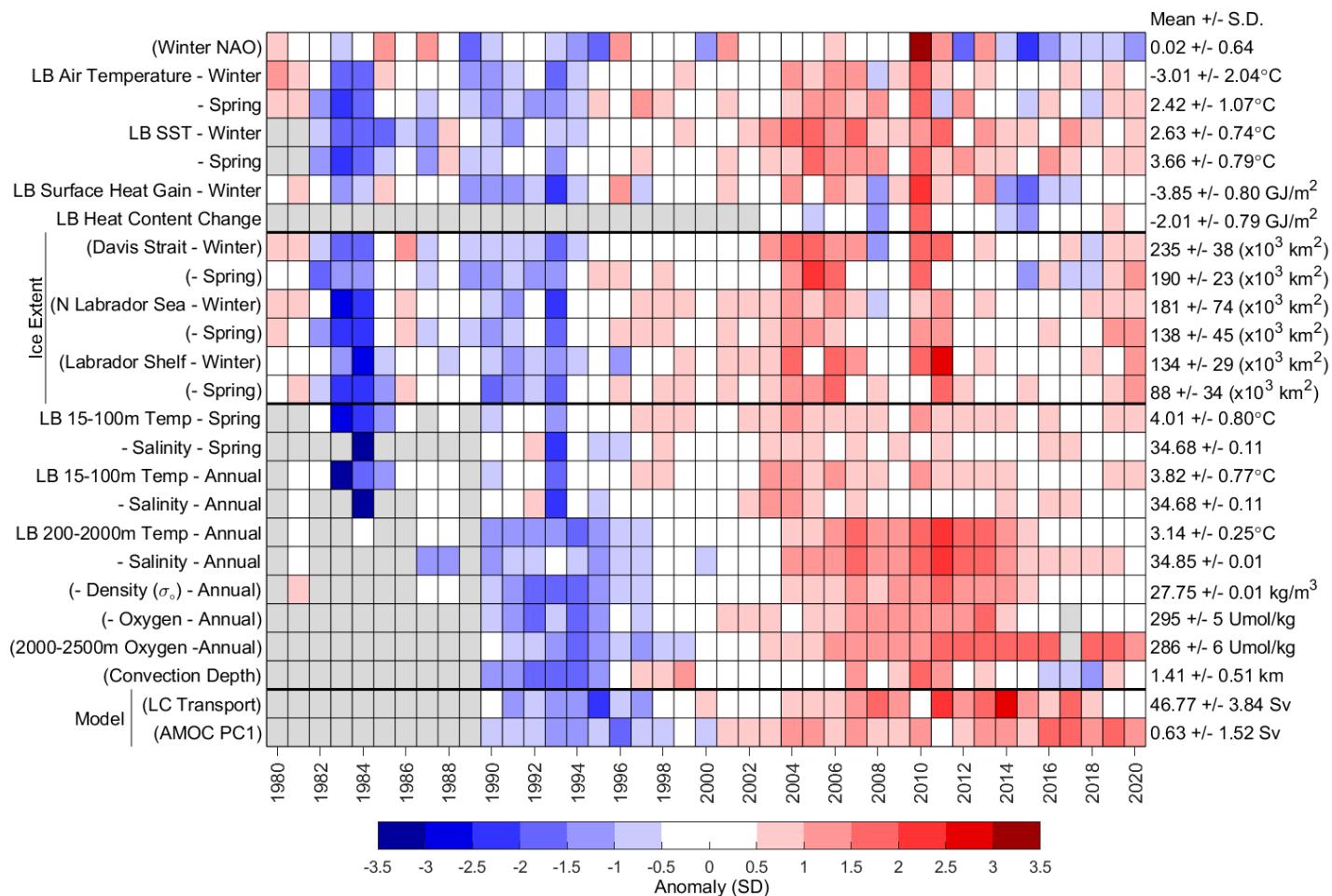
Figure 27. Scorecard for 1980-2020 oceanographic series. A grey cell indicates missing data, a white cell is a value within 0.5 SD of the long-term mean based on data from 1981–2010 when possible; a red cell indicates above normal conditions, and a blue cell below normal. Variables whose names appear in parentheses have reversed colour coding, whereby reds are lower than normal values that correspond to warm conditions. More intense colours indicate larger anomalies. Long-term means and standard deviations are shown on the right-hand side of the figure. North Atlantic Oscillation [NAO], Labrador Basin [LB], Labrador Current [LC].
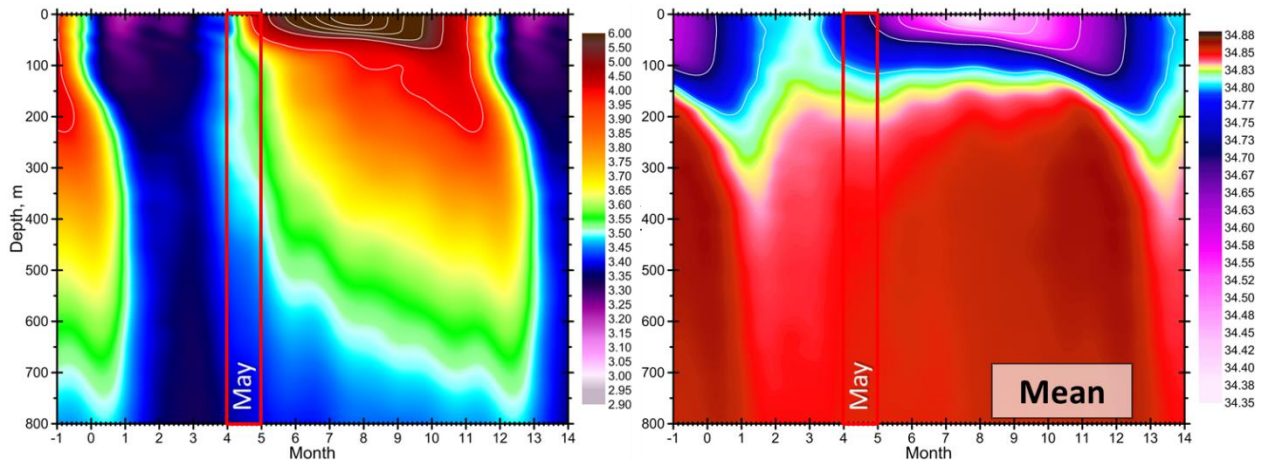
Figure A1. Regular seasonal cycles of temperature (left) and salinity (right) in the central Labrador Sea based on the iterative time series analysis technique by Yashayaev applied to all ship and Argo data.
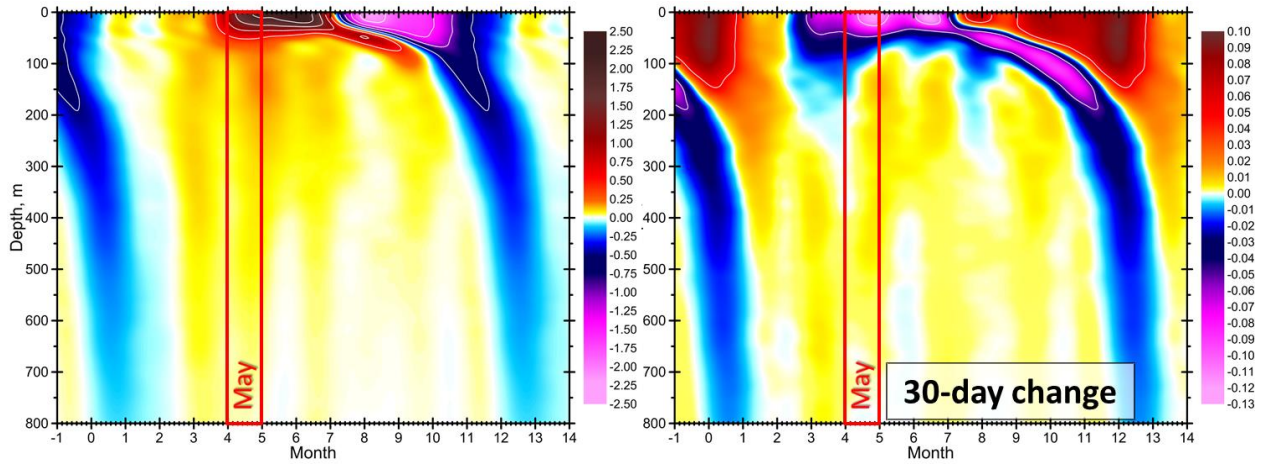

Figure A2. Ranges of temperature (left) and salinity (right) climatological normal values, shown in Figure A1, confined to 30-yearday-long seasonal intervals starting at each consecutive yearday.
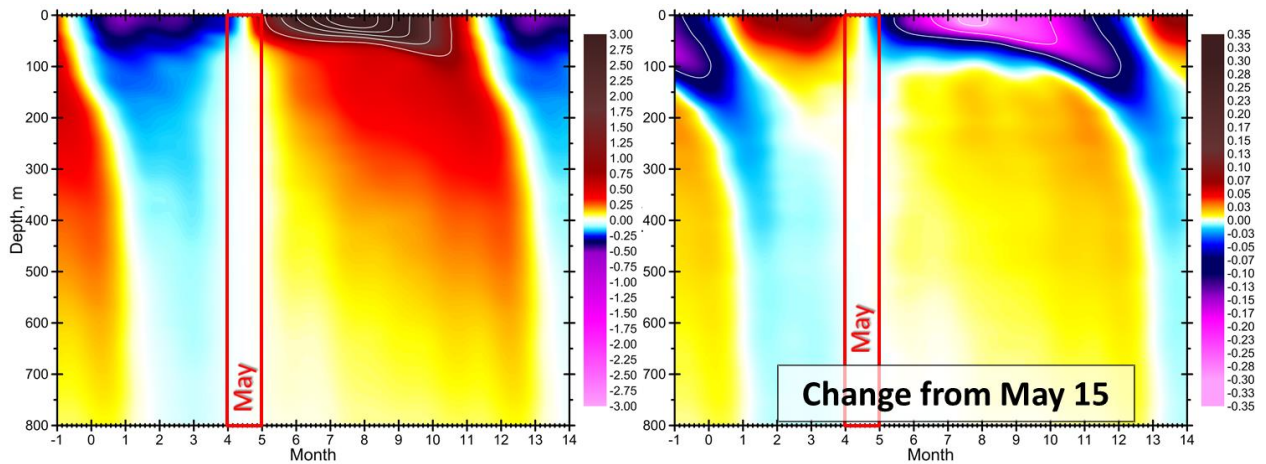

Figure A3. Seasonal changes of temperature (left) and salinity (right) referenced to the 15th of May (zero changes on that day).
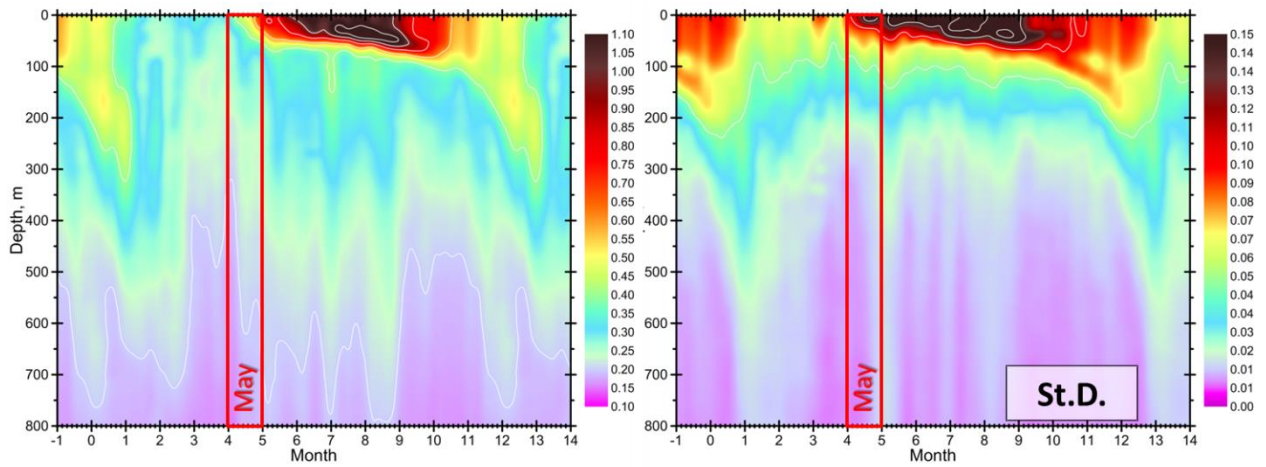
Figure A4. Standard deviations of temperature (left) and salinity (right) anomalies in the central Labrador Sea computed for data from all years selected within individual 10-yearday-long seasonal bins. The starting points of these bins are separated by 5 yeardays. The anomalies were computed by subtracting the harmonic seasonal cycle (Figure A1) from all multiyear observations at each depth. The data have been quality controlled (outliers removed) using the iterative seasonal cycle estimation techniques. Note that the standard deviations of temperature anomalies is smaller than the 30-day seasonal temperature change in May (Figure A2).
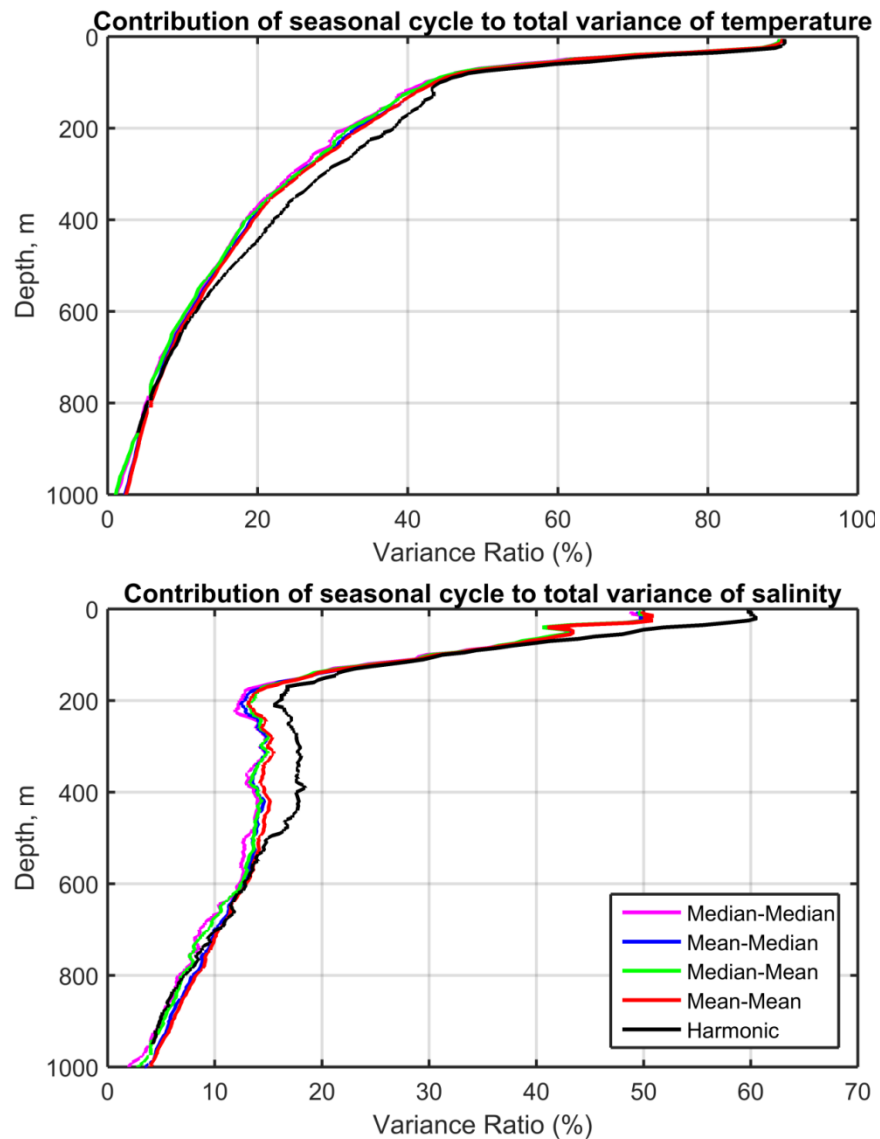
Figure A5. Contribution of computed seasonal cycle to the total variance of temperature (top) and salinity (bottom). The seasonal cycles were estimated by using data binning with 10-day bins spaced at 5-day intervals (coloured lines) and by using the iterative time series analysis technique based on harmonic analysis (black line) developed by Yashayaev. The data have been quality-controlled (outliers removed) as part of the same time series analysis.

The contributions are computed by dividing the variance of the respective seasonal cycle by the total variance and multiplying by 100%. This measure, for example, indicates that 90% of the total temperature variance at the sea surface is associated with the seasonal cycle. The contribution of the seasonal cycle below 200 m is less than 40% for temperature and less than 20% for salinity, and it rapidly declines with depth. This means that the annual averaging is permissible without applying a seasonal correction only below 200-300 m, but not above.
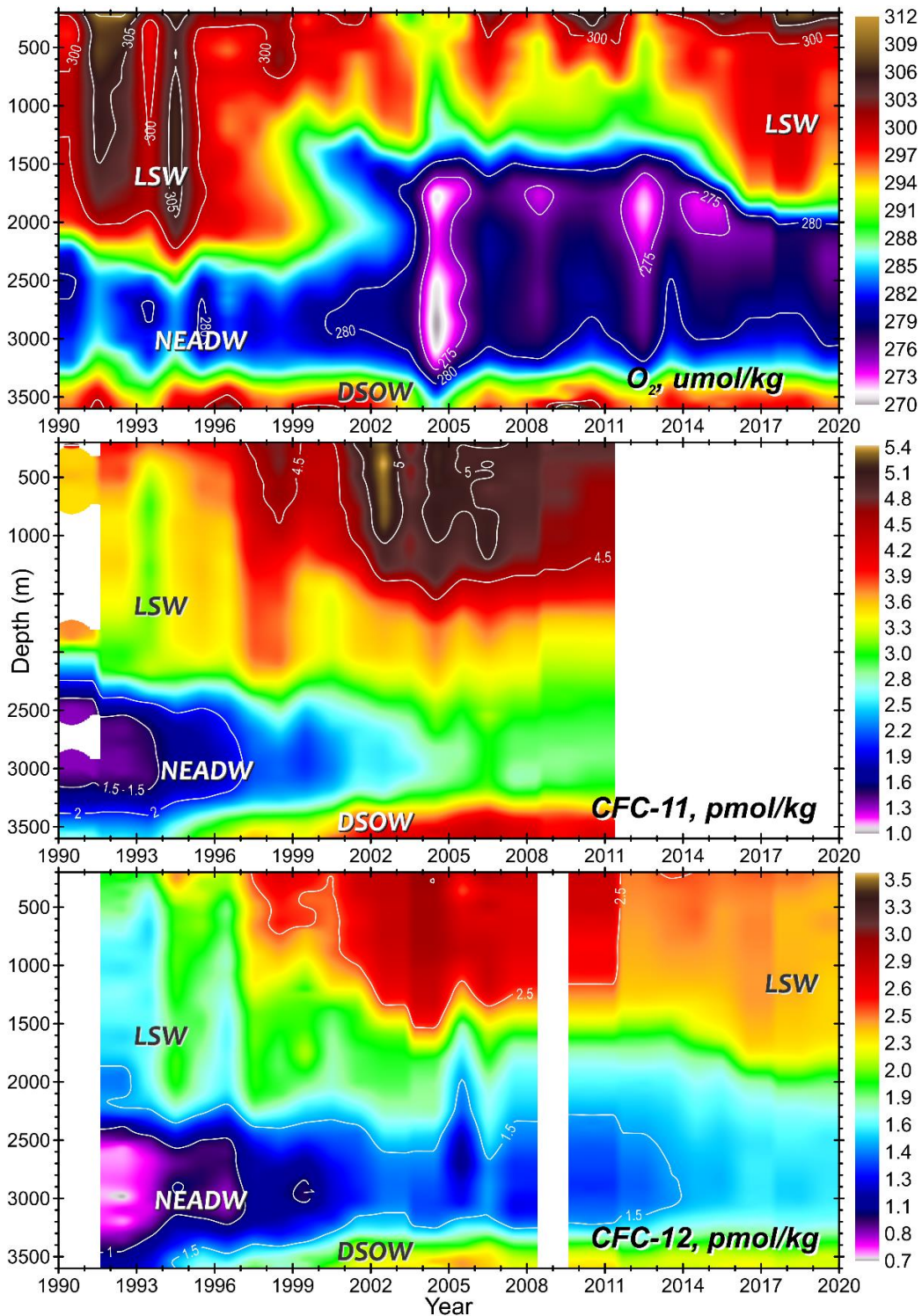
Figure A6. Annual composite profiles of dissolved oxygen (upper panel), CFC-11 (middle panel) and CFC-12 (lower panel) concentrations in the central region of the Labrador Sea (time period: 1990-2019, depth range: 200-3500 m). LSW, NEADW and DSOW indicate Labrador Sea Water, Northeast Atlantic Deep Water and Denmark Strait Overflow Water, respectively. Extensive quality control and data cleaning actions were applied to the data sets before averaging. The time-dependent corrections applied in Figure 11 *were not applied when constructing the annual profiles for the present figure.*
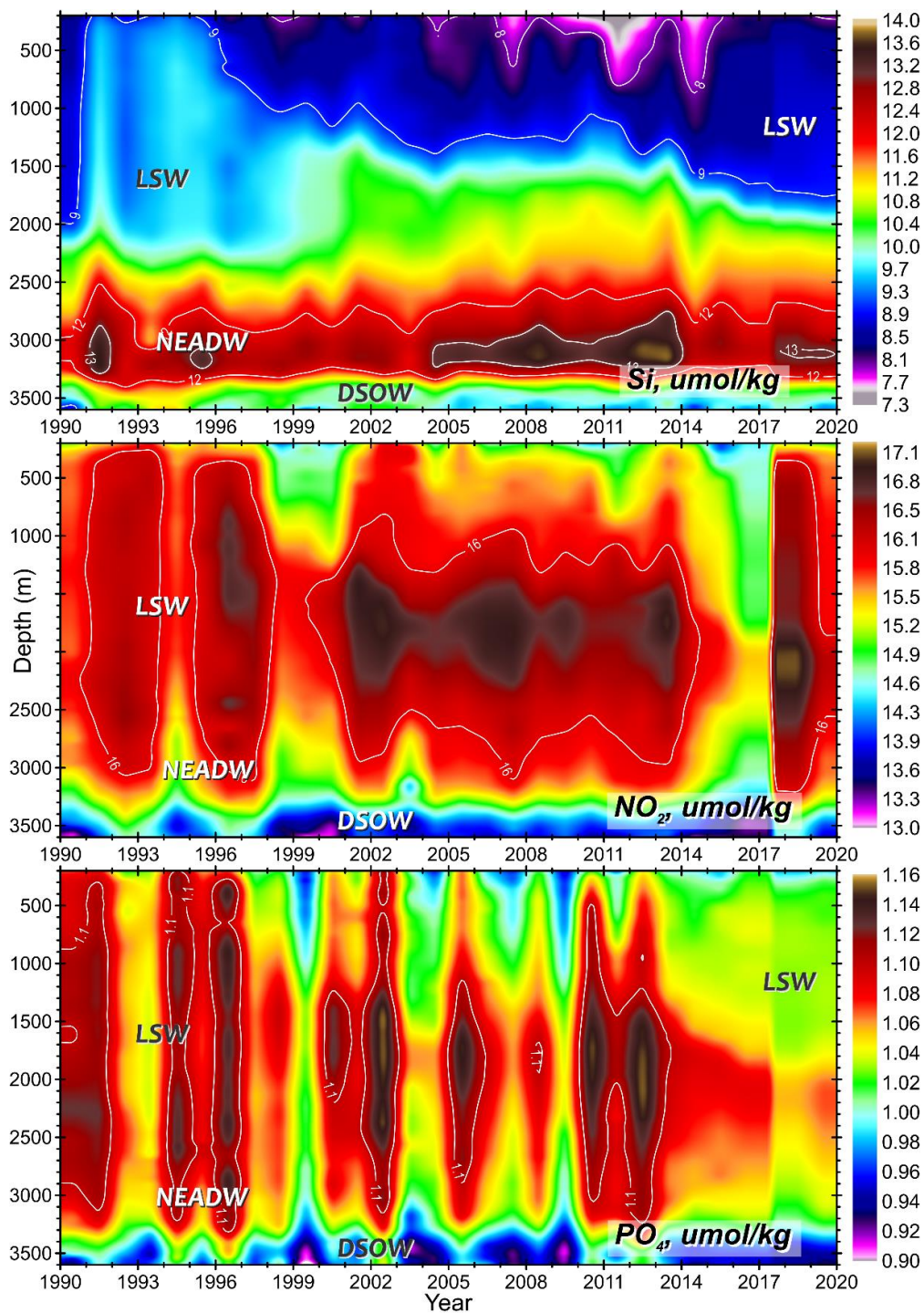
Figure A7. Annual composite profiles of dissolved silicate (upper panel), nitrate (middle panel) and phosphate (lower panel) concentrations in the central region of the Labrador Sea (time period: 1990-2019, depth range: 200-3500 m). LSW, NEADW and DSOW indicate Labrador Sea Water, Northeast Atlantic Deep Water and Denmark Strait Overflow Water, respectively. Extensive quality control and data cleaning actions were applied to the data sets before averaging. The time-dependent corrections applied in Figure 12 were not applied when constructing the annual profiles for the present figure.